BRITISH COLUMBIA

MESOZOIC MAGMATISM AND METALLOGENY OF THE HOTAILUH BATHOLITH, NORTHWESTERN BRITISH COLUMBIA

By B.I. van Straaten, J.M. Logan, and L.J. Diakow

Ministy of Energy, Mines and Natural Gas, British Columbia Geological Survey, Victoria, B.C., Canada

With contributions from:
J. Gabites (Pacific Centre for Isotopic and Geochemical Research, University of British Columbia, Vancouver, B.C., Canada)
R. Donelick (Apatite to Zircon, Viola, ID, U.S.A.)
P. O'Sullivan (Apatite to Zircon, Viola, ID, U.S.A.)

This report is accompanied by a 1:50,000 scale geology map

BRITISH COLUMBIA GEOLOGICAL SURVEY

Geoscience BC

OPEN FILE 2012-06

REPORT 2012-10
MAP 2012-10-1

ABSTRACT

A regional-scale reconnaissance bedrock mapping study was conducted in the Hotailuh batholith area, near the town of Dease Lake. The 2275 km^2 composite Late Triassic to Middle Jurassic batholith occurs within the Stikine terrane of northern British Columbia. The investigation aimed to refine the temporal magmatic and geochemical evolution of the batholith, and specifically focussed on relating mineralization with magmatic events.

This study combines one summer of field bedrock mapping with detailed petrography, geochemistry of both altered/mineralized and unaltered samples, geochronological data and integration with airborne geophysical survey results.

The Late Triassic plutonic suite comprises the Gnat Lake ultramafic to mafic bodies, Cake Hill felsic pluton and Beggerlay Creek ultramafic to mafic pluton. The absence of equivocal crosscutting relationships, lack of absolute crystallization age determinations for the ultramafic to mafic intrusions, and the absence of detailed mineral chemistry data makes it difficult to determine the genetic and temporal relationships between the different Late Triassic intrusions. The Late Triassic intrusions are spatially associated with, and in places intrude, poorly exposed and poorly dated, intermediate-mafic volcanic and sedimentary rocks of the Triassic Stuhini group. The Middle Jurassic Three Sisters pluton comprises at least four phases, namely the fine-grained mafic-intermediate phase, a mafic phase, central felsic phase, and a crosscutting potassic phase. U-Pb zircon crystallization ages and Ar-Ar cooling ages confirm that all phases formed during a relatively short time span in the Middle Jurassic. The northern and eastern margin of the batholith is nonconformably overlain by a succession of Early Jurassic basal sedimentary rocks grading upward into Early-Middle Jurassic volcanic rocks. The volcanic rocks were previously mapped as Triassic Stuhini group, but new geochronological data and mapping suggest they are part of the Jurassic Hazelton group.

Geochronology and geochemistry confirm the presence of at least two discrete magmatic events in the Late Triassic and Middle Jurassic. Both magmatic events have a strong calc-alkaline subduction-modified subcontinental mantle geochemical signature, and formed in a volcanic island arc to continental volcanic arc setting. At least two episodes of mineralization associated with Late Triassic and Middle Jurassic magmatism are found in the area. In addition to the known mineral occurrences within the batholith and its immediate surroundings, this study identified several new mineral occurrences. The intrusion-related magmatic-hydrothermal mineralization comprises predominantly copper, gold, silver, molybdenum and/or tungsten occurrences. Mineral occurrences occur peripheral to the main batholith and along contact zones between different magmatic phases within the batholith. The Gnat Pass ductile to brittle shear zone on the western margin of the batholith appears especially well endowed with mineral occurrences, and includes the newly dated (ca. 216.5 Ma) porphyry copper prospect at Gnat Pass.

TABLE OF CONTENTS

INTRODUCTION

This report summarizes the results of a reconnaissance study on the magmatic history and metallogeny of the Hotailuh batholith, and is part of a larger BC Geological Survey Dease Lake Geoscience Project (Logan *et al.*, 2012a). The BCGS project is funded through Geoscience BC's QUEST-Northwest initiative, a program launched in early 2011 to stimulate mineral exploration in the northwestern part of the province along Highway 37. The 2011 Geoscience BC program includes two high-resolution airborne magnetic surveys (Simpson, 2012; Aeroquest Airborne, 2012; Geo Data Solutions, 2012), the collection of new regional stream sediment data and reanalysis of stream sediment samples (Jackaman, 2012a, b, c, d), as well as new bedrock mapping (Logan *et al.,* 2012b, c; this report; Moynihan and Logan, 2012; Iverson *et al.,* 2012; Iverson, 2012). Collectively, these programs provide detailed, high quality geoscience data that is intended to enhance metallic mineral exploration in an area of prospective geology adjacent to Highway 37, near Dease Lake, in northwestern British Columbia.

The study area is located within the Stikine terrane of the Canadian Cordillera, an aggregate of Late Paleozoic to Mesozoic magmatic arc successions accreted onto the North American margin during Middle Jurassic time (e.g. Gabrielse, 1991). The Stikine terrane comprises predominantly Triassic to Jurassic volcanic, sedimentary and plutonic rocks. This study focuses on the composite Hotailuh batholith (Figure 1), which has traditionally been subdivided into three plutonic suites of Late Triassic, Early Jurassic and Middle Jurassic age (Anderson, 1983; Gabrielse, 1998).

The main objectives of the Hotailuh project were to:

- further refine the temporal magmatic and geochemical evolution of the batholith;
- build a metallogenic framework that relates mineralization to magmatic events; and
- identify prospective areas for mineralized magmatic-hydrothermal systems.

Here, we present the 2011 field results, as well as results from assay analyses of mineralized samples, petrography, lithogeochemistry of least altered samples, geochronology and integration with Geoscience BC's geophysical survey.

The composite Hotailuh batholith is exposed in a 2275 km^2 area southeast of Dease Lake. Nine weeks of 1:20,000 scale mapping by a two person team in summer 2011 included visits to 331 field stations and collection of 134 samples for laboratory study and analysis. The 2011 study focused on mapping within the Gnat Pass area and seven smaller areas to the east (Figure 1). The field areas were chosen for their mineral occurrences and suitability for understanding the internal geology and external contact relationships for various phases of the batholith. The study areas are covered by the 1:50,000 NTS map sheets 104I/04, 104I/03W, the southernmost part of 104I/05, and northernmost part of 104H/13. The Gnat Pass area is accessible by truck from Highway 37. Except for a section between Upper Gnat Lake and a point 7 km further south, the abandoned BC railroad grade is driveable by truck up to the southern boundary of the study area. The remaining areas were mapped from fly camp

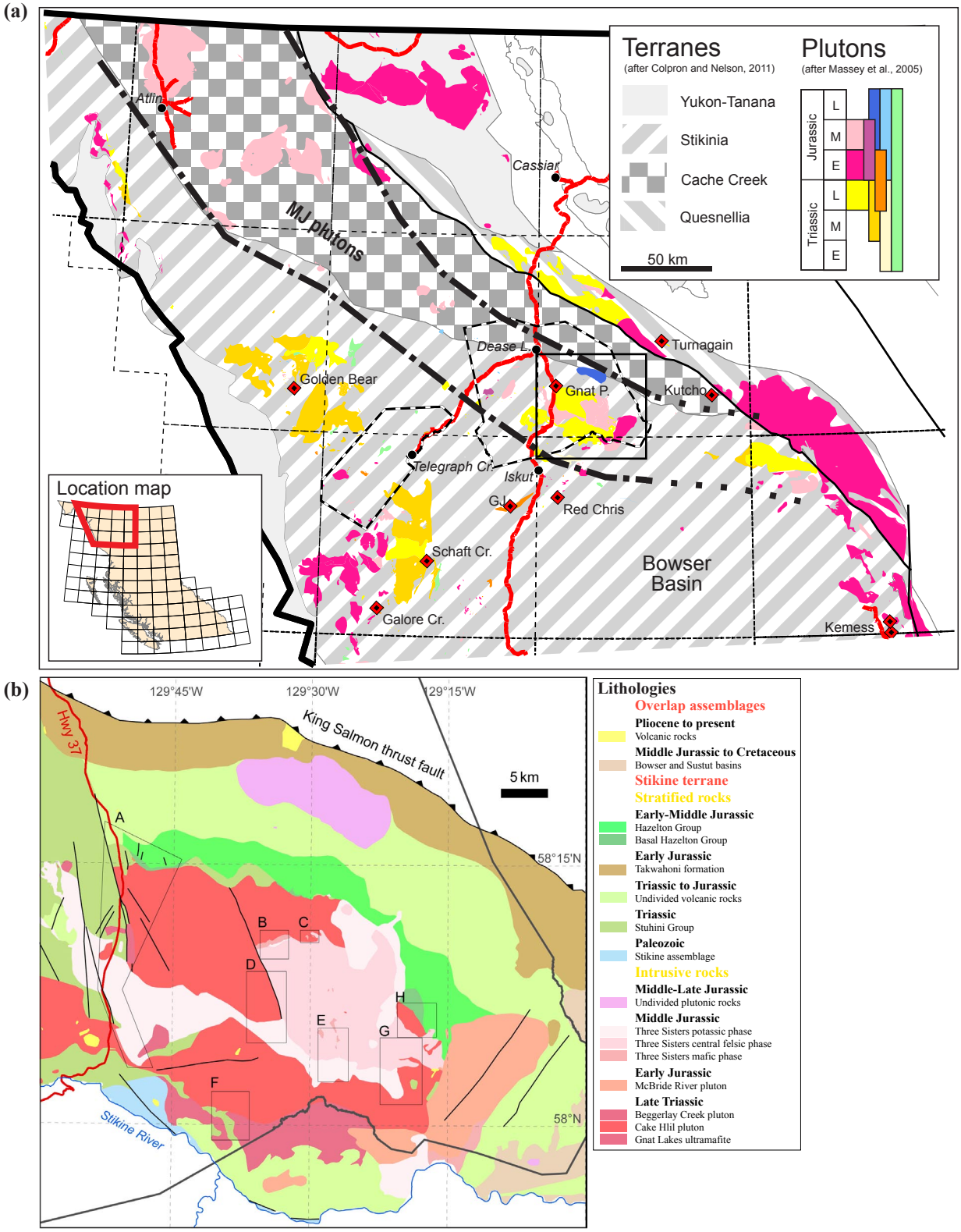

Figure 1: Regional setting of the Hotailuh batholith. (a) Distribution of Triassic and Jurassic intrusive rocks in northwestern B.C. Geology adapted from Massey et al. (2005) using geochronology data from Friedman and Ash (1997), Gabrielse (1998), Scott et al. (2008), Logan et al. (2012c). The QUEST-NW geophysical footprint is shown for reference. (b) Regional geology map of the Hotailuh batholith area, showing main lithologies, faults and the eight study areas.

locations accessed by helicopter chartered from Dease Lake.

The bedrock exposure is poor to moderate (5-10%) in the forested and brush-covered Gnat Pass area, except for exposures along road cuts, abandoned rail cuts and in old exploration trenches. The rock exposure improves dramatically above tree line, at approximately 1500 m. Exposure is best (10-30%) in the topographically higher areas of the Hotailuh batholith, with excellent exposure along alpine ridges, steep valley walls and cirques. However, glacial deposits and colluvium cover many alpine valleys, with only limited exposure in some creeks. Many of the exposures below, and especially above, treeline have an intense lichen cover. A notable exception is the lee side of alpine ridges where the thicker wind-accumulated winter snowpack appears to have inhibited lichen growth. These are prime locations for observing complex crosscutting relationships among the intrusive phases of the batholith.

REGIONAL GEOLOGY

The study area is located near the north-northeastern margin of the Stikine terrane of the Canadian Cordillera (Figure 1), a volcanic island-arc complex accreted onto the North American margin during Middle Jurassic time (Gabrielse, 1991; Nelson and Mihalynuk, 1993). The basement of the Stikine terrane is characterized by carbonate and volcanic rocks of the Devonian to Permian Stikine assemblage, overlain by calc-alkaline volcanic and associated sedimentary rocks of the Triassic Stuhini group and Early to Middle Jurassic Hazelton group (Marsden and Thorkelson, 1992; Currie and Parrish, 1997). The Stuhini group volcanic rocks are predominantly mafic to intermediate in composition, whereas the Hazelton group volcanic rocks are predominantly intermediate in composition with lesser felsic and mafic horizons (Marsden and Thorkelson, 1992).

Late Permian to Middle Triassic tholeiitic volcanism of the Kutcho assemblage formed a proto-arc on the inboard margin of the Stikine terrane, and was the subsequent locus for arc marginal clastic sedimentation in the Early Jurassic (English and Johnston, 2005; Schiarizza, 2011). Sedimentation within this forearc sedimentary basin (Whitehorse trough) comprises proximal conglomerates and more distal sandstones of the Takwahoni and Inklin formations, respectively. Closure of the Cache Creek ocean, subsequent collision with the Whitehorse trough and thrusting overtop the inboard margin of Stikinia occurred in the late Early to earliest Middle Jurassic (Ricketts *et al.*, 1992; Nelson and Mihalynuk, 1993). The rocks of the Cache Creek ocean and Whitehorse trough are currently exposed in a north-northwest striking belt north of Dease Lake (Figure 1), and are found in the hanging wall and footwall of the King Salmon thrust fault. The latter is generally interpreted as a major terrane bounding structure, separating autochthonous rocks of the Stikine terrane to the south from allochthonous rocks of the Cache Creek terrane to the north (e.g. Gabrielse, 1998). The Stikinia – Cache Creek accretionary event was complete by the Middle Jurassic (Bajocian), as indicated by sedimentation of Cache Creek derived chert clasts deposited in the molasse-type Bowser Basin to the south of the study area (Figure 1; Ricketts *et al.*, 1992).

Large granitoid plutons were emplaced during the Late Triassic to Middle Jurassic, and are exposed in an arcuate belt on the northern margin of the Bowser basin. This belt, commonly referred to as the Stikine arch, is centered on the Hotailuh batholith,

and includes the Stikine pluton to the southeast and the Hickman batholith to the southwest (Anderson, 1983; Woodsworth *et al.*, 1991). Several smaller Late Jurassic to Cretaceous plutons are present within the Dease Lake area (Anderson and Bevier, 1992; Logan *et al.*, 2012b, c).

Mineralization in the northern Stikine terrane comprises several Late Triassic to earliest Jurassic calc-alkaline porphyry Cu-Mo±Au and alkaline porphyry Cu-Au deposits; notable examples include Galore Creek, Schaft Creek, KSM and GJ to the southwest, Red Chris to the south, and Kemess to the southeast (Ash *et al.*, 1997; Logan *et al.*, 2000; Duuring *et al.*, 2009; Norris *et al.*, 2011). These porphyry copper deposits are roughly located on the southwestern and southeastern apexes of the Stikine magmatic arch. Interestingly, despite the presence of similar rocks in the centre of the arch, no major porphyry copper deposits have yet been found in the immediate area of the Hotailuh batholith. Southwest of the study area, the Au-Ag-enriched Eskay Creek volcanogenic massive sulphide deposit is hosted in felsic volcanic rocks within the Early-Middle Jurassic Hazelton group (Bartsch 1993), and represents a relatively underexplored deposit type elsewhere in the Stikine terrane (Massey *et al.*, 1999).

GEOLOGICAL UNITS

Eight areas were mapped in detailed during this study, and are shown on the accompanying 1:50,000 scale geological map (labelled ‘a’ to ‘h’ on Figure 1b). The detailed geological maps incorporate data from Anderson (1983) and Gabrielse (1998), as well as Read and Psutka (1990) and Evenchick and Thorkelson (2005) in the far south. The detailed Gnat Pass compilation map ‘a’ also incorporates data from Read (1984), Nixon *et al.* (1989; 1997) around the Gnat Lakes ultramafite, Dircks (1974) around the BCR property, Wetherill (1989; 1990) around the Dalvenie claims, Smith and Garagan (1990) and Page and Scott (2006) around the Gnat Pass prospect, and detrital zircon results from near peak 2096 m (Iverson *et al.*, 2012; Iverson, 2012). The position of geological contacts were refined in areas lacking geological information using the QUEST-Northwest aeromagnetic survey data (Aeroquest Airborne, 2012) . Additional U-Pb LA-ICP-MS zircon crystallization ages and Ar-Ar hornblende and biotite cooling ages are reported as part of this study (see ‘Geochronology’ section).

The regional geological information surrounding the detailed geological maps on the accompanying 1:50,000 scale map are modified from the digital BC geological map compilation of Massey *et al.* (2005) and the above mentioned sources.

Rock classification schemes used throughout this paper follow those developed by the British Geological Survey (Gillespie and Styles, 1999; Hallsworth and Knox, 1999). Notably, the reported crystal size in igneous rocks is the volumetrically dominant size; the mineral qualifying suffixes *–bearing* and *–rich* indicate that <5% and >20% of the rock comprises the mineral in question, respectively. In the field, a *gabbro* has been defined as a rock plotting in the diorite QAPF field, but containing ≥50% mafic minerals. Elevations for unnamed peaks (“peak ... m”) are spot heights from BC’s TRIM database. All coordinates are in UTM NAD83 zone 9V.

Magnetic susceptibility values for all rock units were measured in the field with a Terraplus KT-10 hand-held magnetic susceptibility meter. Magnetic susceptibility data is summarized in Figure 2, and shows

consistent variability and distinctive ranges for several of the major units.

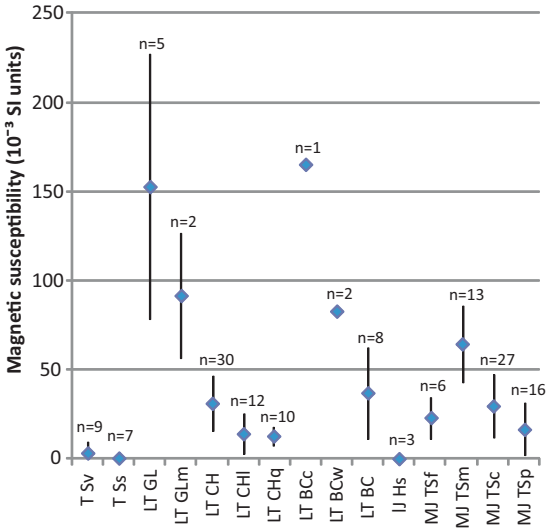

Figure 2: Graph showing the magnetic susceptibility values and one standard deviation for all major rock units. n = number of measurements, where each measurement represents the average of ten field measurements at one station point.

Rock units encountered in the field are summarized in Table 1, and are described in order from oldest to youngest.

Stratified rocks

Triassic rocks

Rocks in the central and western part of the Gnat Pass valley predominantly comprise massive to foliated augite-phyric coherent rocks with lesser massive fine-grained sedimentary rocks (units T Sv and T Ss in Table 1 respectively), that are assigned to the Triassic Stuhini group (Anderson, 1983; Gabrielse, 1998). The coherent rocks represent either volcanic extrusives and/or sub-volcanic intrusions. The complex map pattern of the volcanic and sedimentary lithologies could be due to a number of factors such as faulting, folding, rapid lateral and vertical facies changes and/or irregular intrusion of augite porphyry into the sedimentary strata. The Stuhini augite-phyric rocks are cut by felsic dikes, likely genetically related to the Gnat Lakes ultramafite (unit LT GLf), and appear to be intruded and partially assimilated by the Cake Hill pluton (unit LT CH, 221-218 Ma). The Stuhini group augite-phyric coherent rocks in the Gnat Pass valley north of Lower Gnat Lake are crosscut by the Gnat Pass intrusive (unit LT GP, 216 Ma). These relationships, as well as their foliated nature (discussed below), suggest a pre 221-216 Ma age for these rocks.

South of the Hotailuh batholith (map 'f'), Stuhini group rocks consists of a lower predominantly sedimentary package grading into predominantly coherent rocks exposed at higher elevations (units T Ss and T Sv in Table 1, respectively). The change from laminated and very thinly bedded siltstones and medium-grained sandstones with minor concordant intervals of massive augite-phyric coherent rocks to massive augite-phyric coherent rocks with rare fine-grained sandstone intervals is well-exposed in a steep gully. Here, laminated to very thinly bedded augite-bearing medium-grained volcaniclastic sandstones to granule-sized volcaniclastic conglomerates (unit T Sv) occur between these two rock units. Unfortunately, poor exposure and lichen-covered outcrops dominate the remainder of the area making it difficult to differentiate coarse-grained augite-bearing sediments from augite-phyric coherent rocks. This could explain the apparent lack of augite-bearing sediments at other locations near this contact. Way-up criteria were not observed in the area, and although bedding in the southeastern half of the Stuhini succession has a uniform moderate southeasterly dip, structural disturbance appears to have affected rocks in the western half (map 'f'). Based on the presence of augite-bearing volcaniclastic sediments, the augite-phyric coherent rocks most likely are

Table 1a: Stratified rocks

Group	Area	Unit	Age	Code	Lithology
		Undivided	TJ	v	Includes lmJ Hv, lmJ Hsc, lmJ Hs, lJ Hs, T Sv and T Ss; see below
Jurassic Hazelton group	Northwestern area	Volcanic rocks	lmJ	Hv	Granule, pebble and cobble-sized volcaniclastic conglomerate and pyroclastic breccia; contains Plag-Aug, Plag, Aug, Plag-Hbl-phyric, amygdaloidal clasts. Volcanic sediments commonly contain Aug crystals
		Coarse-grained sedimentary rocks	lmJ	Hsc	Medium grey, medium bedded, medium- and (very) coarse-grained sandstone. Feldspathic ± lithic arenite. Minor interbedded siltstone; minor interbedded pebble conglomerate
		Fine-grained sedimentary rocks	lmJ	Hs	Dark grey to black, parallel laminated to (very) thinly bedded siltstone and fine-grained sandstone. Often recessive
		Coarse-grained quartz-bearing sedimentary rocks	lJ	Hs	Basal unit nonconformably(?) overlies Cake Hill pluton. Very coarse-grained sandstone and pebble-sized conglomerate with granitoid clasts. Includes conglomerate, quartz-bearing feldspathic-arenite, graphitic siltstone and micrite of Anderson (1983), Smith and Garagan (1990)
	Eastern area	Volcanic rocks	lmJ	Hv	Pyroclastic breccia and volcaniclastic pebble-sized conglomerate; contains Hbl(?)-Plag-phyric clasts
		Sedimentary rocks	lJ	Hs	Alternating medium-dark grey (parallel) laminated siltstones, calcareous siltstones, fine- to medium-grained sandstone and rare very thick bedded, likely Qtz-bearing, (very) coarse-grained sandstone and granular conglomerate
Triassic Stuhini group	Entire area	Stuhini volcanic rocks	T	Sv	Dark green, 1-5 mm euhedral, 20-40% Aug-phyric coherent rocks; rare Plag-Aug-phyric. Local volcanic breccia, volcaniclastic conglomerate and sandstone
		Stuhini fine-grained sedimentary rocks	T	Ss	Medium to dark grey, laminated to very thinly bedded siltstone and fine- to medium-grained sandstone. With minor concordant 0.5-1 m intervals of 2-5 mm 30-40% Aug-phyric coherent rocks

Age abbreviations: T = Triassic, J = Jurassic; stratified rocks: l = lower, m = middle, u = upper; intrusive rocks: E = early, M = middle, L = late
Mineral abbreviations after Kretz (1983)

Table 1b: Intrusive rocks

Suite	Pluton	Unit	Age	Code	Lithology
Middle Jurassic Three Sisters plutonic suite		Tees Creek intrusive	≤ MJ	TC	Altered Hbl-Fsp-porphyritic hypabyssal intrusive
	Three Sisters pluton	Three Sisters potassic phase	MJ	TSp	Bt-bearing granite, Qtz-syenite and Qtz-monzonite with Kfs>Plag. Equigranular 1 mm to 4 mm; often 5-20 mm Kfs porphyritic. Includes pink Bt porphyritic dikes
		Three Sisters central felsic phase	MJ	TSc	Bt and Hbl-Bt (rare Bt-Hbl) Qtz-monzonite and Qtz-monzodiorite with Plag>Kfs. Equigranular, 2-3mm; 4-5 mm Kfs porphyritic in places; dioritic xenoliths locally present
		Three Sisters mafic phase	MJ	TSm	Hbl-rich (minor Bt-Cpx Hbl-rich) Qtz-diorite. Acicular Hbl 0.5-4 mm to 2-7mm; equant Hbl 1-2mm to 4-10 mm
		Three Sisters fine-grained mafic-interm. phase	MJ	TSf	Hbl-Bt Qtz-diorite. Equigranular, 1-1.5 mm, often 10 vol.% 1.5-3 mm Plag porphyritic
Early Jurassic	McBride River	McBride River pluton	EJ	MR	Hbl-Bt granodiorite and Qtz-monzodiorite. Equigranular, 1-5 mm; contains abundant rounded, clear to grey Qtz (Anderson, 1983)
Late Triassic Stikine plutonic suite		Gnat Pass intrusive	LT	GP	Plag-porphyritic hypabyssal intrusive (sparse Qtz and/or Hbl porphyritic in places). Inequigranular 2 mm euhedral-subhedral Plag, rarely 2-4 mm Qtz-porphyritic
	Beggerlay Creek pluton	Beggerlay Creek potassic dikes	LT	BCp	Coarse pink Kfs (± Ep) dikes
		Beggerlay Creek websterite body	LT	BCw	Serpentinized websterite. Equigranular, 5 mm, massive
		Beggerlay Creek pluton	LT	BC	Cpx-Hbl-rich to Hbl-Cpx-rich gabbro (BC) to rare Plag-bearing clinopyroxenite (BCc). Equigranular, 3-5 mm, massive to moderately foliated
	Cake Hill pluton	Cake Hill quartz-rich phase	LT	CHq	Hbl monzogranite and granodiorite. Equigranular, 3 to 3-4 mm, with minor ubiquitous 4-7 mm Qtz blebs; tabular Hbl common
		Cake Hill foliated phase	LT	CHf	Bt(?)-Hbl diorite and Qtz-diorite. Foliated, equigranular, 1-3 mm
		Cake Hill leucocratic phase	LT	CHl	Light-coloured and Ep altered Hbl Qtz-monzodiorite, granodiorite, Qtz-diorite, tonalite(?). Equigranular, 1-2 to 2-3 mm, common tabular Hbl
		Cake Hill pluton	LT	CH	Hbl to lesser Bt-Hbl Qtz-monzodiorite and Qtz-monzonite. Equigranular, 3-4 mm; tabular Hbl bearing, trace Ttn usually ubiquitous; trace Mag in places; massive to moderately foliated
	Gnat Lakes ultramafite	Gnat Lakes felsic phase	LT	GLf	Hbl granodiorite, monzodiorite and diorite. Equigranular 2 mm
		Gnat Lakes mafic phase	LT	GLm	Cpx Hbl-rich gabbro. Equigranular 1-5 mm Hbl
		Gnat Lakes ultramafite	LT	GL	Plag-bearing hornblendite to Cpx Hbl-rich gabbro. Equigranular 2-100 mm euhedral-subhedral Hbl, anhedral Plag

extrusive in origin. The volcano-sedimentary rocks close to the Beggerlay Creek pluton contact are cut by coarse K-feldspar dikes that are presumed to be cogenetic with the latter pluton, implying a Late Triassic or older age for this Stuhini succession.

A limited number of Stuhini group xenoliths occur within the Hotailuh batholith. A 0.5-1 km^2 raft or pendant of Stuhini is present within the Cake Hill leucocratic phase (map 'g') and comprises predominantly volcanic breccia and volcaniclastic conglomerate (unit T Sv). To the north, a much smaller inclusion of augite-phyric coherent rocks (unit T Sv; map 'h') within the Cake Hill quartz-rich phase is intruded and partly assimilated by the Three Sisters mafic phase.

All Stuhini group rocks on the accompanying 1:50,000 map have been assigned a lower-middle Triassic (lmT Ss), middle Triassic (mT Sv) or upper Triassic age (uT Sv) based on Gabrielse's (1998) regional work.

Jurassic rocks

Sedimentary and volcanic rocks of Jurassic age were identified in the northwestern (map 'a') and eastern (map 'h') parts of the Hotailuh batholith.

Northwestern margin of the batholith

A succession of normal-facing Jurassic sedimentary rocks overlies the Cake Hill pluton (map 'a'). It was mapped previously as a Lower Jurassic unit of the Takwahoni formation overthrust by Lower to Upper Triassic Stuhini group (Anderson, 1983; Gabrielse, 1998). However, U-Pb detrital zircon dates suggest the hanging wall rocks are also Jurassic in age (Iverson *et al.*, 2012; Iverson, 2012).

The base of this succession comprises a coarse-grained, quartz-rich sedimentary unit (lJ Hs; Table 1), which was recognized at one outcrop location and in drill core at the Gnat Pass prospect. In outcrop it consists of a granitoid clast-bearing conglomerate and very coarse-grained sandstone (Figure 3). The lower contact lies within ten metres of intrusive rocks and likely represents a nonconformable contact. Fossils from a sandy micrite associated with limey, quartz-bearing, feldspathic-arenite located 4.5 km east of Lower Gnat Lake suggest an Early (to Middle?) Jurassic age (Henderson and Perry, 1981; Anderson, 1983, p. 209-214; Gabrielse, 1998, Appendix 2; map 'a'). Conglomerate, quartz-bearing feldspathic-arenite and graphitic siltstone intersected in drill core from the Gnat Pass prospect (Smith and Garagan, 1990; this study) appear similar to the rocks described above, and have been included in the basal unit.

The stratigraphically overlying package of rocks can be traced along most of the south-facing slopes of peak 2096 m, and consists of two coarsening-upward sequences of predominantly sedimentary rocks (map 'a'; see also Figure 2, Iverson *et al.*, 2012; Iverson, 2012). Results from three detrital zircon samples show distinct Middle Jurassic and Late Triassic populations (Iverson *et al.*, 2012; Iverson, 2012) and indicate that these rocks must be younger than the Triassic Stuhini group. These sedimentary rock units (lmJ Hs and lmJ Hsc in Table 1) dip moderately to the north, and are stratigraphically overlain by augite-phyric volcanic breccias (unit lmJ Hv in Table 1). The coarse-grained quartz-bearing basal unit had traditionally been separated from these overlying, presumed Triassic Stuhini group, rocks by the Hotailuh thrust (Anderson, 1983; Gabrielse, 1998). However, the new detrital zircon results and the stratigraphic continuity between these

Figure 3: Very coarse-grained sandstone to granule-sized conglomerate with several pebble-sized granitoid clasts (arrow; unit lJ Hs). Altered Cake Hill pluton is exposed 10 m to the southeast and suggests a nonconformable contact. Hammer for scale.

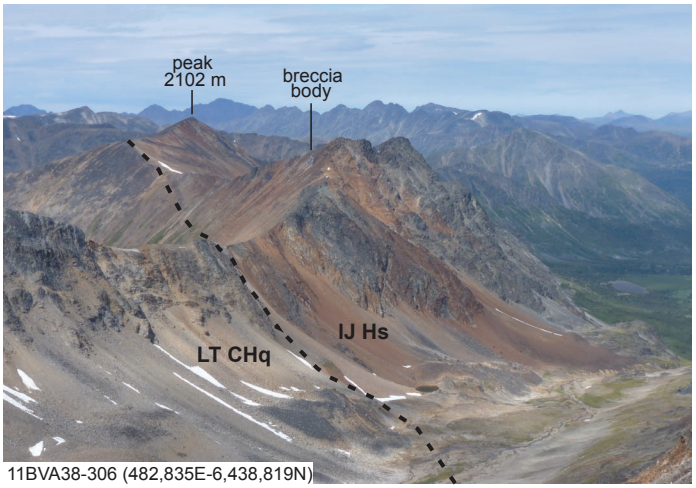

Figure 4: View northwest towards peak 2102 m (on left) showing the contact between grey quartz-rich phase of the Cake Hill pluton on the left (unit LT CHq) and rusty red, stratified sedimentary rocks (unit lJ Hs) on the right. Note light grey breccia body on the southwest face of the central peak.

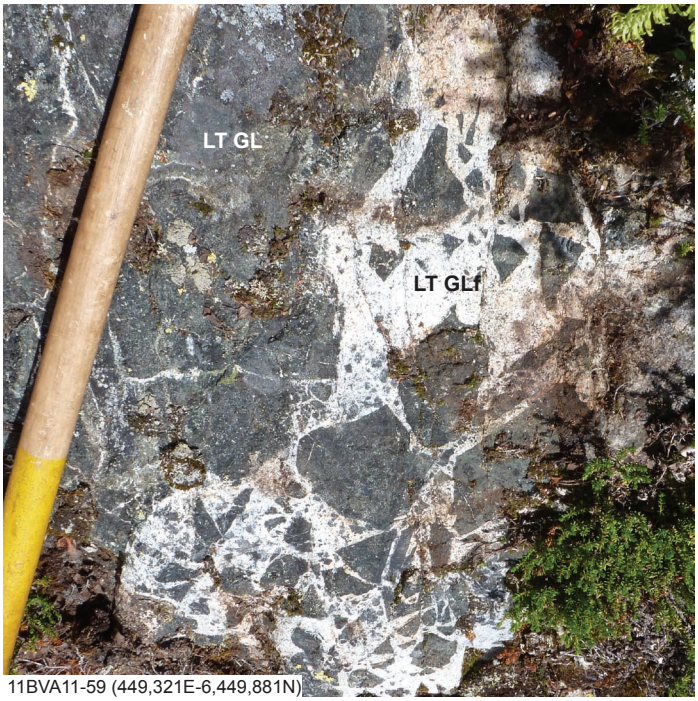

Figure 5: Hornblende-bearing granodiorite (Gnat Lake felsic phase, LT GLf) intruding and brecciating the Gnat Lake ultramafite (LT GL). Hammer for scale.

units eliminates the necessity for a thrust fault in this area (map 'a'). A large outcrop of (hornblende)-plagioclase-phyric volcanic breccia is present southwest of peak 2096 m, between the basal quartz-bearing and the overlying fine-grained sedimentary rock succession (map 'a'). It does not appear to extend further east or west. The overlying fine-grained sediments contain two 10 m thick concordant columnar jointed augite-phyric coherent rock intervals, either representing fluidal flows or sills. The upper coarse-grained sediments in this unit comprise alternating medium-grained sandstones and concordant augite to plagioclase-augite-phyric coherent rocks. The coherent intervals either represent fluidal flows or sills. These exposures are correlated with similar plagioclase-augite-phyric coherent rocks exposed in Gnat Creek. The fine- to coarse-grained stratified sedimentary rocks are overlain by volcanic breccias, and the entire sequence is cut by north-trending sub-vertical faults.

The Jurassic rocks in this area are age equivalent with both the Takwahoni formation and the Hazelton group. Marsden and Thorkelsen's (1992) definition for the Hazelton group includes all Lower to Middle Jurassic volcanic and related sedimentary rocks on Stikinia, including the basinal sedimentary equivalents of the volcanic successions, but excludes distal strata whose origin is generally unrelated to Hazelton volcanism. Following this definition, the entire succession exposed along the northern margin of the Hotailuh area is best assigned to the Hazelton group.

Eastern margin of the batholith

A second succession of Jurassic sediments is present near peaks 2102 and 2214 m (map 'h'). It had been previously correlated with the western succession and mapped as Lower Jurassic Takwahoni formation overthrust by Upper Triassic Stuhini Group rocks (Anderson, 1983; Gabrielse, 1998). The area around peak 2102 m at the eastern margin of the Hotailuh batholith comprises extensive exposures of reddish sedimentary rocks (map 'h', Figure 4), previously assigned to the Takwahoni formation (Gabrielse, 1998). The rocks comprise alternating medium to dark grey, parallel laminated siltstone, calcareous siltstone, fine- to medium-grained sandstone and rare, very thickly bedded, likely quartz-bearing, coarse-grained sandstone to granule-sized conglomerate (unit lJ Hs in Table 1). The fine-grained sedimentary rocks commonly contain a few percent disseminated and stratiform, very fine-grained (0.05 mm) pyrite and are commonly iron oxide-stained. A sedimentary – intrusive rock contact is exposed in the south-facing headwall of peak 2102 m (map 'h', Figure 4). Sedimentary rocks proximal to the margin of the adjacent Cake Hill intrusion exhibit contact metamorphism (see 'Structure and Metamorphism' section). Fossils collected from this area suggest an Early to possibly Middle Jurassic (Toarcian and possibly Bajocian) age for these rocks (Gabrielse, 1998, Appendix 2).

The exposures northeast of Lower Gnat Lake are part of a semi-continuous band of rocks previously assigned to the Triassic Stuhini group on the north and northeastern margin of the Hotailuh batholith (Figure 1; Anderson, 1983; Gabrielse, 1998). The volcanic rocks in the eastern part of the batholith (map 'h') are presumed to be the easternmost extension of this belt. On the lower southwest ridge of peak 2214 m, black-weathering, hornblende(?)-plagioclase-phyric pyroclastic breccia and volcaniclastic pebble-sized conglomerate (unit lmJ Hv in Table 1) stratigraphically overlie contact-metamorphosed, well-stratified fine-grained sedimentary rocks

similar to those exposed on peak 2102 m. No evidence for a thrust fault separating these two units could be found, and if the section is right-way-up, the volcanic rocks are likely Early to Middle Jurassic in age, comparable to the succession northeast of Lower Gnat Lake.

Similar to interpretations for the Jurassic rocks in the northwestern area, the basal Lower (-Middle) Jurassic sedimentary rocks may represent deposition related to the Hazelton group. Further work will need to address whether these rocks, and the entire band of volcanic and sedimentary rocks on the north and northeastern margin of the batholith, are part of the Hazelton group.

Intrusive rocks

Late Triassic plutonic suite

The Late Triassic plutons within the Cry Lake (104I) and Dease Lake (104J) 1:250,000 map sheets comprise the Stikine plutonic suite of Gabrielse (1998). Late Triassic plutonic rocks comprise about two-thirds of the Hotailuh batholith, and are exposed mainly in the west, northwest and southern part of the batholith (Figure 1). Here, we will only discuss the Late Triassic plutonic bodies within the main part of the Hotailuh batholith; namely the Cake Hill pluton, Beggerlay Creek pluton and Gnat Lakes ultramafite.

Gnat Lakes ultramafite

The Gnat Lakes ultramafite is a small 2.2 x 0.7 km body exposed both west and east of Highway 37, about three kilometres south of Upper Gnat Lake (Anderson, 1983; map 'a'). It has been described as an Alaskan-type ultramafic body based on the presence of hornblende clinopyroxenite, hornblendite and gabbro lithologies, minor zoning and distinctive whole-rock and mineral chemistry data (Nixon *et al.*, 1989, 1997). The body comprises clinopyroxene hornblende-rich gabbro and plagioclase-bearing ultramafite (predominantly hornblendite; unit LT GL). The cumulate-textured ultramafic rock types are characterized by a cumulus framework of touching hornblende and/or clinopyroxene crystals with intercumulus plagioclase (terminology following Irvine, 1982). The ultramafic body is locally brecciated by irregular coalescing hornblende-bearing dikelets of granodiorite, monzonite and diorite composition (Figure 5). These leucocratic phases (unit LT GLf in Table 1) have not been found outside of the Gnat Lake body, and are tentatively interpreted as cogenetic with the ultramafic body. Hornblende from the body has been dated by Zagorevski *et al.* (2011) as 223.2±2.0 Ma using the ^{40}Ar-^{39}Ar method.

Anderson (1983) interpreted the Cake Hill pluton to predate the Gnat Lakes ultramafite, based on observations southwest of Lower Gnat Lake along the abandoned railroad grade. He reports (p. 85): "Irregular, dun weathering apophyses of hornblende pyroxenite engulf sphene-bearing, well-foliated hornblende diorite and include rounded xenoliths of it." Upon revisiting these outcrops, we could not confirm these observations but found intimately mixed ultramafic and mafic rock types, both cut by a felsic dike of Cake Hill composition (Figure 6). The mafic rocks exposed at this location are foliated, clinopyroxene hornblende-rich gabbros, which both intrude and are intruded by plagioclase-bearing hornblendite. The mafic rocks are more hornblende and/or clinopyroxene-rich (40-60% mafic minerals) than typical Cake Hill. The felsic dike comprises foliated titanite-bearing hornblende diorite, and apart from the relatively low K-feldspar content (0-5% K-feldspar) appears similar to typical Cake Hill. Based on these observations we

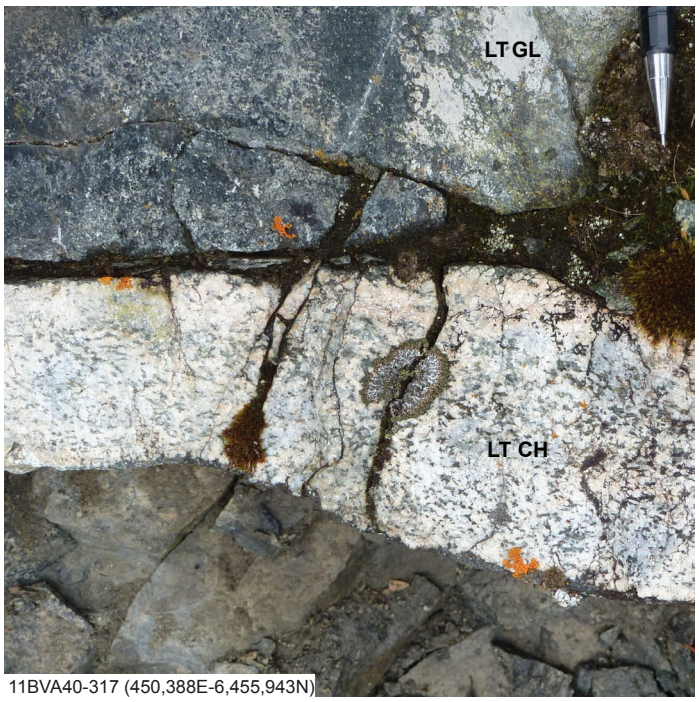

11BVA40-317 (450,388E-6,455,943N)

Figure 6: Titanite-bearing hornblende diorite dike (LT CH) intruding hornblende-rich gabbro to plagioclase-bearing hornblendite (LT GLm, LT GL). Pencil for scale.

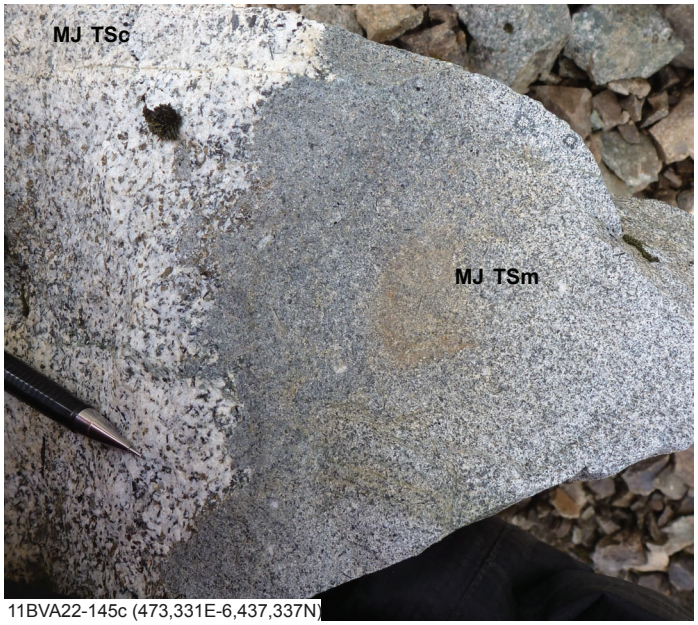

11BVA22-145c (473,331E-6,437,337N)

Figure 7: Irregular xenolith of acicular hornblende diorite (MJ TSm) within hornblende-biotite quartz-monzodiorite (MJ TSc). Note decrease in grain size within mafic xenolith from core to rim. Pencil for scale.

suggest that the Gnat Lakes body might predate the Cake Hill pluton.

A mineralogically similar, but non-foliated, clinopyroxene hornblende-rich gabbro body is exposed immediately east of the main Gnat Lakes ultramafic body. It also contains a decimetre-scale xenolith of ultramafic material similar to the Gnat Lakes ultramafic body. These relationships suggest a stronger genetic link between the mafic phases and the Gnat Lakes ultramafite than to the Cake Hill pluton. However, the non-foliated nature of this phase suggests it post-dates ductile shear zone development associated with intrusion of the Cake Hill pluton (see 'Structural geology and metamorphism' section) and conflicts with crosscutting relationships southwest of Lower Gnat Lake. It is unlikely that the non-foliated body is Middle Jurassic in age, since it does not contain any quartz, which is common in the hornblende-rich quartz-diorites of the mafic phase of the Three Sisters pluton. We have tentatively reassigned these rocks to a mafic subphase (LT GLm, see Table 1, map 'a') of the Gnat Lakes body. The mafic exposures located immediately east of the Gnat Lakes ultramafite and about 3 km south have been described as augite metagabbro by Read (1984) and Gabrielse (1998). To be consistent, these exposures have also been reassigned to the Gnat Lakes mafic subphase.

Cake Hill pluton

The Cake Hill pluton is the most areally extensive pluton of the Hotailuh batholith (Figure 1). The pluton is relatively homogeneous, xenolith-free, comprises equigranular hornblende quartz-monzodiorite to quartz-monzonite, and contains trace amounts of titanite (LT CH in Table 1). Generally, the Cake Hill can be distinguished from the Three Sisters central felsic phase by the presence of abundant tabular hornblende rather than biotite, presence of trace titanite, rare presence of a moderately developed fabric, and possibly also a lack of fine-grained dioritic xenoliths. A new U-Pb zircon crystallization age of 218.2 ±1.3 Ma and a new hornblende Ar-Ar cooling age of 220.5 ± 2.2 Ma from the southern part of the Cake Hill pluton determined by this study corroborates the 221±3 Ma age reported by Anderson and Bevier (1992).

A light-coloured, epidote-altered, hornblende quartz-monzodiorite, granodiorite, quartz-diorite to tonalite(?) phase occupies the southeast corner of the batholith (map 'g'). These rocks were mapped as the leucocratic phase of the Three Sisters by Anderson (1983, p. 287), and were reinterpreted as Cake Hill by Gabrielse (1998). The rocks contain tabular, epidote-altered hornblende, appear K-feldspar-poor in the field, and resemble the main Cake Hill pluton. In addition, the unit contains several irregular metre-scale domains of hornblende quartz-monzonite to quartz-monzodiorite containing tabular hornblende and trace titanite, characteristic of the Cake Hill pluton. We adopt Gabrielse's interpretation, and assign the leucocratic unit to the Cake Hill pluton (unit LT CHl in Table 1).

A foliated, finer-grained biotite(?)-hornblende diorite to quartz-diorite is present in the southeast of map 'd', and has been assigned to the Late Triassic Cake Hill pluton due to the presence of hornblende and its foliated nature (LT CHf in Table 1).

An intrusive body originally mapped as the Late Triassic Cake Hill pluton in the southeastern part of the study area (Anderson, 1983; Gabrielse, 1998; map 'h') is composed of massive, equigranular (3-4 mm) hornblende monzogranite and

granodiorite that are significantly more quartz-rich than typical Cake Hill, and contain minor but ubiquitous 4-7 mm quartz blebs. We report a new U-Pb zircon crystallization age of 216 ± 1.2 Ma for this intrusive body, and interpret the body as a more quartz-rich phase of the Cake Hill pluton (LT CHq).

The presence of a ~4 km wide WNW-ESE corridor of Cake Hill rocks connecting the south-easternmost exposures with the main pluton has not been confirmed during this study (cf. Figure 1, map 'e'), and remains to be tested. Several <1 km enclaves of hornblende quartz-monzodiorite to quartz-monzonite, presumed to represent Cake Hill, are hosted by the Three Sisters central felsic phase in the southeast (map 'g'). However, gradational contacts complicate distinguishing these domains from surrounding biotite-hornblende to hornblende-biotite quartz-monzodiorite and quartz-monzonite of the Three Sisters central felsic phase. Similar relationships are found in the north-central part of the batholith, where differentiating Cake Hill from the Three Sisters central felsic phase is problematic (map 'c'). In this area, rocks previously mapped as Three Sisters central felsic phase (Anderson *et al.*, 1982; Gabrielse, 1998) are reinterpreted as Cake Hill based on the presence of tabular hornblende and trace titanite. Some of the ambiguity in distinguishing the Cake Hill from the Three Sisters central felsic phase is likely due to the (partial to complete) assimilation of Cake Hill by the Three Sisters central felsic phase pluton.

The presence of Cake Hill rocks in the far southeast and eastern parts of the Hotailuh batholith suggests that this pluton occupied much of eastern half of the batholith before intrusion of the Three Sisters pluton.

Beggerlay Creek pluton

The Beggerlay Creek pluton is confined to the southern part of the Hotailuh batholith, and straddles the boundary between the NTS 104I and 104H map sheets north of the Stikine River. The pluton has been studied previously by Anderson (1983), Read and Psutka (1990), Gabrielse (1998) and Evenchick and Thorkelson (2005). We visited the pluton where it forms the southernmost part of the Hotailuh batholith (map 'f'). All but the southwestern exposures in this area are comprised of clinopyroxene-hornblende-rich gabbro (unit LT BC) with minor plagioclase-bearing clinopyroxenite domains (unit LT BCc). Exposures in the southwest comprise highly serpentinized ultramafic rocks, interpreted as websterite (unit LT BCw in Table 1). A thin section of this unit contains equal proportions of relatively fresh clinopyroxene and completely serpentinized pyroxene, the latter is interpreted to be preferentially altered orthopyroxene. The cumulate-textured ultramafic rock types are characterized by a cumulus framework of touching hornblende and/or clinopyroxene crystals with intercumulus plagioclase (BCc) or a cumulus framework of touching clinopyroxene and orthopyroxene (BCw; terminology following Irvine, 1982). From field observations the nature of the Beggerlay Creek – Cake Hill contact has been reinterpreted, and now includes all clinopyroxene-hornblende-rich gabbro up to an abrupt change (over a 10 m covered interval) to titanite-bearing, hornblende quartz-monzonite of the Cake Hill pluton (map 'f'; cf. Anderson, 1983, p. 84-85, p. 139-140, Appendix 2.3c). Clinopyroxene-hornblende-rich gabbro closest to the contact, now assigned to the Beggerlay Creek pluton, is intensely foliated roughly parallel to the trace of the contact.

Minor coarse K-feldspar ± epidote dikes (unit LT BCp) crosscut the northwestern portions of the Beggerlay Creek pluton, and may be related to a 5 x 1 km biotite metasyenite phase of the Beggerlay Creek pluton mapped about 7 km to the east (Read and Psutka, 1990). Coarse K-feldspar dikes, similar to those within the Beggerlay Creek pluton, also crosscut the augite-phyric coherent rocks of the Stuhini group near the contact with the mafic phases of the Beggerlay Creek intrusion.

Intrusive relationships between the Beggerlay Creek and Cake Hill plutons were not observed, however Anderson (1983, p. 84-85, Appendix 2.3c) reports that in two locations a gabbro dike of suspected Beggerlay Creek affinity intrudes quartz-monzodiorite of the Cake Hill. A new hornblende Ar-Ar date from a clinopyroxene-bearing hornblende-rich gabbro (map 'f') yielded a 210.9 ± 1.6 Ma cooling age. The hornblende in this sample is present within the groundmass and replaces clinopyroxene, clearly confirming that the Ar-Ar age is a minimum age.

Early Jurassic McBride River pluton

The McBride River pluton underlies an 8 x 20 km area at the easternmost margin of the Hotailuh batholith, dissected by the McBride River (Figure 1). The McBride River pluton was not visited during this study, but has been described as an equigranular hornblende-biotite granodiorite and quartz-monzodiorite containing abundant rounded quartz crystals (Anderson, 1983, p. 377). Anderson and Bevier (1992) established a 184 ± 8 Ma U-Pb zircon age for the pluton.

Middle Jurassic Three Sisters pluton

The Three Sisters pluton comprises about one-third of the Hotailuh batholith. It is predominantly exposed in the eastern half of the batholith and also forms a significant exposure around and west of Highway 37 (Figure 1). The Three Sisters pluton is internally heterogeneous, and has been subdivided into four separate phases by Gabrielse (1998). The four phases studied include the fine-grained mafic-intermediate phase, mafic phase, central felsic phase and potassic phase (Table 1).

Fine-grained mafic-intermediate phase

The Three Sisters fine-grained mafic-intermediate phase is restricted to an 8 x 2 km body in the southeast of the Hotailuh batholith (map 'g'); it also occurs as centimetre- to decimetre-sized xenoliths within parts of the Three Sisters central felsic phase. The fine-grained mafic-intermediate phase comprises massive, equigranular to sparsely plagioclase-porphyritic, hornblende-biotite quartz-diorite with a 1-1.5 mm crystal size. Hornblende tonalite dikes intrude the fine-grained mafic-intermediate phase. A new hornblende Ar-Ar cooling age of 173.2 ± 1.4 Ma was established in this study.

Mafic phase

The mafic phase comprises a volumetrically small portion of the Three Sisters pluton. Overall, it is fairly uniform compositionally, and comprises massive, equigranular, hornblende-rich quartz-diorite. Texturally, the rocks are varied, and contain either acicular hornblende or equant blebby hornblende, with both types exhibiting wide variations in crystal size (1-20 mm). The mafic phase occurs as small- to medium-sized (<1-2 km^2) bodies within the Three Sisters central felsic phase (map 'e'). The

central felsic phase intrudes into, as well as assimilates and includes fluidal fragments of the mafic phase. Furthermore, the fluidal domains of mafic phase within central felsic phase rocks often show a decrease in grain size towards the clast edge (Figure 7), interpreted as chilled margins. All evidence suggests that the two phases formed roughly at the same time. Similar mafic plutonic rocks crop out as several small (<0.5 km^2) bodies within the Cake Hill pluton close to the contact with the main Three Sisters pluton (map 'c', 'h'). Where the mafic phase is present within these older plutonic rocks, the latter are observed intruding, and often including, the mafic phase rocks. Anderson (1983, p. 86) reports similar observations at these locations, but also reports irregular mafic phase dikelets intruding Cake Hill, features interpreted to reflect remelting and remobilization of felsic rocks by intrusion of hot mafic melts. In the southeast (map 'e'), the mafic phase intrusions form subhorizontal tabular bodies confined to the highest ridge tops. In the north (map 'b'), a body several square kilometres in size forms the margin of the Three Sisters pluton. A new hornblende Ar-Ar cooling age of 171.9 ± 1.7 Ma was established for this phase.

Central felsic phase

The areally most extensive phase occupies the central portion of the Three Sisters pluton. It consists of massive, equigranular (2-3 mm) biotite and lesser hornblende-biotite quartz-monzonite and quartz-monzodiorite, locally with K-feldspar phenocrysts. In addition to the internal variation in composition and texture, the central felsic phase encloses several other intrusive phases. For example, an estimated 15 to 50% of the north-south traverses along ridges in maps 'e', 'g' and 'h' comprise either older (partly assimilated?) Cake Hill pluton, roughly coeval Three Sisters mafic phase, or crosscutting Three Sisters potassic phase. Notably, certain ridges that have been mapped by Anderson (1983) and Gabrielse (1998) as solely central felsic phase (north-south trending ridge in northwestern part of map 'e'), comprise substantial proportions of other rock types. The age of the central felsic phase was only constrained by K-Ar dates reported in the '70s and early '80s (see compilation in Anderson and Bevier, 1992). A U-Pb zircon crystallization age from a biotite quartz-monzonite exposed along the eastern margin of the Three Sisters pluton yielded a 169.0 ± 1.2 Ma age, identical to a biotite Ar-Ar cooling age of 169.0 ± 1.1 Ma obtained for the same sample (map 'h', this study).

Potassic phase

The Three Sisters potassic phase comprises massive, equigranular (1-4 mm crystal size) to locally K-feldspar porphyritic (5-20 mm crystal size), biotite to biotite-bearing, granite, quartz-syenite and quartz-monzonite. This phase occurs as a large body straddling Highway 37 that appears to be connected to the main part of the Three Sisters pluton through a relatively narrow (~1.5 km wide) corridor occupied by associated potassic phase rocks (Figure 1; Anderson, 1983; Gabrielse, 1998). Elsewhere, several medium sized bodies of the potassic phase form the margin of the Three Sisters pluton in the eastern half of the batholith. Several smaller potassic phase bodies crosscut the central felsic phase pluton, and immediately adjacent plutons (maps 'e', 'g', 'h').

A U-Pb zircon crystallization age of 169.1 ± 0.7 Ma (this study) is only slightly younger than a 171±1 Ma date by Anderson and Bevier (1992) for these coarse-grained intrusive rocks. Abundant fine-grained, pink, biotite-phyric dikes, likely related to the potassic phase, cut almost all adjacent plutonic and sedimentary rocks. The

potassic and central felsic phases are distinguished by more quartz, less biotite and more K-feldspar than plagioclase in the potassic phase. In places, the potassic phase can be difficult to distinguish from the central felsic phase. Some areas mapped previously as the potassic phase corridor (Figure 1; Anderson, 1983; Gabrielse, 1998) consist of massive, relatively fine-grained (1-2 mm crystal size), biotite quartz-diorite (maps 'd', 'e'). Further investigations are needed to fully characterize distinctions between these phases. The QUEST-NW geophysical survey (Aeroquest Airborne, 2012) indicates a complex aeromagnetic signature over the area between the BCR showing and newly discovered "BCR north" mineral occurrence (map 'a'). The high aeromagnetic response at BCR north coincides with a high magnetic susceptibility measurement on biotite-bearing hornblende syenite ($42 \cdot 10^{-3} \pm 15 \cdot 10^{-3}$ SI units), and appears to represent a different sub-phase of the Three Sisters potassic phase (unit MJ TSpm). The lower aeromagnetic response to the south coincides with more typical biotite-bearing granites (measured magnetic susceptibility of $21 \cdot 10^{-3} \pm 6.8 \cdot 10^{-3}$ SI units).

Other intrusive rocks

In addition to the plutonic rocks described above, several small intrusive bodies and numerous dikes are present throughout the study area. A mineralized intrusive body is the "Gnat Pass intrusive" (unit LT GP in Table 1). Where unaltered, it comprises plagioclase-phyric hypabyssal rocks (with sparse quartz and/or hornblende phenocrysts present in places). The intrusive occupies an area of ~0.1 km^2 in the "hill zone" (main zone) of the Gnat Pass mineral prospect (Smith and Garagan, 1990). A U-Pb zircon crystallization age from the Gnat Pass intrusive at the hill zone yielded a 216.4 ± 1.3 Ma age (this study), only slightly younger than the Late Triassic plutons in the area. Similar intrusive bodies and dikes 1-10 m in width, generally also associated with minor sulphides, are found along Gnat Creek downstream of Lower Gnat Lake ("creek zone" of the Gnat Pass prospect) as well as along Highway 37 north of Lower Gnat Lake. In all areas, the intrusive rocks cut Triassic Stuhini group augite-phyric coherent rocks. Interestingly, Asbury (1967) reports a 0.5 x 1 km-size granodiorite intrusion approximately 3.5 km northwest of Lower Gnat Lake. The body is described as "... a medium-grained, granular rock containing grey to pink plagioclase, an estimated 15% free quartz and 1% to 2% mafic minerals." This body is not shown on the regional geological map of Gabrielse (1998), and warrants additional study to determine its spatial extent and possible association with mineralization. In addition, possible cogenetic Fe-carbonate-altered rhyodacite dikes that postdate all other units and are typically associated with sulphide mineralization are reported at the Dalvenie showing (Wetherill, 1990, p.13).

A small intrusion located further south of Gnat Pass is tentatively named the "Tees Creek intrusive". This altered hornblende-feldspar porphyry is exposed along the abandoned railroad about 1.5-3.5 km south of the Gnat Lakes ultramafite; it also occurs as irregular dikes intruding the coarse-grained potassic phase of the Three Sisters pluton. The intrusive is associated with minor pyrite at the "BCR north" mineral occurrence.

Abundant subvertical north to northeast striking 8-10 m wide augite-plagioclase-porphyritic, augite hornblende-rich diabase dikes cut the Cake Hill pluton in the centre of the Hotailuh batholith (map 'd'). Their petrological, geochemical (see

'Lithogeochemistry' section) characteristics and crosscutting relationships suggest that these hypabyssal dikes are most likely subvolcanic feeders to the Middle Jurassic Hazelton Group volcanics.

STRUCTURAL GEOLOGY AND METAMORPHISM

Whereas the Hotailuh batholith appears to be mostly unaffected by post-intrusion contractional deformation, most surrounding sedimentary and volcanic rocks have been deformed. The area north of the Hotailuh batholith comprises predominantly moderately north-dipping strata, ascribed to result from south-directed thrusting along the King Salmon and Hotailuh faults (Gabrielse, 1998). The Gnat Pass area appears to be a major structural zone with evidence for several north-northeast- to north-northwest-striking ductile to brittle fault zone localized along part of the western margin of the Cake Hill pluton. Faulting and folding is common in Triassic sedimentary and volcanic rocks east of this fault zone (Read, 1984; Gabrielse, 1998). The structural style in the area south and east of the batholith is poorly understood. Two regional-scale faults inferred along the Stikine River include the Beggerlay Rapids and Pitman faults (Evenchick and Thorkelson, 2005).

Anderson (1983, p. 67-76) and Gabrielse (1998, p. 64) described the Cake Hill pluton as pervasively or well-foliated. However, we found the fabric within the Cake Hill pluton to be only moderately-developed to absent, except in a north-northwest-striking zone in the Gnat Pass area where it is well-developed. The fabric is defined by alignment of tabular hornblende crystals. Although moderately aligned hornblende is regularly observed in outcrop within the main part of Cake Hill pluton, it is commonly inconsistent over the metre scale. Where present, the orientation of the foliation measured herein is generally similar to the NW-SE striking, sub-vertical orientations reported by Anderson (1983). Except within the Gnat Pass zone (see below), the foliation is likely magmatic in origin.

Gnat Pass fault zone

The Gnat Pass fault has been described as a 25 km long, north-northwest striking, possible dextral strike-slip to east-side-down dip-slip, fault (Gabrielse, 1998, p. 94). According to this author the fault is cut on its southern end by the Three Sisters pluton, occurs on (or near) the western margin of the Cake Hill pluton in the Gnat Pass area, terminates the Hotailuh thrust northwest of Lower Gnat Lake, and is terminated by the King Salmon thrust fault near Dease Lake (Figure 1).

An outcrop immediately south of Upper Gnat Lake shows intensely foliated felsic intrusive rocks containing relict 3-5 mm euhedral augite-crystal porphyroclasts. Augite-phyric coherent rocks up to 250 m east of this location, as well as granitoid rocks of the Cake Hill pluton up to 250 m west of this location, are intensely foliated. Foliation orientations in all rock types are sub-vertical and strike approximately north-northwest. The foliation in the Stuhini Group augite-phyric coherent rocks comprises newly formed chlorite wrapped around relict augite phenocrysts, indicating greenschist facies metamorphic conditions. In the Cake Hill pluton, the foliation is defined by alignment of tabular hornblende that is macro- and microscopically indistinguishable from magmatic hornblende. Outcrops of intensely foliated Stuhini Group and Cake Hill pluton lithologies are found in a up to 1 km wide, generally north-northwest trending zone

coincident with the approximate western edge of the Cake Hill pluton (map 'a'). Based on these observations, we infer the presence of a north-northwest-striking, sub-vertical, ductile shear zone, roughly situated on the western margin of the Cake Hill pluton. Syn-intrusion shear would explain the relatively narrow band of foliated and metamorphosed country rocks, as well as the presence of a well-developed fabric formed by igneous hornblende in the pluton. The north-northwest-striking belt of foliated rocks continues at least 3 km to the north and 5 km to the south where it appears to be cut by undeformed plutonic rocks of the Three Sisters potassic phase.

A sub-vertical north-northwest striking brittle fault is exposed in a 2 m wide recessive zone in an exposure along the abandoned railroad (map 'a'). The fault separates intensely foliated augite-phyric coherent rocks on the east wall of the fault, with unmetamorphosed, non-foliated, sedimentary rocks on the west wall. Folation in the augite-phyric coherent rocks as well as bedding attitudes in the sedimentary rocks are roughly parallel to the brittle fault. This fault has been interpreted by Gabrielse (1998) as the main Gnat Pass fault.

Several north-northwest trending aeromagnetic lineaments are evident within the Gnat Pass area (Aeroquest Airborne, 2012). All major geophysical lineaments are interpreted here as brittle faults (see map 'a'). An induced polarization survey carried out by Bearclaw Capital Corp. in 2005 (Page and Scott, 2006) indicates a significant north to north-northwest striking sub-vertical resistivity low (< 500 Ωm) between the creek and hill zones of the Gnat Pass prospect. The Gnat Pass shear zone does not show up as a geophysical lineament on the aeromagnetic survey, likely due to the lack of magnetite-destructive alteration associated with the shear zone. The Gnat Pass shear zone could not be traced beyond the northern margin of the Gnat Lakes mafic phase. This clinopyroxene hornblende-rich gabbro body is not foliated and may post-date formation of the Gnat Pass shear zone.

We interpret the Gnat Pass structural zone as an up to 1 km wide, >10 km long ductile shear zone developed on the western margin of the Cake Hill pluton during Late Triassic time. The ductile shear zone became the locus of brittle faulting during subsequent cooling and/or exhumation. The brittle fault exposed along the abandoned railroad that separates foliated and metamorphosed rocks from non-foliated and unmetamorphosed rocks likely represents such a subsidiary brittle fault. The geophysical lineaments at Upper Gnat Creek, Tees Creek, and at the Gnat Pass showing most likely represent major brittle faults related to the Gnat Pass structural zone.

Hotailuh thrust fault

An exposure of the Hotailuh thrust could not be found during current mapping between Highway 37 and peak 2096 m (map 'a'). Reported evidence for the fault is the presence of presumed Triassic Stuhini rocks overlying Early Jurassic fossil-bearing siliciclastic sedimentary rocks assigned to the Takwahoni formation (Anderson, 1983; Gabrielse, 1998). However, detrital zircon results (Iverson *et al.*, 2012; Iverson, 2012) suggest a Middle Jurassic or younger age for the overlying package, leaving no requirement for the presence of a thrust fault in this particular location. A seismic reflector interpreted as the Hotailuh thrust fault by Evenchick *et al.* (2005) may just represent the change from Triassic Stuhini and Cake Hill to Jurassic volcanic and sedimentary rock types.

On the eastern margin of the batholith (map 'h'), the Hotailuh thrust has been inferred within steep and largely inaccessible topography surrounding peak 2214 m (Anderson, 1983; Gabrielse, 1998). Study of the lower southwest ridge of peak 2214 m found no evidence for a thrust fault, and if the section is right-way-up, the volcanic rocks previously assigned to the Triassic Stuhini group may be Early to Middle Jurassic in age, comparable to the succession further west that yielded Jurassic detrital zircon populations.

Other structures and metamorphism

The succession of Middle Jurassic sedimentary and volcanic rocks around peak 2096 m is cut by several north-northeast- to north-northwest-trending, sub-vertical faults with stratigraphic offset suggesting a dextral strike-slip and/or east-side-down dip-slip motion. Another important structure is the Dalvenie fault, which hosts the Dalvenie copper-gold-silver prospect (map 'a'). Many roughly parallel topographic lineaments, aeromagnetic lineaments and/or possible faults are present in the immediate area (selected lineaments shown on the 1:50,000 scale map).

At the eastern margin of the Hotailuh batholith, sedimentary rocks with Early (to Middle?) Jurassic fossils (Gabrielse, 1998) exhibit contact-metamorphism adjacent to the 216 Ma hornblende monzogranite to granodiorite of the Cake Hill pluton (map 'h'). Several skarn bodies comprising brown garnet, dark green diopside and/or white fibrous wollastonite occur within about 50 m of the contact with the intrusive, and represent contact-metamorphosed calcareous, fine-grained sedimentary rocks. Three irregular altered felsic intrusive dikes cut the sedimentary rocks. Based on the biostratigraphic and geochronological constraints, the intrusive to sedimentary contact represents a nonconformity or a fault. We tentatively interpret the calcic exoskarn development to be due to increased fluid flow along the permeable (nonconformable or fault) contact and injection of dikes accompanying intrusion of the nearby Middle Jurassic Three Sisters pluton.

Mafic intrusive rocks of the Beggerlay Creek pluton are intensely foliated in a 500-750 m wide zone adjacent to the Cake Hill contact (map 'f'). The steeply dipping, east- to east-northeast-striking foliation is defined by elongated hornblende and plagioclase, imparting an almost gneissic compositional banding in places.

LITHOGEOCHEMISTRY

Analytical Techniques

A total of 46 least altered lithogeochemical samples were collected from nine different plutonic phases and one mafic dike. The samples were jaw crushed at the Geological Survey sample preparation facilities in Victoria. The crushed samples were further processed at Activation Laboratories in Ancaster (Ontario), pulverized in a mild steel mill to prevent Cr and Ni contamination and analyzed for major and trace elements using a lithium metaborate plus lithium tetraborate fusion technique. At Activation Laboratories, the samples were mixed with a flux of lithium metaborate and lithium tetraborate and fused in an induction furnace at 1150 °C. The melt was immediately poured into a solution of 5% nitric acid, and mixed continuously until completely dissolved. This aggressive fusion technique ensures that the entire sample, including resistate phases, dissolves. The samples were analyzed for major oxides

using an Inductively Coupled Plasma (ICP) technique and trace elements using an Inductively Coupled Plasma – Mass Spectrometry (ICP-MS) technique. Nickel was also analyzed by four acid digestion; beginning with hydrofluoric acid, followed by a mixture of nitric and perchloric acid, and final hydrochloric acid dissolution. Samples were analyzed using an ICP technique. With this near total digestion technique, certain resistate phases (e.g. zircon, monazite, sphene, gahnite, chromite, cassiterite, rutile and barite) may be only partly solubilized. Chromium was analyzed using Instrumental Neutron Activation Analysis (INAA), where samples were irradiated in a nuclear reactor, and following a 7-day decay, gamma rays measured on germanium detectors. Analytical techniques and detection limits for all major oxides and trace elements are listed in Appendix 2. Two blind CANMET standards (see Govindaraju, 1994 for reference values) and two blind duplicates of the jaw crushed material were included in the sample batch (see Appendix 3). Additional Activation Labs' internal quality control duplicate analyses on powdered samples are also listed in Appendix 3.

During sample collection and preparation every effort was taken to avoid sampling altered material. We avoided and/or removed any obvious surface weathering, altered areas, veins and open space fill. A summary of the rock type and intensity of alteration of feldspars and mafic minerals for all lithogeochemistry samples are presented in Appendix 1. Geochemical results presented in Appendix 2 show normal total weight percent values (between 97.5 and 101 wt.%) and loss on ignition values (below 2 wt.%).

Results

Major oxide diagrams (Figure 8a-c) indicate that the bulk of the samples plot within the metaluminous to weakly peraluminous calc-alkaline (subalkaline) fields. A small number of samples fall within the alkaline field (Figure 8a). The latter samples likely do not represent original melt compositions, possibly due to crystal addition (phenocrysts accumulation, cumulate origin) and/or minor alteration. The Gnat Lakes and some of the Beggerlay Creek samples are unusually clinopyroxene and/or hornblende-rich (and SiO_2-poor) due to their cumulate origin, which causes them to plot within the alkaline field. All samples define a good calc-alkaline trend on an AFM diagram (Figure 8c), with a clear trend from alkali-poor primitive ultramafic to mafic suites to alkali-enriched intermediate to felsic suites. All intermediate to felsic plutonic rocks plot within the Island Arc Granite (IAG) to Continental Arc Granite (CAG) fields of Maniar and Piccoli (1989). The Middle Jurassic plutonic rocks tend to have a slightly higher Aluminum Saturation Index (ASI, Figure 8b) compared to Late Triassic rocks. Most samples are metaluminous in nature, whereas the Three Sisters potassic phase is weakly peraluminous. Lithogeochemical analyses from the latter phase are corundum normative (based on the CIPW norm, Hutchinson, 1974), indicating that the samples contain more aluminum than can be accommodated in feldspars. This agrees well with petrological observations that show biotite as the dominant mafic phase in these rocks. Trace element tectonic discrimination diagrams of Pearce *et al.* (1984) indicate a Volcanic Arc Granite (VAG; Figure 8d) affinity for all but one or two rock samples. The Pearce *et al.* (1984) trace element plot and Frost *et al.* (2001) ASI classification plot, suggests a subduction-related origin for the magmas

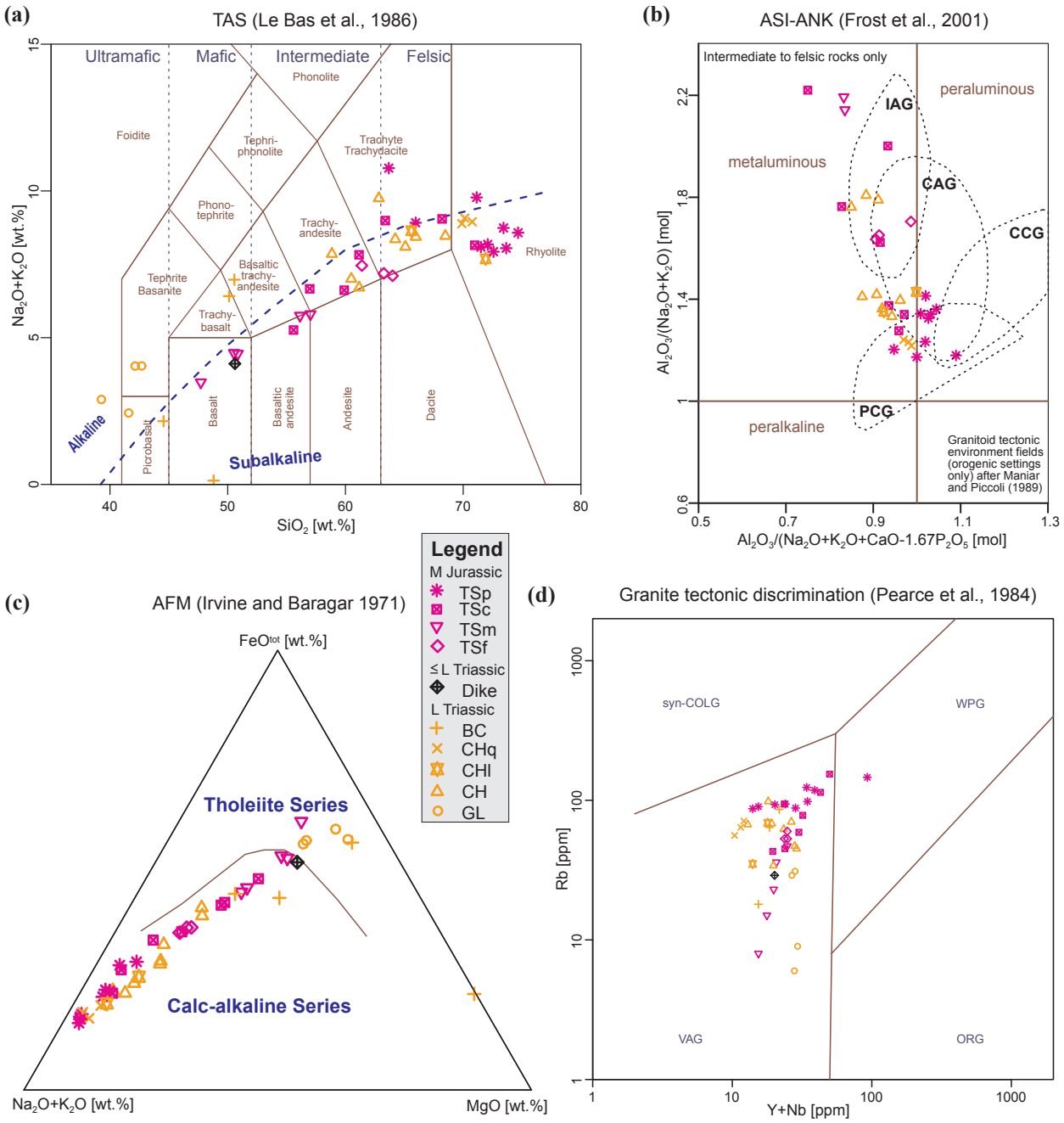

Figure 8: Major and trace element diagrams for different plutonic phases of the Hotailuh batholith. (a) Total Alkali vs. Silica diagram of Le Bas et al. (1986). (b) Aluminum Saturation Index vs. $Al_2O_3/(Na_2O + K_2O)$ diagram of Frost et al. (2001) with granitoid tectonic fields after Maniar and Piccoli (1989). IAG = Island Arc Granite, CAG = Continental Arc Granite, CCG = Continental Collision Granite, PCG = Post-Collision Granite. (c) Alkali – Iron –Magnesium oxide plot of Irvine and Baragar (1971). (d) Y+Nb vs. Rb trace element granite tectonic discrimination plot of Pearce et al. (1984). VAG = Volcanic Arc Granites, ORG = Ocean Ridge Granites, WPG = Within Plate Granites, syn-COLG = syn-Collision Granites.

that formed the Hotailuh batholith. Lastly, the presence of trace magnetite in most rocks and magnetic susceptibility values above ~$3.0 \cdot 10^{-3}$ SI (see 'Geological units' section) indicate that the plutonic rocks are part of the relatively oxidized magnetite-series granitoids of Ishihara (1977; 1981) and Ishihara *et al.* (2000).

The Rare Earth Element (REE) and trace element concentration within the different plutonic suites supports the field and petrographic separation of different intrusive phases (Figure 9, Figure 10). The Gnat Lakes ultramafite has a flat La-Nd Light Rare Earth Element (LREE) pattern, which is distinctly different from other ultramafic-mafic-intermediate intrusive phases within the Hotailuh batholith (Figure 9a). The Late Triassic Beggerlay Creek pluton, the Middle Jurassic Three Sisters mafic and fine grained mafic-intermediate phases have broadly similar REE patterns with an increase in REE abundance towards more silicic compositions. The serpentinized websterite (LT BCw) has a flat to slightly irregular REE pattern with very low REE concentrations (Figure 9a). The REE concentration and negative LREE slope increase from plagioclase-bearing clinopyroxenites (LT BCc) to hornblende-clinopyroxene and clinopyroxene-hornblende gabbro (LT BC). There is also an increase in the negative LREE slope from the mafic phase to fine grained mafic-intermediate phase. The augite-plagioclase basalt dike that cuts the Cake Hill pluton has a similar REE pattern and concentrations as samples from the mafic Beggerlay Creek pluton and the Three Sisters mafic phase and fine grained mafic/intermediate phase. The Late Triassic Cake Hill felsic phases (LT CH, CHl, CHq) and Middle Jurassic Three Sisters central felsic (MJ TSc) and potassic phases (MJ TSp) have overlapping REE concentrations and broadly similar REE patterns (Figure 9b, c). The Late Triassic Cake Hill quartz-rich phase (LT CHq) is depleted in REE relative to the main Cake Hill pluton (LT CH). The Cake Hill leucocratic phase (LT CHl) shows overlapping, but slightly depleted REE concentrations relative to the main Cake Hill pluton (Figure 9b). The Middle Jurassic Three Sisters central felsic and potassic phases (MJ TSc, TSp) show overlapping REE patterns and moderately negative Eu anomalies (Figure 9d). This indicates that the melt was at one time in equilibrium with now-absent plagioclase, either at the source, or due to removal of plagioclase phenocrysts from the melt. The potassic phase shows steeper negative LREE slopes, and overlapping to lower Heavy Rare Earth Element (HREE) concentrations, relative to the central felsic phase (Figure 9d). One sample from the potassic phase in the Gnat Pass area is highly anomalous and shows very high REE concentrations indicative of a late-stage, incompatible element-enriched melt (Figure 9d). The outcrop also returned much higher magnetic susceptibility readings than measurements on the Three Sisters potassic phase further east, and is associated with a zone of a much higher airborne magnetic response interpreted as a subphase of the potassic phase (MJ TSpm). In addition, a second sample from the potassic phase in the Gnat Pass area has a steeper negative LREE slope than any of the other samples. Relative to N-type Mid Ocean Ridge Basalt (N-MORB), the rock types are all enriched in LREE and contain similar to depleted HREE concentrations (Figure 9e). The HREE pattern suggests that the mantle source for these rocks was similar to, or more depleted than, a typical MORB mantle source region.

Multi-element N-MORB normalized diagrams modelled after Sun and McDonough (1989) are shown in Figure 10.

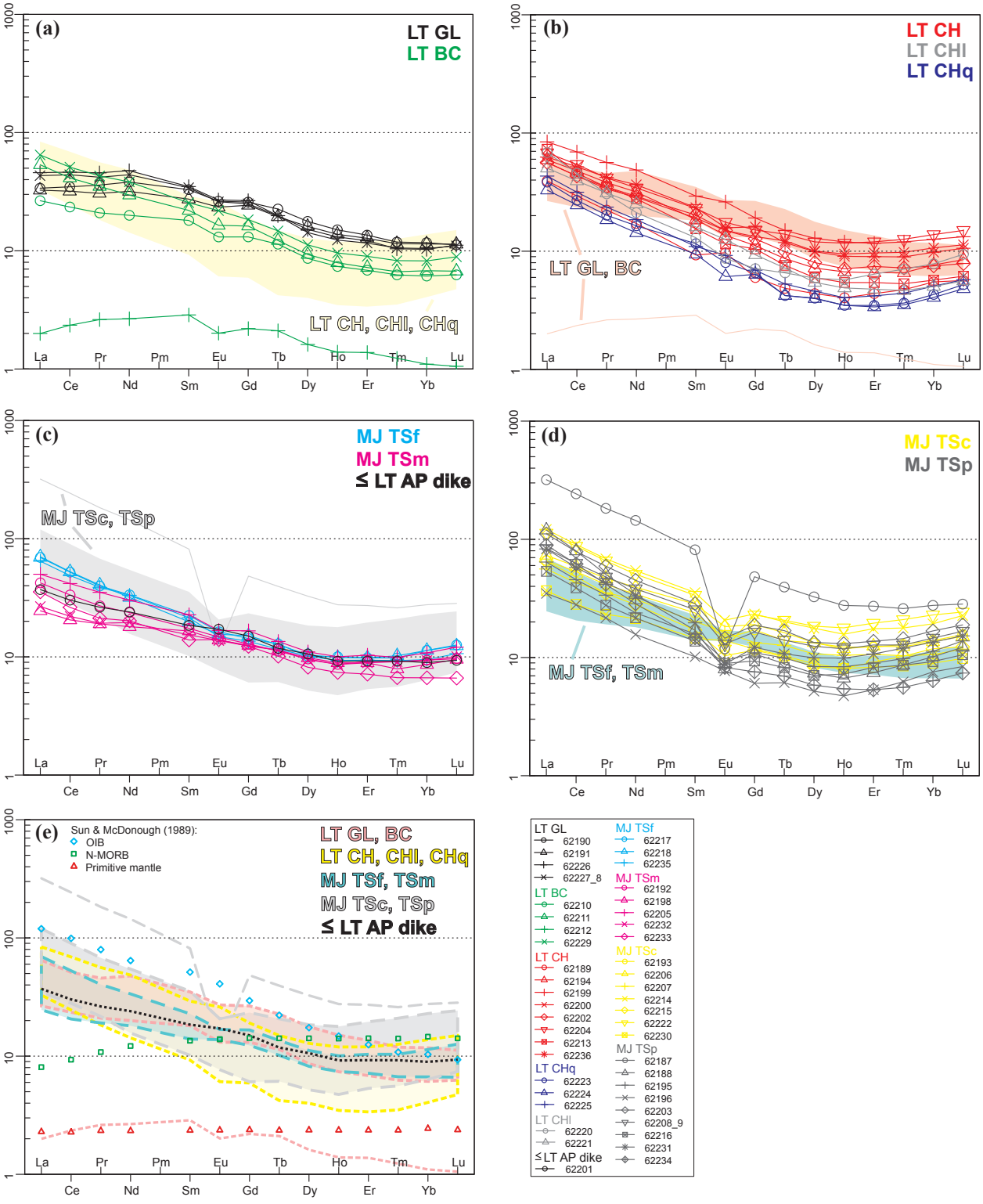

Figure 9: Chrondrite normalized rare earth element diagram for ultramafic-mafic-intermediate (a,c) and intermediate-felsic (b,d) suites of the Late Triassic (LT) and Middle Jurassic (MJ) plutonic suites within the Hotailuh batholith. Normalization values of Boynton (1984). Ocean Island Basalt (OIB), N-type Mid-Ocean Ridge Basalt (N-MORB) and Primitive Mantle values of Sun and McDonough (1989) plotted for reference in diagram (e).

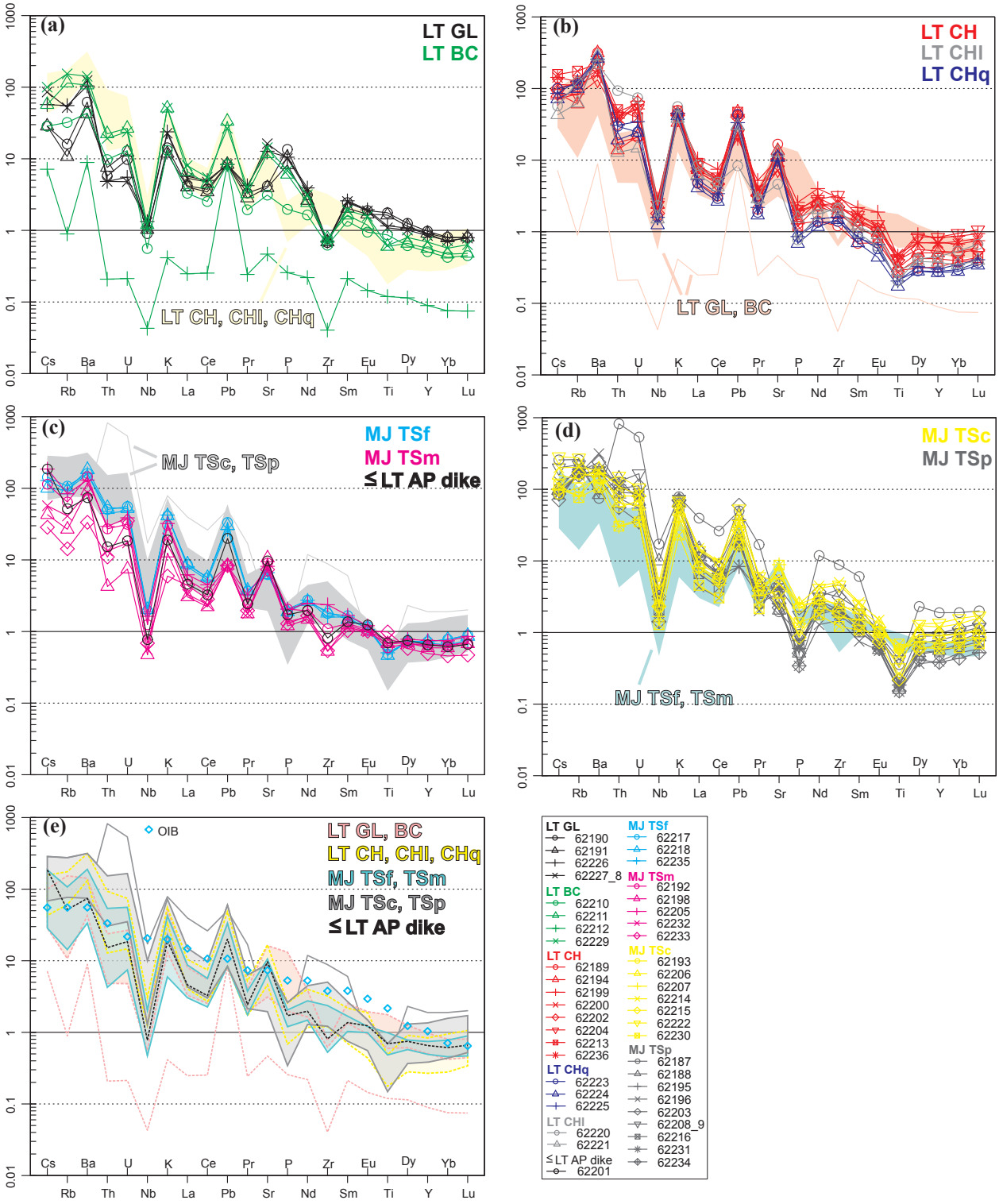

Figure 10: N-MORB normalized multi-element diagram for ultramafic-mafic-intermediate (a,c) and intermediate-felsic (b,d) suites of the Late Triassic (LT) and Middle Jurassic (MJ) plutonic suites within the Hotailuh batholith. Normalization and ordering scheme of Sun and McDonough (1989). Ocean Island Basalt (OIB) values of Sun and McDonough (1989) plotted for reference in diagram (e).

The elements in the diagram are organized by increasing compatibility towards the right, as shown by typical Ocean Island Basalt (OIB) concentrations (Figure 10e). Notable diversions from a negative sloping trend in Figure 10 include a strong depletion in Nb (a High Field Strength Element; HFSE), and a strong enrichment in hydrous fluid-mobile Large Ion Lithophile Elements (LILE) such as K and Pb. These patterns are typical of subduction-generated magmas where LILE-enriched aqueous fluids derived from dehydration reactions within the down-going slab induce partial melting in the overlying mantle wedge.

GEOCHRONOLOGY

In this study we used modern radiogenenic isotopic dating techniques to determine the ages of seven different plutons and plutonic phases that comprise the Hotailuh Batholith, as well as one porphyritic hypabyssal intrusion associated with copper mineralization at Gnat Pass. Historical dating of the Hotailuh batholith (Wanless *et al.*, 1972; Stevens *et al.*, 1982) does not reliably constrain crystallization ages or provide adequate coverage of the 2,275 km^2 area of the batholith.

Five intermediate to felsic intrusive rocks were processed for zircons and subsequently analyzed for U-Pb using a Laser Ablation Inductively Coupled Mass Spectrometer (LA-ICP-MS) at the University of Washington. The U-Pb results presented here supersede preliminary ages presented in van Straaten *et al.* (2012a, b). In addition, five mafic to intermediate intrusive rocks were processed for hornblende and/or biotite mineral separation, subsequently irradiated and analyzed using the $^{40}Ar/^{39}Ar$ method method at the Pacific Centre for Isotopic and Geochemical Research, University of British Columbia. Detailed methodologies are described in Appendix 4.

Previous geochronological studies (Wanless *et al.*, 1972; Anderson *et al.*, 1982; Stevens *et al.*, 1982; Anderson and Bevier, 1992) included 29 K-Ar hornblende, biotite and whole rock age dates and three U-Pb zircon dates to estimate the ages of the major plutonic suites within the Hotailuh batholith. More recently Ar-Ar dating on hornblende from the Gnat Lakes ultramafite established a minimum cooling age of 223.2±2.0 Ma for this body (Zagorevski *et al.*, 2011).

Results

All samples analyzed are summarized in Table 2, and shown in detail in Figure 11. Complete datasets are presented in Appendices 5 and 6.

Of the five zircon U-Pb LA-ICP-MS analyses, none suggests the presence of any significant inherited age populations, and only one sample is interpreted to contain a significant number of grains affected by lead loss (Figure 11a-e). Data points were excluded from the U-Pb age determinations based on 1) large degree of discordance in a conventional Tera-Wasserburg diagram (isotopic ratios not corrected for common lead), 2) large 2 standard deviation (SD) errors in the $^{206}Pb/^{238}U$ age, and 3) $^{206}Pb/^{238}U$ age values suggesting the data points are outliers with respect to the main population of data points, i.e. data points that plot away from the cumulative relative probability peak. The interpretation of most samples is straightforward; for sample 11BVA31-232 no data points were excluded, and for samples 11BVA38-304 and 11BVA42-333 only 3-4 outliers were excluded for each sample. Inclusion of these grains does not significantly alter the final age determinations. Sample 11JLO32-319 contains a small population (n=3) of older

Table 2: Summary of zircon U-Pb and hornblende/biotite Ar-Ar geochronology samples taken from the Hotailuh batholith.

Sample no.	Type	UTM E	UTM N	Unit	Rock description	Age (Ma)*	Population	Statistics
11BVA31-232	U/Pb, Zrn	478,755	6,434,626	MJ TSp	Hbl-bearing Bt monzogranite	169.1±0.8	50/50 grains	MSWD=0.93, p=0.62
11BVA35-276	Ar/Ar, Bt	480,640	6,439,273	MJ TSc	Hbl-bearing Bt Qtz-monzonite to monzogranite	169.0±1.1	13/25 steps, 54.7% of ^{39}Ar	MSWD=1.12, p=0.34
11BVA35-276	U/Pb, Zrn	,,	,,	,,	,,	169.0±1.3	29/49 grains	MSWD=0.64, p=0.93
11BVA42-329	Ar/Ar, Hbl	466,997	6,448,398	MJ TSm	Acicular Hbl-rich Qtz-diorite	171.9±1.7	6/11 steps, 81.6% of ^{39}Ar	MSWD=1.13, p=0.34
11BVA42-332	Ar/Ar, Hbl	479,794	6,436,014	MJ TSf	Fine grained Hbl-Bt Qtz-diorite	173.2±1.4	4/12 steps, 54.2% of ^{39}Ar	MSWD=0.114, p=0.95
11BVA27-199	Ar/Ar, Hbl	462,983	6,427,463	LT BC	Cpx-bearing Hbl-rich gabbro	210.9±1.6	5/17 steps, 53.3% of ^{39}Ar	MSWD=1.16, p=0.32
11JLO32-319 (DDH G-89-8 55.47-60.05 m)	U/Pb, Zrn	451,832	6,457,090	LT GP	Plag-porphyritic hypabyssal intrusion	216.5±1.4	44/49 grains	MSWD=0.78, p=0.85
11BVA38-304	U/Pb, Zrn	481,362	6,439,991	LT CHq	Hbl-bearing granodiorite to monzogranite	216.2±1.2	45/49 grains	MSWD=0.73, p=0.90
11BVA42-333	Ar/Ar, Hbl	463,692	6,431,161	LT CH	Hbl Qtz-monzonite	220.5±2.2	6/9 steps, 94.2% of ^{39}Ar	MSWD=1.20, p=0.31
11BVA42-333	U/Pb, Zrn	,,	,,	,,	,,	218.2±1.3	47/50 grains	MSWD=0.76, p=0.88

* Crystalization age for U-Pb zircon analyses. Cooling age (plateau age) for Ar-Ar analyses. 2 SD error

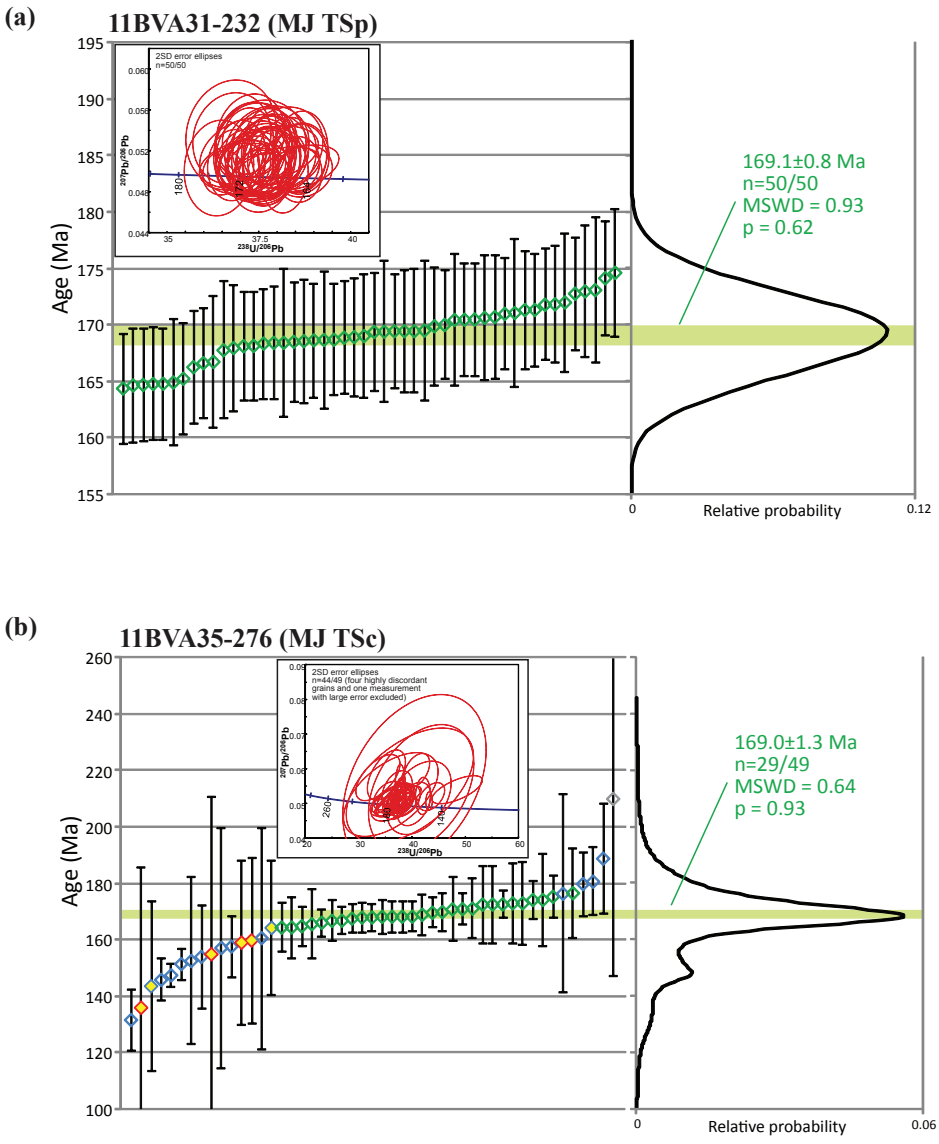

Figure 11: Geochronology plots for samples from the Hotailuh batholith. Graphs (a-e) show U-Pb zircon LA-ICP-MS ages, cumulative relative probability plots and Tera-Wasserburg diagrams (inset). Plotted values are $^{206}Pb/^{238}U$ ages, except for yellow data points in samples 11BVA-35-276 and 11JLO32-319 which are common lead-corrected ages. Data points in red, grey and blue are excluded from the age determination based on a high degree of discordance, high error, or outlier nature (respectively). Green data points are included. Error bars represent 2 standard deviations. Graphs (f-j) show Ar-Ar plateau ages for biotite or hornblende crystals. Red heating steps are excluded and green heating steps are included in the age determination. Errors are reported at 2 standard deviations.

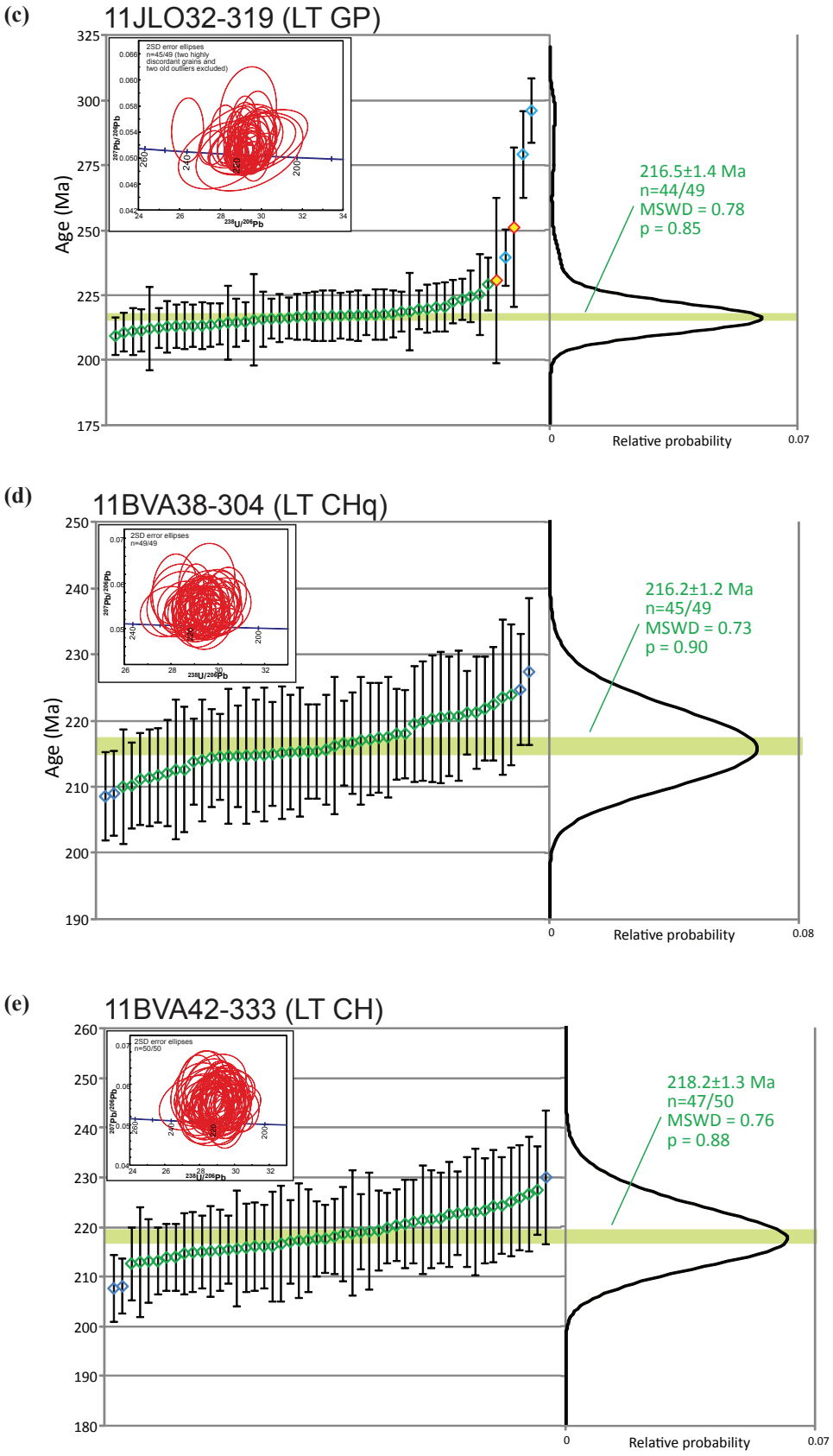

Figure 11: (cont.)

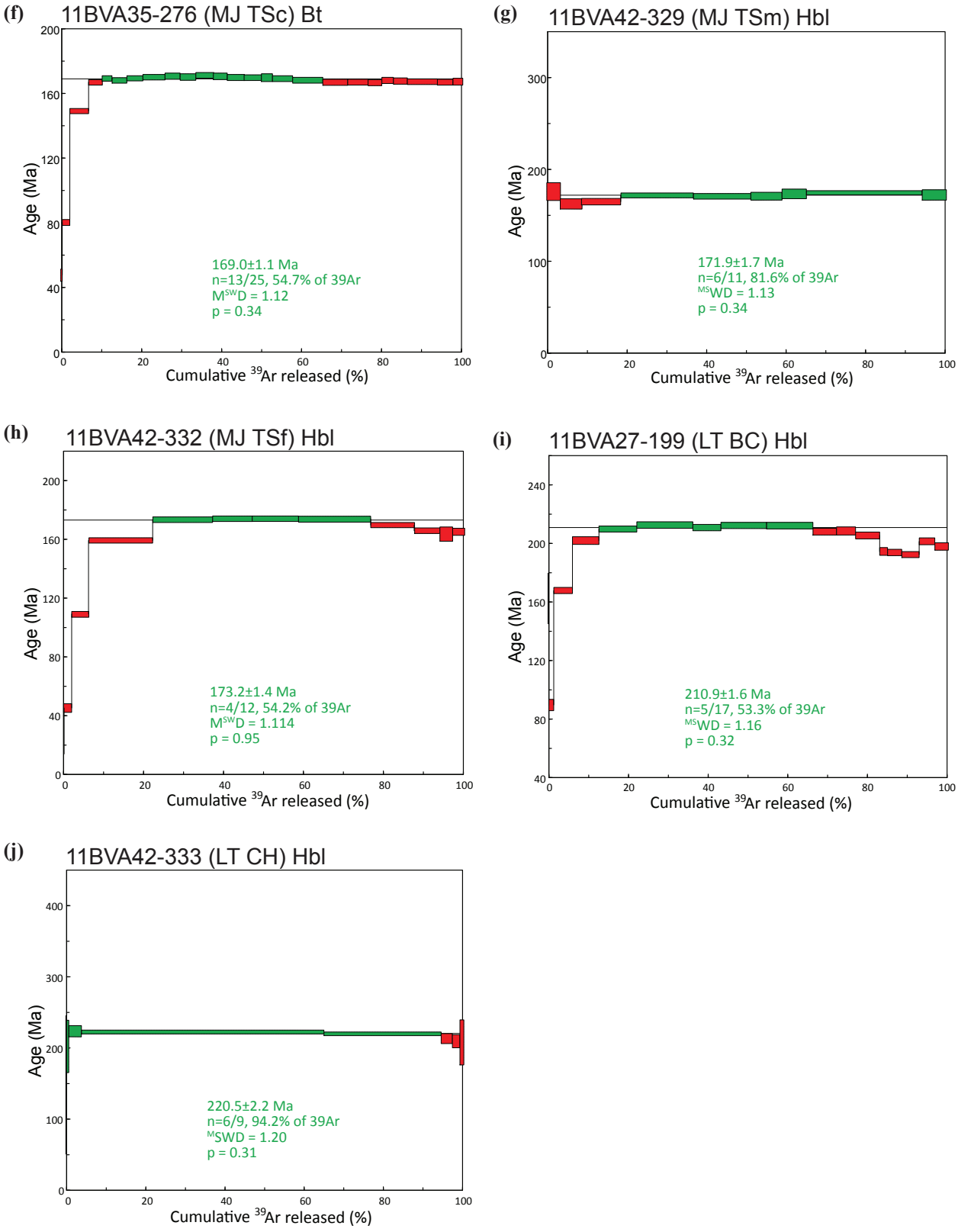

Figure 11: (cont.)

grains interpreted to be inherited from Paleozoic basement rocks, as well as two discordant grains. Sample 11BVA25-276 is complex in nature. The 15 youngest grains have been excluded from the age determination, based on their moderately to highly discordant nature (when not corrected for common lead) and relatively high 2SD errors. The sample contains a relatively robust population of 29 grains with $^{296}Pb/^{238}U$ ages ranging from 164 to 177 Ma. The mean of 169.0 (±1.3) Ma coincides with the main cumulative relative probability function peak, suggesting this represents the crystallization age of this sample. This age is within error of the biotite Ar-Ar age (Figure 11f) from the same sample. This sample would benefit from a follow-up study to determine the validity of the Middle Jurassic age. If the age is correct, it is unclear why about one third of the zircon grains were affected by lead loss, whereas the biotite Ar-Ar cooling age remained unaffected.

One biotite Ar-Ar and four hornblende Ar-Ar cooling ages are shown in Figure 11f-j. Plateau ages are based on 4 to 13 heating steps, and 53 to 94% of released ^{39}Ar.

Sample 11BVA42-333 was analyzed using both U-Pb and Ar-Ar, and the results are the same age within error. Note however, that the cooling age is 2.3 Myr older than the crystallization age. Sample 11BVA35-276 was also analyzed using both U-Pb and Ar-Ar, and has been discussed above. Statistical parameters show no reason for rejection of the U-Pb or Ar-Ar age data (Table 2), with Mean Squared Weighted Deviation (MSWD) values below $1+2(2/(n-1))^{0.5}$ (with n = number of data points; Wendt and Carl, 1991) and Probability (P) values well above 0.05.

MINERALIZATION

Five mineralized prospects and showings in the MINFILE database (BCGS, 2012) have been visited within the Hotailuh study area. Most of these occur in the easily accessible Gnat Pass area where rock exposure is poor to moderate. An additional nine new mineral occurrences were identified, three within the Gnat Pass area, and six on well-exposed ridges within the Hotailuh batholith (see enclosed 1:50,000 scale map).

A total of 20 mineralized (grab) samples were collected from 4 MINFILE locations, as well as 7 from the newly identified mineral occurrences. The samples were jaw crushed and pulverized in a Cr-steel mill at the Geological Survey sample preparation facilities in Victoria and analyzed at AcmeLabs in Vancouver. The samples were dissolved using a four-acid digestion followed by multi-element Inductively Coupled Mass Spectroscopy (ICP-MS) analysis. Gold was analyzed by lead-collection fire assay fusion followed by Inductively Coupled Plasma Emission Spectroscopy (ICP-ES) analysis. Values reported in Table 3 include analysis of one repeat on a jaw crushed reject sample, an external standard, and Acme's internal quality control duplicate samples and standard. The assay results are given in Table 3.

MINFILE prospects and showings

Gnat Pass (MINFILE 104I 001)

The Gnat Pass copper developed prospect is located immediately north to northeast of Lower Gnat Lake (map 'a'), and comprises two different zones. The "hill zone" is about 1.1 km east of the lake outlet and was drilled in 1965 and 1989 (Smith and Garagan, 1990). Indicated resources (non-NI 43-101-

Table 3: Assay results and coordinates of mineralized rock samples collected during 2011 field work in the Hotailuh area.

Mineral occur.	Element				Au*	Ag	Cu	Mo	W	Sn	Bi	As	Sb	Ba	Pb	Zn	Rb	Sr	Cd	Ni	Co
	Units				ppb	ppm	ppm	ppm	ppm	ppm	ppm	ppm	ppm	ppm	ppm	ppm	ppm	ppm	ppm	ppm	ppm
	Detection limit				2	0.1	0.1	0.1	0.1	0.1	0.1	1	0.1	1	0.1	1	0.1	1	0.1	0.1	0.2
	Station no.	UTM E	UTM N	Unit																	
Gnat P.	11BVA5-30	450,034	6,458,207	LT GP	12	0.1	161	<0.1	1.0	0.3	0.9	30	4.2	463	4	5	79	211	<0.1	3	109
	11BVA9-48	450,502	6,457,572	LT GP	4	<0.1	34	0.4	0.5	0.6	0.1	7	2.4	598	2	23	66	182	<0.1	2	6
	11JLO32-319	451,832	6,457,090	LT GP	41	0.6	7221	16.7	0.6	0.6	0.1	5	1.0	510	7	32	134	315	0.2	4	8
Dalv.	11BVA11-62a	448,489	6,449,977	T Ss	14	<0.1	87	<0.1	29.5	0.9	4.8	535	54.9	53	2	3	64	38	<0.1	230	31
Gnat Cr.	11BVA11-62b	448,489	6,449,977	T Ss	570	2	463	0.5	9.8	1.2	61.0	>10000	204.7	36	32	21	38	121	<0.1	53	93
	11BVA2-12	451,163	6,451,183	LT CH	1703	81.7	>10000	5.5	<0.1	0.1	482.6	<1	1.4	50	79	125	62	599	0.5	5	18
Gnat L. um.	11BVA11-57	449,665	6,450,261	T Ss	<2	<0.1	72	1.9	0.3	3.9	0.3	<1	0.3	341	11	33	64	21	<0.1	21	11
	11BVA11-58b	449,472	6,449,706	LT GLf	<2	0.1	87	8.2	0.8	0.9	0.1	5	1.8	1005	8	78	19	689	<0.1	39	22
	11BVA11-59	449,321	6,449,882	LT GL	5	0.2	402	3.7	0.2	1.3	0.1	2	1.9	245	4	93	5	424	0.2	30	96
	Acme Dup	,,	,,	,,	*4*																
Mat	11BVA26-184	462,220	6,428,961	T Ss	2	0.2	139	7.0	0.4	0.7	<0.1	4	<0.1	27	5	129	2	80	0.4	146	20
	11BVA26-187	461,821	6,429,303	T Ss	<2	0.1	133	0.9	0.2	0.6	<0.1	22	0.4	36	73	57	2	272	0.2	63	39
Mat N	11BVA25-172	461,904	6,431,947	LT CH	39	9.1	>10000	0.7	0.2	0.2	5.4	<1	0.4	3102	13	86	32	1120	0.1	25	22
Pat	11BVA13-74	470,681	6,449,148	LT CH?	32	1.1	2962	2.2	0.4	1.8	1.0	12	0.7	392	4	24	25	568	<0.1	10	20
Pat W	11BVA14-82	467,697	6,447,881	MJ TSc	21	0.7	7079	0.1	2.4	1.1	0.6	19	1.3	1083	2	49	117	159	0.2	2	15
	11BVA15-90	466,323	6,447,968	MJ TSp	<2	<0.1	131	2.0	0.1	0.5	<0.1	4	<0.1	1179	4	7	84	461	<0.1	2	8
3 Sis. N	11BVA30-216	480,344	6,438,583	MJ TSc	9	0.2	3645	6.4	>200	3.4	<0.1	3	0.4	130	3	92	19	195	0.2	5	51
3 Sis.	11BVA32-241	480,590	6,435,596	MJ TSf	80	<0.1	3520	0.8	6.1	0.7	0.2	<1	0.2	41	2	59	2	270	<0.1	3	15
	11BVA32-246	481,249	6,435,903	LT CH	<2	<0.1	144	3.8	3.2	2.7	<0.1	<1	<0.1	188	3	9	4	550	<0.1	2	15
3 Sis. S	11BVA33-253	481,447	6,433,699	T Sv	<2	<0.1	55	6.8	1.1	0.8	0.1	5	0.2	40	1	3	2	1028	<0.1	10	124
	11BVA33-257	481,525	6,433,380	T Sv	14	0.4	3367	314.3	33.3	3.1	2.4	11	2.7	51	2	58	9	521	<0.1	11	123
	Acme Dup	,,	,,	,,		*0.3*	*3452*	*331.8*	*38.9*	*3.2*	*2.3*	*9*	*2.6*	*51*	*2*	*59*	*9*	*537*	*<0.1*	*11*	*122*
	11BVA33-257Dup	,,	,,	,,	*14*	*0.3*	*2925*	*240*	*31.9*	*4.6*	*2.4*	*8*	*3.1*	*50*	*2*	*54*	*7*	*560*	*<0.1*	*12*	*105*
Standards	*Standard RU-1*	-	-	*Standard*	*238*	*3.9*	*7546*	*10.9*	*8.5*	*9.9*	*18.9*	*67*	*0.9*	*31*	*380*	*>10000*	*9*	*88*	*60*	*32*	*104*
	*Expected***	-	-	,,	*3·10²*	*7*	***8.54·10³***									***2.237·10⁴***			*7·10¹*	*7·10¹*	
	OREAS45C	-	-	*Standard*		*0.2*	*595*	*2.2*	*1.0*	*2.8*	*0.2*	*11*	*0.8*	*279*	*24*	*81*	*23.8*	*35*	*0.2*	*317*	*100*
	OREAS45C	-	-	,,		*0.1*	*591*	*2.6*	*1.2*	*3.0*	*0.2*	*10*	*0.8*	*272*	*25*	*79*	*24.3*	*39*	*0.1*	*302*	*98*
	*Expected***	-	-	,,		*0.28*	*620*	*2.26*	*1.06*	*2.9*	*0.21*	*10.1*	*0.79*	*270*	*24*	*83*	*24*	*36.4*	*0.15*	*333*	*104*

Significant values in yellow, anomalous values in orange, slightly elevated values in blue. Abbreviations used for mineral occurrences: Gnat P. = Gnat Pass, Gnat Cr. = Upper Gnat Creek, Dalv. = Dalvenie, Gnat L. um. = Gnat Lakes ultramafite, 3 Sis. = Three Sisters, W = west, N = north, S = south. For unit abbreviations, see Table 1.

* Analyzed by lead-collection fire assay fusion followed by ICP-ES. All other elements analyzed by four-acid digestion followed by ICP-MS.

** Recommended values for CANMET standard RU-1 in bold (Faye *et al.*, 1977). Expected values for AcmeLabs internal standard.

Table 3 *(cont.)*

Mineral occur.	Element	Cr	V	Nb	Y	Zr	Sc	La	Hf	Ta	Ce	Th	U	Li	Be	Mn	Ti	Al	Fe	Mg	Ca	Na	K	P	S
	Units	ppm	ppm	ppm	ppm	ppm	ppm	ppm	ppm	ppm	ppm	ppm	ppm	ppm	ppm	ppm	%	%	%	%	%	%	%	%	%
	Detection limit	1	1	0.1	0.1	0.1	1	0.1	0.1	0.1	1	0.1	0.1	0.1	1	1	0.001	0.01	0.01	0.01	0.01	0.001	0.01	0.001	0.1
	Station no.																								
Gnat P.	11BVA5-30	63	24	2.0	2	22	1	2	0.9	<0.1	5	0.7	0.8	4	<1	23	0.08	7.7	2.5	0.1	0.1	4.09	1.82	0.01	1.6
	11BVA9-48	30	39	3.3	3	40	3	5	1.3	0.2	12	1.6	1.0	7	2	103	0.15	7.9	1.5	0.1	0.2	4.53	2.39	0.05	0.2
	11JLO32-319	32	53	3.7	8	24	4	8	1.0	0.2	16	1.8	1.2	5	<1	221	0.20	7.1	1.3	0.2	0.5	2.10	5.76	0.08	0.5
Dalv.	11BVA11-62a	769	168	0.3	9	13	23	21	0.5	<0.1	41	0.2	0.4	16	<1	4597	0.22	3.9	3.9	0.7	5.0	0.03	1.75	0.10	0.1
	11BVA11-62b	299	91	0.4	2	17	10	43	0.5	<0.1	60	0.5	1.3	22	<1	336	0.08	2.9	10.2	0.1	0.0	0.03	1.02	0.04	4.0
Gnat Cr.	11BVA2-12	17	77	0.2	2	2	<1	6	<0.1	<0.1	6	0.2	7.1	10	<1	815	0.02	4.0	24.8	0.7	1.5	0.03	2.31	0.01	9.7
Gnat L. um.	11BVA11-57	64	22	1.1	4	13	9	7	0.3	<0.1	22	1.0	0.3	17	<1	1088	0.11	3.9	1.3	1.0	0.1	0.10	1.76	0.02	0.4
	11BVA11-58b	60	326	1.9	17	20	31	8	1.0	<0.1	19	0.7	0.4	4	<1	1249	0.65	7.6	6.5	3.6	5.8	3.57	0.84	0.30	0.1
	11BVA11-59	88	511	1.9	17	31	64	4	1.3	<0.1	13	0.4	0.2	3	<1	1544	1.06	5.8	13.3	6.3	7.9	1.15	0.60	0.06	1.9
	Acme Dup																								
Mat	11BVA26-184	105	333	6.0	21	24	22	14	0.8	0.4	27	2.9	1.4	2	<1	833	0.47	8.0	4.7	1.1	1.2	7.67	0.12	0.07	1.3
	11BVA26-187	499	212	1.0	10	17	51	5	0.7	<0.1	12	1.1	0.5	11	<1	1741	0.31	4.8	5.9	6.4	10.4	1.88	0.09	0.18	1.0
Mat N	11BVA25-172	27	107	4.2	6	4	<1	19	0.2	0.3	35	2.0	2.4	27	2	827	0.58	8.6	3.3	2.5	2.0	3.75	1.34	0.13	0.2
Pat	11BVA13-74	61	69	3.6	12	8	4	16	0.5	0.2	35	3.5	1.7	8	1	592	0.21	7.2	4.6	0.9	3.5	2.99	0.65	0.06	0.2
Pat W	11BVA14-82	52	85	3.7	18	8	9	11	0.5	0.2	26	7.6	6.9	8	<1	811	0.22	6.8	3.3	0.8	0.5	2.23	3.05	0.09	<0.1
	11BVA15-90	66	18	4.0	12	17	2	20	0.6	0.3	39	7.5	2.5	6	1	162	0.13	7.1	1.6	0.4	1.0	3.63	2.82	0.05	0.5
3 Sis. N	11BVA30-216	40	244	1.7	24	11	31	11	0.5	0.1	24	4.7	27.5	6	3	1683	0.18	5.1	22.0	2.0	3.2	1.11	0.70	0.07	<0.1
3 Sis.	11BVA32-241	53	99	2.8	15	41	9	14	1.4	0.2	29	4.2	6.2	5	<1	627	0.26	6.6	5.4	1.9	1.6	3.53	0.09	0.07	<0.1
	11BVA32-246	32	54	6.2	19	31	10	70	1.2	0.3	105	3.7	2.9	1	2	310	0.28	7.8	1.8	0.8	3.3	4.38	0.21	0.06	0.6
3 Sis. S	11BVA33-253	36	136	5.4	21	55	17	17	1.5	0.3	34	3.8	1.1	2	1	258	0.55	9.6	7.1	2.4	4.9	3.55	0.17	0.16	2.4
	11BVA33-257	58	180	4.1	22	57	18	15	1.6	0.2	31	2.4	2.2	5	1	1906	0.43	5.7	16.3	3.5	3.3	0.68	0.20	0.10	1.8
	Acme Dup	*59*	*182*	*4.2*	*22*	*61*	*17*	*15*	*1.5*	*0.2*	*32*	*2.5*	*2.3*	*5*	*1*	*1978*	*0.44*	*6.0*	*15.7*	*3.6*	*3.3*	*0.70*	*0.20*	*0.11*	*1.8*
	11BVA33-257Dup	*67*	*182*	*3.8*	*23*	*56*	*19*	*17*	*1.6*	*0.2*	*34*	*2.5*	*2.5*	*5*	*1*	*1805*	*0.41*	*5.8*	*15.6*	*3.2*	*3.7*	*0.69*	*0.19*	*0.10*	*1.6*
Standards	*Standard RU-1*	*53*	*59*	*1.4*	*9*	*34*	*11*	*8*	*1.0*	*<0.1*	*17*	*1.2*	*0.8*	*5*	*<1*	*778*	*0.12*	*3.5*	*22.9*	*3.1*	*2.6*	*0.40*	*0.26*	*0.02*	*>10.0*
	*Expected***															*1·10³*	*0.2*	*4.3*	***24.40***	*3.3*	*2.8*	*0.8*	*0.6*		***21.6***
	OREAS45C	*934*	*252*	*23.1*	*13*	*160*	*59*	*26*	*4.1*	*1.4*	*49*	*10.1*	*2.2*	*15*	*<1*	*1111*	*1.05*	*6.9*	*17.5*	*0.2*	*0.5*	*0.10*	*0.34*	*0.05*	*<0.1*
	OREAS45C	*925*	*239*	*22.9*	*12*	*173*	*58*	*25*	*4.2*	*1.5*	*52*	*10.7*	*2.3*	*15*	*<1*	*1113*	*1.11*	*7.2*	*18.5*	*0.3*	*0.5*	*0.10*	*0.34*	*0.05*	*<0.1*
	*Expected***	*962*	*270*	*23.1*	*12.9*	*170*	*59.0*	*26.2*	*4.27*	*1.43*	*54*	*10.2*	*2.4*	*15.7*		*1160*	*1.131*	*7.59*	*18.33*	*0.25*	*0.48*	*0.097*	*0.36*	*0.051*	*0.02*

compliant) are 30.4 million tonnes grading 0.389 % copper, including 20 % dilution with wall rock grading 0.15 % copper (Lytton Minerals Ltd., 1972, reported in MINFILE 104I 001; BCGS, 2012). The "creek zone" is exposed along the creek draining Lower Gnat Lake, about 750 m north of the lake outlet, and has not been drill tested.

Apart from minor outcrop at the hill zone and along Gnat Creek, very few exposures are present in the immediate area. Mapping conducted during this study indicates that the area is underlain by predominantly augite-phyric coherent rocks of the Triassic Stuhini group. The augite-phyric rocks are cut at several locations by altered intrusive rocks. These intrusive rocks are plagioclase-phyric hypabyssal rocks (with sparse quartz and/or hornblende phenocrysts present in places), termed here the "Gnat Pass intrusive". These intrusive rocks are found both in the hill and creek zones, as well as one small outcrop along Highway 37. A U-Pb zircon crystallization age of 216.5 ± 1.4 Ma was obtained from drill core samples of the Gnat Pass intrusive. The sample was collected from diamond drill hole G-89-8 drilled vertically into the hill zone. This age implies that these intrusive rocks are part of the Late Triassic plutonic suite, and indicate a pre-216.5 Ma age for the augite-phyric coherent rocks. The Stuhini augite-phyric coherent rocks and associated intrusive rocks are overlain by a northeast-dipping sequence of conglomerate, quartz-bearing feldspathic-arenite and graphitic siltstone, as evident in the 1989 drill core (Smith and Garagan, 1990; this study). We have tentatively assigned these rocks to an Early (-Middle) Jurassic coarse-grained quartz-rich sedimentary rock unit (lJ Hs, map 'a'). The contact between the Stuhini and siliciclastic rocks is generally brecciated (Smith and Garagan, 1990), and most likely represents an unconformable contact. Assay results of 1989 drill core (Smith and Garagan, 1990) indicate that mineralization is mostly associated with the Stuhini Group and intrusive rocks; minor copper occurs in the brecciated contact zone, and only trace copper is present within the siliciclastic succession. An Induced Polarization (IP) survey (Page and Scott, 2006) indicates a significant north to north-northwest striking sub-vertical resistivity low between the creek and hill zones, and is interpreted here as a fault. In addition, the IP survey (Page and Scott, 2006) identified a significant chargeability high centred on the hill zone, likely caused by abundant disseminated sulphides in this area. The 12.5mV/V inverted chargeability contour at 40 m depth is shown on the 1:50,000 geological map.

Silicification, tourmaline veining and Fe-carbonate-cemented breccias are common in the hill zone. Here, chalcopyrite and pyrite range up to several percent, occur in disseminations or fracture-fillings, and are also found within tourmaline veins and Fe-carbonate cement in brecciated zones. A grab sample from subcrop of quartz and plagioclase porphyritic granodiorite on the G-89-8 drill pad returned 0.7% Cu and slightly elevated Au and Mo (sample 11JLO32-319, Table 3). Several percent of pyrite associated with possible K-feldspar alteration is found just north of the creek zone, and pyrite associated with Fe-carbonate alteration is found in the small intrusion along Highway 37. Assay samples of altered intrusive rocks from both locations (11BVA09-48, 11BVA05-30) returned no significant mineralization.

Thin section study of the plagioclase±quartz-phyric hypabyssal intrusions near Highway 37 indicate the presence of a few percent disseminated pyrite and selective replacement of

plagioclase by sericite. Samples from the "hill zone" contain disseminated and fracture-hosted chalcopyrite and pyrite in plagioclase-phyric hypabyssal intrusive rocks containing weakly sericite-altered plagioclase and patchy carbonate alteration.

Dalvenie (MINFILE 104I 003)

The Dalvenie gold-copper-silver prospect is located immediately west of the Gnat Lakes ultramafite (map 'a'). The prospect was mapped, trenched and drilled in the 1960's. Results from the program indicated a 1146 m long mineralized shear zone (Dalvenie shear) with short intercepts of up to 1.5 m containing 4.8 g/tonne gold and 3.73% copper (Wetherill, 1990). The report describes a 10-15 m wide, steeply west-dipping shear zone that separates the Gnat Lakes ultramafic body on the east from sedimentary and volcanic rocks on the west side of the fault zone. The shear zone contains abundant, weathered grey quartz; 5 cm-wide zones of massive pyrite, chalcopyrite and arsenopyrite; disseminated pyrite and chalcopyrite; and is locally silicified (Wetherill, 1990). Bornite, hematite, siderite, barite, magnetite, pyrrhotite and sphalerite have also been reported (MINFILE 104I 003; BCGS, 2012). A polymictic breccia zone was identified along the trace of the Dalvenie shear, and associated mineralization was sampled (Table 3). Two assay samples were taken about 2 m apart and show the highly variable metal content of the prospect. A sulphide rich sample (11BVA11-62b) returned values of 0.57 g/t Au, > 1% As, anomalous Sb and Bi and slightly elevated Cu and Ag. A pervasively silicified, sericitized and carbonate-altered sample (11BVA11-62a) contained 535 ppm As as well as slightly elevated Sb, Bi and W. Trace fine grained euhedral arsenopyrite, predominantly associated with carbonate, was identified in a polished thin section taken from the same sample.

BCR (MINFILE 104I 068)

The BCR copper-zinc-lead-molybdenum showing is located along the abandoned BC railway grade, about 12.5 km south of Upper Gnat Lake (map 'a'). It is hosted within biotite granites and quartz-syenites mapped as the potassic phase of the Middle Jurassic Three Sisters pluton. The rocks are reported to contain chalcopyrite with minor sphalerite, galena and molybdenite in north-trending sets of fractures, locally with argillic and quartz-sericite alteration envelopes (MINFILE 104I 068; BCGS, 2012). Fifteen percussion holes with a total length of 437 m were drilled along the BC railway grade and drill roads marked 'BCR' on map 'a', and intersected predominantly granitic rocks (Dircks, 1974). Samples from drill core returned low copper (<112 ppm) and zinc values (<81 ppm; Dircks, 1974). In the current study we examined all outcrops along the BC railroad grade. Sparse outcrop within 1 to 2.5 km north and 1 km south of the drilled area are intensely iron-oxide stained and contain several percent disseminated and fracture-hosted pyrite (marked on map 'a'). Salmon pink K-feldspar alteration developed along epidote±pyrite-filled fractures is common within the plutonic rocks of the Gnat Pass area, and locally increases in intensity to pervasive K-feldspar alteration at the BCR showing. The southernmost outcrop of granitic rocks visited along the railroad grade (map 'a') shows completely chlorite-altered mafic minerals, locally abundant chlorite veins and specular hematite coated fractures. The latter outcrop appears to have suffered significant magnetite-destructive hydrothermal alteration (measured magnetic susceptibility of $0.35 \cdot 10^{-3} \pm 0.12 \cdot 10^{-3}$ SI units), and coincides with an aeromagnetic low (Aeroquest Airborne, 2012). A major

aeromagnetic (and partially, topographic) lineament immediately west of the BCR showing likely indicates the presence of a north-northwest trending brittle fault. Despite discouraging shallow percussion drill results, the large alteration footprint of this showing warrants additional investigation.

Pat (MINFILE 104I 043)

The Pat copper-molybdenum showing is centred on a drift covered valley north of peak 2196 m (map 'c'). In addition to copper ± molybdenum soil anomalies, several small mineralized outcrops have been described to the south and southeast of the valley (Sadlier-Brown and Chisholm, 1971; Sadlier-Brown and Nevin, 1977). The mineralization reported by these authors comprises disseminations and siliceous veins carrying chalcopyrite and/or molybdenite. One mineralized outcrop identified in this study is characterized by 1-10 mm pyrite + chalcopyrite veins with silicic and potassic altered haloes. An assay sample from this location returned 0.3% Cu and slightly elevated Au and Ag (11BVA13-74 in Table 3). The veins are hosted by biotite-hornblende to hornblende-biotite quartz-monzonite and quartz-monzodiorite, which could be related to the Cake Hill pluton or Three Sisters central felsic phase intrusion. Biotite quartz-monzonite and quartz-monzodiorite, interpreted as the central felsic phase of the Three Sisters pluton, is exposed 100 m to the northeast of this mineral occurrence (map 'c').

Mat (MINFILE 104I 034)

The Mat copper-lead-zinc showings are located in a deeply incised forested valley system on the southern margin of the Cake Hill pluton, several kilometres north of the Stikine River (Figure 1, map 'f'). The area south and southwest of the showing is part of the Stikine River Provincial Park. Poorly exposed fine-grained, stratified sedimentary rocks are found in the valleys and are overlain by more competent augite-phyric coherent rocks exposed at topographically higher levels (map 'f'). Both the sedimentary and volcanic rocks, as well as surrounding foliated hornblende diorites and gabbros, ultramafic rocks and hornblende quartz-monzonites, have been reported to host copper, lead and/or zinc sulphide occurrences (McAusland, 1971). In addition, a soil survey (McAusland, 1971) indicated moderately elevated values of nickel (>300 ppm) over part of the survey area, likely related to occurrences of ultramafic rocks. We identified several sulphide occurrences in the fine-grained sedimentary rocks, and one within the Cake Hill pluton (see "Mat north" new mineral occurrence). The mineralization within the sedimentary rocks occurs in laminated to very thinly bedded siltstones to medium-grained sandstones, and forms stratiform and more irregular-shaped bodies up to 20 m wide. The sulphides occur as fine to very fine-grained disseminations, stratiform horizons and/or within veinlets. Silicification and/or quartz-pyrite veins occur locally. No copper oxides, copper sulphides, galena or sphalerite were observed in the field, possibly due to their very fine grain size. Two assay samples returned no significant metal values (11BVA26-184, 187 in Table 3). Trace, very fine grained chalcopyrite inclusions in pyrite were observed in two thin sections of the assay samples.

New mineral occurrences

Nine new mineralized and/or altered zones were discovered within the Hotailuh batholith. Mineralized samples were collected and submitted for base and precious metal assay analysis. The locations have been described as 'mineral

occurrences' rather than 'showings', pending their inclusion into the MINFILE database.

Triassic occurrences

Four of the new zones are hosted in probable Late Triassic rocks, and include the "Upper Gnat Creek", "Mat north", "Gnat Lakes ultramafite" and "Three Sisters south" mineral occurrences.

The "Upper Gnat Creek" occurrence is located 1.5 km south of Upper Gnat Lake, on a brush- and forest-covered ridge about 750 m east of the BC railroad grade. The occurrence comprises a 1-10 cm wide vein of massive chalcopyrite (locally widening to a 20 x 20 cm pod) within well-foliated Cake Hill plutonic rocks. The wider mineralized zone is associated with brecciated pink K-feldspar altered wall-rocks (Figure 12). An assay sample of the massive sulphide breccia returned significant results of 1.7 g/t Au, 82 g/t Ag, >1 % Cu and 483 ppm Bi (11BVA02-12a in Table 3). A thin section of this material shows abundant massive chalcopyrite, with minor replacement by covelite and goethite. Epidote was identified in thin section, and is present within fractures in the host rock and associated with massive chalcopyrite. An outcrop containing copper sulphide-bearing veinlets was found in the same host rock about 140 m further southeast along the ridge. The host rock immediate surrounding the area of the main mineral occurrence, as well as similar intrusive rocks within approximately 1 km, contain mm to cm wide epidote veins, often associated with epidotization of the wall rock and/or iron-oxide staining. Further south in the Gnat Pass area, epidote + pyrite veins with K-feldspar alteration haloes are also found within the potassic phase of the Three Sisters pluton (see BCR showing above). Given the similar vein style, and proximity to intrusions of the potassic phase of the Three Sisters pluton, the mineralization at "Upper Gnat Creek" may be related to Middle Jurassic intrusive activity.

The "Mat north" mineral occurrence is found on the east face of an alpine ridge, a couple of kilometres north of the Mat showing. It is hosted by the Late Triassic Cake Hill pluton, and comprises decimetre-size pods containing about 5% disseminated sulphides (pyrite, bornite; chrysocolla and malachite staining common). One assay sample returned >1 % Cu and slightly elevated Ag, Au and Bi (11BVA25-172 in Table 3). Abundant coarse-grained euhedral biotite immediately surrounds the mineralized pods, but is absent further away in the plutonic rocks. A thin section of the assay sample shows bornite with minor chalcopyrite, both partly replaced by chalcocite ± covelite. Feldspar in the sample is selectively altered to fine grained sericite, whereas biotite is partially altered to chlorite. The occurrence might be similar to an undisclosed location described by McAusland (1971) where bornite is found in epidote stringers within the Cake Hill pluton.

The "Gnat Lakes ultramafite" occurrences occur within, or immediately surrounding, the Gnat Lakes ultramafite. They are spatially associated with significant topographic lineaments, interpreted as faults, and might be genetically related to the Dalvenie prospect. Subcrop of intensely silicified and sericite-altered, fine-grained, Stuhini sedimentary rocks containing several percent disseminated pyrite occurs along strike of a topographic lineament (sample 11BVA11-57 in Table 3). Several ultramafic outcrops contain disseminated pyrite, either directly within ultramafic rocks or associated with later crosscutting felsic dikes (samples 11BVA11-59 and -58b,


11BVA02-12 (451,162E-6,451,183N)

Figure 12: Mineralization at "Upper Gnat Creek". Intensely pink-orange K-feldspar-altered and brecciated plutonic rock clasts within massive chalcopyrite matrix. Pencil for scale.

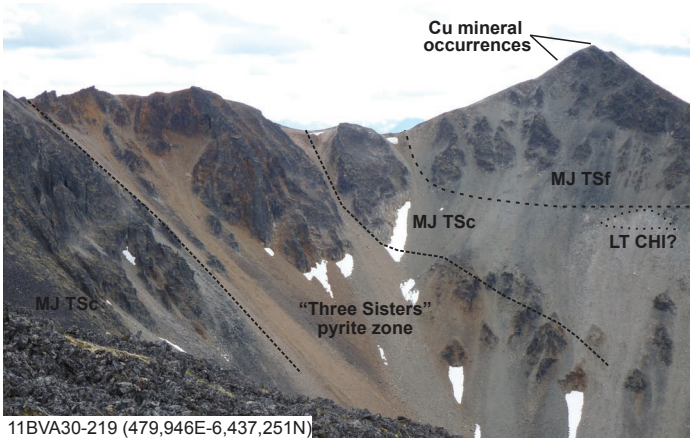

11BVA30-219 (479,946E-6,437,251N)

Figure 13: View south towards westernmost peak hosting the Three Sisters fine-grained mafic-intermediate phase, showing orange-brown altered zone of the "Three Sisters" mineral occurrence and small associated copper showings. The orange-brown zone is intensely goethite-stained, contains abundant disseminated pyrite and pyrite in steeply dipping, west-northwest-striking fractures. The Three Sisters central felsic phase (TSc) is exposed along the ridge in the foreground. Light coloured scree below this peak may be an inclusion of the Cake Hill leucocratic phase (CHl).

respectively). Thin sections of all three assay samples contain predominantly pyrite and trace (microscopic) chalcopyrite. Only one of three samples assayed (11BVA11-59 in Table 3) returned slightly elevated copper values. Sulphides generally occur interstitially within domains of predominantly mafic minerals. In addition, the easternmost exposures of the ultramafic body contain several percent sulphides where they are associated with another north-trending topographic lineament, possibly part of the Gnat Pass fault system.

The "Three Sisters south" mineral occurrence is hosted in a km-size Stuhini inclusion within the leucocratic phase of the Cake Hill pluton (LT CHl in Table 1, map 'g'). Mineralization consists of several zones with 1-5% pyrite disseminated and in veinlets, locally associated with green actinolite. The linear and recessive nature of the gullies suggests that the ≤20 m-wide pyritic zones represent NNW to NE-striking sub-vertical faults cutting the Stuhini succession. One of two assay samples (11BVA33-257 in Table 3) returned 0.3 % Cu, 0.03 % Mo and slightly elevated W. Thin sections of the assay samples contain pyrite and trace chalcopyrite (11BVA33-253) or pyrite, minor chalcopyrite and minor possible bornite (11BVA33-257). Actinolite is present as veins or pervasive replacement in both samples, with chlorite and epidote also abundant in the mineralized sample (11BVA33-257).

Middle Jurassic occurrences

The remaining four new zones, the "Pat west", "Three Sisters", "Three Sisters north" and "BCR north" mineral occurrences, are hosted in Middle Jurassic intrusive rocks of the Three Sisters pluton. One new mineral occurrence at "Red Mountain" is hosted in Early-Middle Jurassic fine-grained sediments, and most likely formed by contact metamorphism associated with Middle Jurassic Three Sisters intrusive activity.

The "Pat west" occurrences are sub-vertical, roughly east- to northeast-trending zones hosted in the Three Sisters pluton, and are spread over the entire local map area (map 'b'). A one-metre-wide zone exposed on the easternmost ridge contains quartz + pyrite ± chalcopyrite veins hosted in biotite quartz-monzonite and quartz-monzodiorite of the central felsic phase, and returned assay values of 0.7% Cu (11BVA14-82). A thin section of this vein material contains trace chalcopyrite. The sample is pervasively potassic altered, feldspars are selectively sericitized, and mafics are completely altered to chlorite. The central and western gossanous exposures are larger in areal extent (30-50 m wide, ≥200-300 m long), contain disseminated pyrite and/or quartz + pyrite veins, and lack copper sulphides. An assay from the latter location (11BVA15-90) failed to return any anomalous values. A thin section of this material shows pyrite, trace chalcopyrite and only partly chloritized mafic minerals.

The "Three Sisters" occurrences are named after the group of peaks on which the fine-grained mafic-intermediate phase of the Three Sisters pluton is exposed (map 'g'). The mineral occurrences are found within the northern margin of the fine-grained mafic-intermediate phase, and within the adjacent central felsic phase and leucocratic Cake Hill pluton. A brown-orange weathering gossan zone, up to 200 m-wide and 2 km-long, is exposed within the Three Sisters central felsic phase close to contact with the fine-grained mafic-intermediate phase (Figure 13). The alteration zone contains abundant WNW-striking and steeply north-dipping goethite-coated fractures after pyrite, and pyrite is also

disseminated throughout the host rock. Three small exposures with quartz + pyrite ± chalcopyrite ± epidote veins, locally associated with in-situ brecciation, are found several hundred metres to the south and southwest of this zone and are hosted in the fine-grained mafic-intermediate phase. One assay sample from the latter location (11BVA32-241) returned 0.35% Cu and slightly elevated Au. The sample is cut by early epidote + chlorite veins, and late quartz + chlorite ± actinolite veins causing local in-situ brecciation. An assay sample from the eastern part of the gossanous pyrite zone (11BVA32-246) returned no anomalous values.

The "Three Sisters north" occurrence is hosted within the Three Sisters central felsic phase. The rocks are intensely veined (roughly 5% veins by volume in a several metre wide interval), with one 10 cm-wide ESE-oriented, steeply north-dipping, epidote + actinolite + magnetite vein. The assay results for this vein indicate 0.36% Cu, >200 ppm W and slightly elevated U (11BVA30-216 in Table 3). A thin section from this vein contains massive magnetite, actinolite, tourmaline and trace apatite.

The "Red Mountain" occurrence is a >1 km^2 zone with 1-5% very fine grained disseminated and minor stratiform pyrite within Lower (-Middle?) Jurassic siltstones (lJ Hs). The whole area is intensely iron-oxide altered. The alteration is centered on the peak located 1 km southeast of Peak 2102 m (map 'h'). One 5 x 30 m NW-SE elongate, steeply SW dipping, grey to white coloured unmineralized breccia body (pipe?) crops out on the upper southwest flank of the above-mentioned peak (see also Figure 4). The breccia body comprises abundant matrix- to clast-supported, cm-sized, angular-subround, plagioclase-phyric clasts within a highly silicified matrix. Common, unmineralized, calcic endoskarn bodies are found in Lower-Middle Jurassic calcareous siltstones within about 20 m of the contact with the Late Triassic Cake Hill quartz-rich phase (LT CHq). Given the age relationship implied by geochronology and biostratigraphy, the skarns likely formed by fluid movement along a permeable fault or non-conformable contact, and originated from the underlying intruding Middle Jurassic Three Sisters pluton.

The "BCR north" occurrence is situated on the BC railroad grade 7 km south of Upper Gnat Lake. It is associated with irregular bodies of potassic(?)-altered hornblende-feldspar porphyry (Tees Creek intrusive, see Table 1) intruding a highly magnetic biotite-bearing hornblende syenite (representing a sub-phase of the Three Sisters potassic phase, MJ TSpm). Minor pyrite is evident in this location, disseminated in both the fringes of the Tees Creek and adjacent intrusive.

DISCUSSION AND CONCLUSIONS

Geological units

The Hotailuh batholith comprises a number of different plutons and plutonic phases. A compilation of crosscutting relationships and previously published and newly reported zircon U-Pb and Ar-Ar dates is shown in Figure 14. The Hotailuh batholith can be subdivided into three plutonic suites, a Late Triassic Stikine plutonic suite (ca. 225-209 Ma), Early Jurassic McBride pluton (ca. 192-176 Ma) and the Middle Jurassic Three Sisters plutonic suite (ca. 175-168 Ma).

The Late Triassic plutonic suite comprises the Gnat Lake ultramafic to mafic bodies, Cake Hill felsic pluton and Beggerlay Creek ultramafic to mafic pluton. The absence of

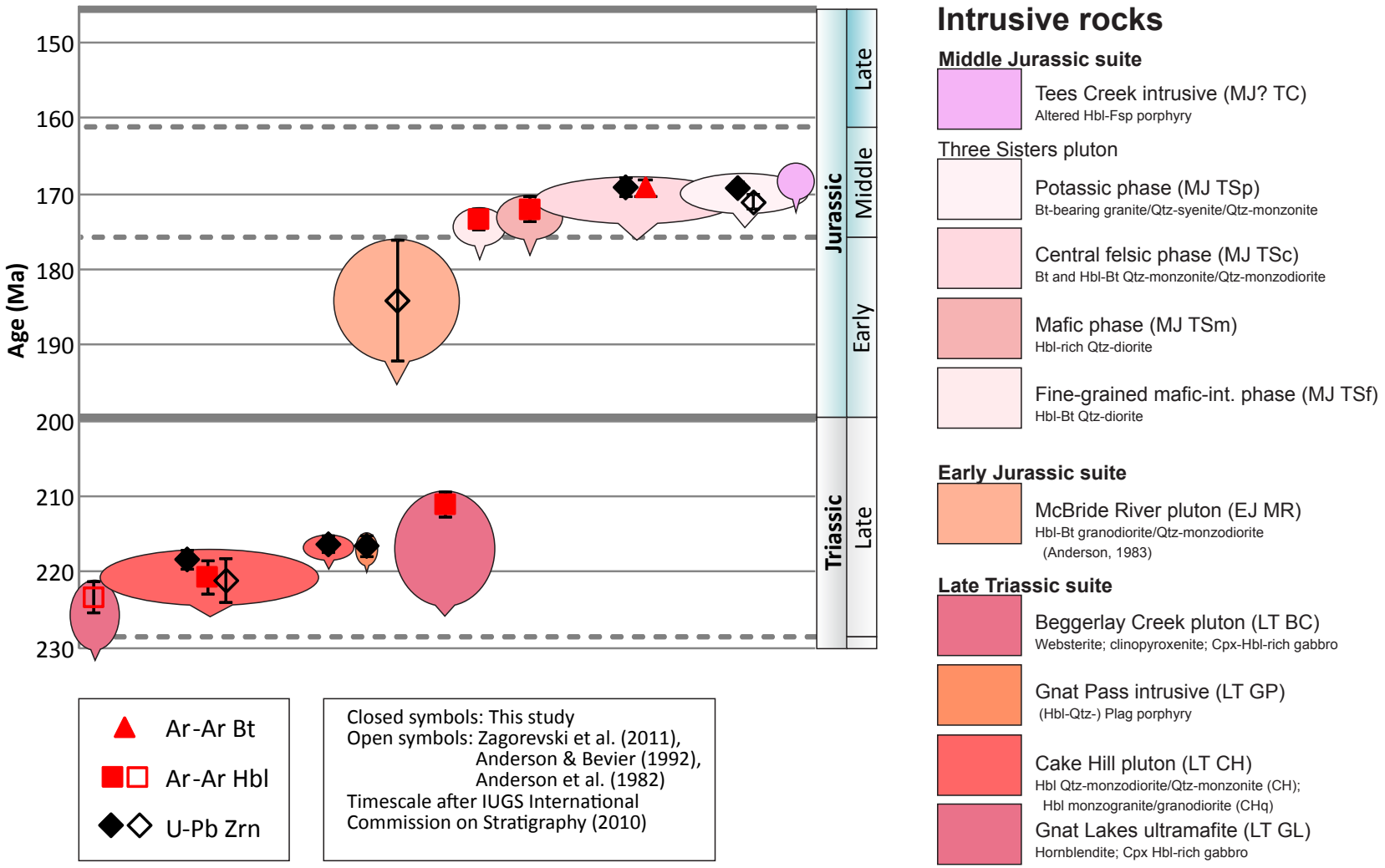

Figure 14: Compilation diagram showing all U-Pb and Ar-Ar geochronological data from the Hotailuh batholith.

equivocal crosscutting relationships, lack of absolute crystallization age determinations for the ultramafic to mafic intrusions, and the absence of detailed mineral chemistry data makes it difficult to determine the genetic and temporal relationships between the different Late Triassic intrusions. The Gnat Lakes ultramafic body lacks orthopyroxene, and can be classified as an Alaskan-type intrusion comprising cumulates derived from a relatively silica undersaturated (alkaline to subalkaline) parental magma (Irvine, 1967; 1974; Nixon *et al.*, 1997). In contrast, the Beggerlay Creek pluton includes a >2 km^2 websterite body interpreted here as cumulates derived from silica saturated (calc-alkaline) parental magma (Irvine, 1967; 1974; Nixon *et al.*, 1997). The calc-alkaline magma that produced the Beggerlay Creek cumulates by fractional crystallization evolved into more felsic compositions, which may be represented by the Cake Hill pluton.

The Late Triassic plutonic suite is spatially associated with, and in places intrudes, poorly exposed and poorly dated, intermediate-mafic volcanic and sedimentary rocks of the Triassic Stuhini group (Figure 15).

The Early Jurassic plutonic suite comprises the McBride River felsic pluton exposed on the easternmost edge of the batholith, and was not studied here. The McBride pluton has not been dated in this study. It may be related to the Texas Creek plutonic suite exposed further southwest near Stewart and the Iskut River (Anderson and Bevier, 1990; Logan *et al.*, 2000), and remains a high-priority target for future geochronology studies in the area.

The Three Sisters pluton comprises at least four phases, namely the fine-grained mafic-intermediate phase, a mafic phase, central felsic phase, and a crosscutting potassic phase. U-Pb zircon crystallization ages and Ar-Ar cooling ages confirm that all phases formed during a relatively short time span in the Middle Jurassic (Figure 14).

Northwest of Lower Gnat Lake, a granitoid clast-bearing conglomerate non-conformably overlies the Cake Hill pluton, and is correlated with Lower (-Middle) Jurassic, quartz-bearing, coarse-grained sedimentary rocks reported within the immediate area. The latter are overlain by rocks previously assigned to the Triassic Stuhini group (Anderson, 1983; Gabrielse, 1998) that in light of new U-Pb detrital zircon data are reinterpreted here as Middle Jurassic sedimentary and volcanic rocks (Iverson *et al.*, 2012; Iverson, 2012; Figure 15). Evidence for the presence of the Hotailuh thrust in the present study areas is lacking. The Lower to Middle Jurassic sedimentary and volcanic successions studied herein (maps ‘a’, ‘h’) are part of a belt of rocks exposed on the north and northeastern margin of the batholith. The Lower Jurassic rocks have previously been assigned to the Takwahoni formation, a formation predominantly composed of greywacke, siltstone, shale, conglomerate and minor limestone exposed in the footwall of the King Salmon thrust fault (Gabrielse, 1998). However, another important Lower to Middle Jurassic unit in Stikinia is the Hazelton group, a succession of volcanic and sedimentary rocks. Following definitions by Marsden and Thorkelson (1992), and in light of the new U-Pb detrital zircon dates (Iverson *et al.*, 2012; Iverson, 2012), the entire succession of volcanic and sedimentary rocks around peak 2096 m (map ‘a’) is reassigned to the Hazelton group. In addition, the entire belt of rocks along the north and northeastern margin of the batholith may be part of the Hazelton group.

Jurassic Hazelton Group (northwest area)

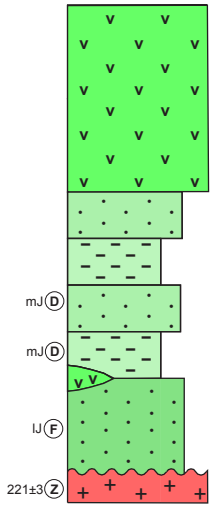

Volcanic rocks (lmJ Hv)

Coarse-grained sedimentary rocks (lmJ Hsc)

Fine-grained sedimentary rocks (lmJ Hs)

Coarse-grained sedimentary rocks (lmJ Hsc)

Fine-grained sedimentary rocks (lmJ Hs)

Coarse-grained quartz-bearing sedimentary rocks (lJ Hs)

Cake Hill pluton (LT CH)

Jurassic Hazelton Group (east area)

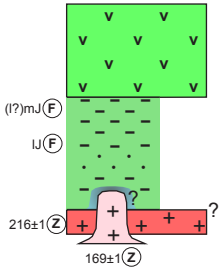

Volcanic rocks (lmJ Hv)

Sedimentary rocks (lJ Hs)

Cake Hill pluton, quartz-rich phase (LT CHq)
Three Sisters, central felsic phase (MJ TSc)

Triassic Stuhini Group (all areas)

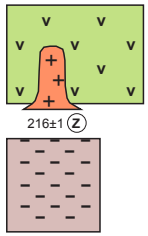

Augite-phyric coherent rocks (T Sv)

Gnat Pass intrusive (LT GP)

Fine-grained sedimentary rocks (T Ss)

Z U-Pb zircon age
(this study; Anderson and Bevier, 1992)
D Detrital U-Pb zircon age
(Iverson et al., 2012; Iverson, 2012)
F Fossil location
(Gabrielse, 1998)

Figure 15: Overview diagram showing all stratified lithologies.

Mineralization

The Gnat Pass area appears especially well endowed with mineral occurrences. In addition to the mineral occurrences described here, many other showings are present just outside of map area 'a'. Examples are Louise (MINFILE 104I 054), Bell (MINFILE 104I 033), Moss (MINFILE 104I 029), Kay 19, 49 (MINFILES 104I 037, 026), and Crown (MINFILE 104I 046). The latter three comprise the Pliny project that is currently under exploration by West Cirque Resources (2011a). The area is cut by the north-northwest-trending Gnat Pass ductile shear zone and similarly trending brittle faults. The shear zone likely formed during emplacement of the Cake Hill pluton in the Late Triassic and was the locus of subsequent brittle faulting. These structures likely played an important role in the introduction of magmas, fluids and associated mineralization in the Gnat Pass area.

Mineralization hosted in Late Triassic rocks varies widely in host rock, metal tenor and mineralization style and comprises:

- Cu only at the Gnat Pass porphyry-style prospect;
- Au+As±Sb (Cu, Ag reported) hosted in a shear/fault zone at the Dalvenie prospect;
- Cu±Mo pyritic fault zones cutting a roof pendant or inclusion of Stuhini volcanics within the Cake Hill pluton at "Three Sisters south";
- Cu with trace Ag as small bodies within the Cake Hill pluton at "Mat north";
- Cu+Pb+Zn (reported) within stratabound to irregular bodies at the Mat showing;

Two mineral occurrences hosted in Late Triassic rocks that may in fact be related to Middle Jurassic magmatism include:

- Au+Cu+Ag massive chalcopyrite vein in felsic plutonic rocks at the newly discovered "Upper Gnat Creek" mineral occurrence, but similar alteration and mineralization to the BCR showing may indicate a Middle Jurassic age for this mineralizing event; and
- Cu (and Mo reported) at the vein-hosted Pat showing, found within the Late Triassic Cake Hill pluton, but close association with the Three Sisters pluton indicates a possible Middle Jurassic age for this mineralizing event.

Mineralization hosted in the Three Sisters pluton appears less variable, and comprises:

- Cu only at the "Pat west" and "Three Sisters" mineral occurrences;
- Cu±W at the "Three Sisters north" mineral occurrence; and
- Cu+Zn+Pb+Mo reported at the BCR showing.

Possible metal zonation is present in both the "Pat west" and "Three Sisters" occurrences, with relatively large, gossanous, pyrite-dominated zones spatially associated with smaller quartz-vein-hosted, pyrite + copper sulphide occurrences. Assay samples indicate 0.3-0.7% Cu in the copper-sulphide-bearing zones, and Cu±W in the possibly related "Three Sisters north" occurrence.

Geological history

In this section we will discuss the results of this study in light of the broader geological

and tectonic framework of northwestern British Columbia.

The Hotailuh batholith provides a unique example of coincident Mesozoic magmatism formed during multiple magmatic episodes spanning the Late Triassic to Middle Jurassic periods. All investigated intrusive phases have a strong calc-alkaline subduction-modified subcontinental mantle geochemical signature, and formed in a volcanic island arc to continental volcanic arc setting (sensu Maniar and Piccoli, 1989).

The Cake Hill pluton is part of the Late Triassic Stikine plutonic suite, which occurs throughout northern Stikinia (Figure 1a). Several large Late Triassic batholiths occur towards the east (Stikine and Pitman batholiths, Anderson, 1984; Read and Psutka, 1990), west (Moosehorn and Sam batholiths around the Golden Bear deposit, Bradford and Brown, 1993), and southwest (Hickman batholith, Brown *et al.*, 1996). Late Triassic magmatism is generally attributed to westward inboard subduction of the Cache Creek ocean below Stikina (English and Johnston, 2005), but eastward outboard subduction may also have occurred at the same time (Figure 16; MacIntyre *et al.*, 2001).

Latest Triassic intrusive activity in northern Stikinia produced relatively small ca. 210 Ma alkaline feldspathoid-bearing intrusions hosting the Galore Creek Cu-Au porphyry deposit (Mortensen *et al.*, 1995), as well as the slightly younger quartz-absent to quartz-bearing 207-204 Ma Groat stock and 205-202 Ma Red stock (host to the GJ and Red Chris Cu-Au porphyry deposits, Ash *et al.*, 1997; Friedman and Ash, 1997; Norris *et al.*, 2011; Hollis, 2011). To date, similar age equivalent rocks have not been identified in the Hotailuh area.

The Early Jurassic McBride River pluton (Anderson and Bevier, 1992) is found on the eastern margin of the Hotailuh batholith. Other Early Jurassic plutons are predominantly found between Stewart and Telegraph Creek, and comprise the Texas Creek and Cone Mountain plutonic suites (Alldrick, 1991; Brown *et al.*, 1996). These intrusions may represent a northern extension of the Coast Mountain plutons (Woodsworth *et al.*, 1991), which formed prior to outboard accretion with the insular terranes (Gehrels, 2001), and a further outboard jump of the subduction zone. Other than the McBride River pluton, only a few Early Jurassic intrusions have been recognized closer to Dease Lake. Notable are the McEwan Creek intrusions east of Iskut (U-Pb zircon age 183.5±0.5 Ma, Evenchick and Thorkelson, 2005 and references therein).

Several Middle Jurassic plutons have been described in northern Stikinia, however most intrusions have only been dated using the older K-Ar technique. Significant improvements in geochronological techniques over the last decades have clearly shown that these earlier-established dates represent minimum age estimates. Notably, the Yeheniko pluton (part of the Hickman batholith to the southwest) was previously interpreted as Middle Jurassic based on several biotite and hornblende K-Ar ages (Brown *et al.*, 1996 and references therein). However, recent U-Pb zircon age dating suggests that the pluton, which is associated with porphyry copper mineralization at Schaft Creek, is Late Triassic in age (Scott *et al.*, 2008). Middle Jurassic plutons are described around the Stikine and Pitman batholiths, but are based on K-Ar biotite/hornblende dates, and need further work to confirm the true crystallization age. During the Middle Jurassic, the Stikine and Quesnel island arc terranes accreted with the

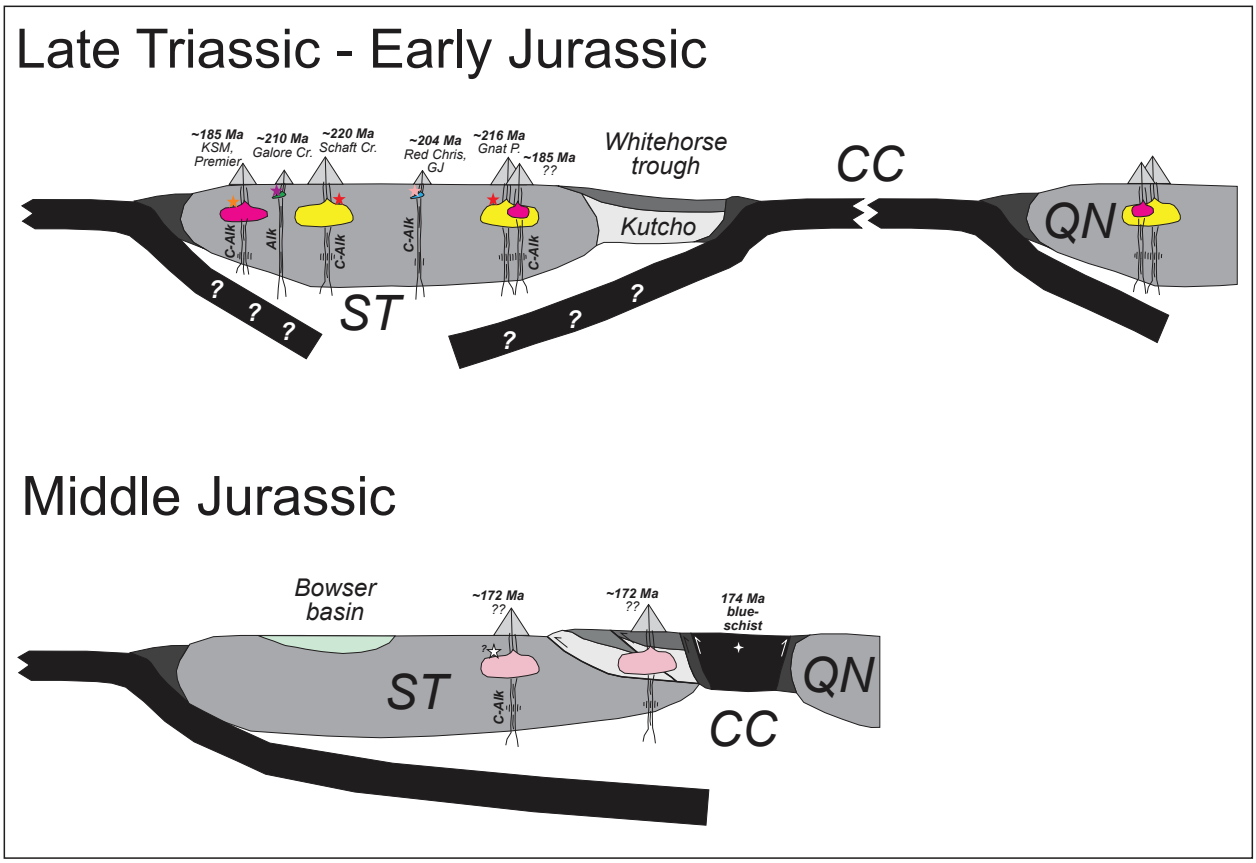

Figure 16: Schematic drawing of possible Late Triassic to Middle Jurassic plate tectonic arrangement, magmatism and associated mineralization. Modified after Mihalynuk et al. (1992), Ricketts et al. (1992), Nelson and Mihalynuk (1993), Mihalynuk et al. (2004), English and Johnston (2005). Abbreviations: ST = Stikinia; CC = Cache Creek; QN = Quesnellia; C-Alk = predominantly calc-alkaline magmatism; Alk = predominantly alkaline magmatism.

North American continent, and enclosed the Cache Creek oceanic terrane (Gabrielse, 1991; Nelson and Mihalynuk, 1993). The completion of the Stikinia – Cache Creek accretionary event (obduction of blueschist metamorphic rocks and intrusion by post tectonic granites) is well constrained as Bajocian (Ricketts *et al.*, 1992; Mihalynuk *et al.*, 1994; 2004). The Three Sisters pluton described here has a similar age and geochemical signature as the Fourth of July pluton that cuts deformed rocks of the Cache Creek terrane (U-Pb zircon ages of 170.4±5.1 Ma, 171.5±3.4 Ma, Mihalynuk *et al.*, 1992), and appear to define a northwest to east-southeast trend of Middle Jurassic, ca. 175-165 Ma, plutons (Figure 1a). Since the Fourth of July pluton is post-kinematic and post-accretion, these plutons formed by eastward outboard subduction below the now-accreted Stikine and Quesnel island arc terranes (Figure 16).

Implications for exploration

The Hotailuh batholith and its environs are highly prospective for intrusion-related magmatic-hydrothermal mineralization, to have formed during at least two magmatic episodes in the Late Triassic and Middle Jurassic. This is indicated by the high number of known intrusion-related MINFILE occurrences and prospects, as well as new mineral occurrences, found peripheral to the main batholith and along contact zones between different magmatic phases within the batholith. The batholith has the same age, chemical composition and tectonic environment as intrusions hosting large precious and base metal deposits within northern Stikinia. The 2275 km^2 batholith proper is prospective for pluton-hosted Cu±Mo±Au deposits associated with late-stage calc-alkaline porphyry intrusions (e.g. similar to Highland Valley), provided the plutons have not been eroded beyond ~3-6 km (Singer *et al.*, 2008). The country rocks are prospective for volcanic and/or sedimentary rock-hosted Cu±Mo±Au deposits associated with high-level calc-alkaline porphyry intrusions (e.g. similar to Schaft Creek). Small volume Latest Triassic alkalic (to calc-alkalic) intrusions with potential for porphyry Cu-Au deposits (e.g. similar to Galore Creek, Red Chris, GJ) were not identified during this study, but their relatively small alteration footprint and intermittent presence throughout the Stikine and Quesnel terrane justifies further attention. Both the Late Triassic and Middle Jurassic magmatic episodes are associated with both pluton- and country rock-hosted copper and/or gold mineral occurrences, which, in many cases are compatible with a porphyry-style deposit type. At Gnat Pass, we dated a plagioclase (±quartz) porphyry stock associated with disseminated, vein- and breccia-hosted copper mineralization, yielding a Late Triassic age. The developed prospect has a similar age, geological setting and mineralization style as the Schaft Creek porphyry Cu±Mo±Au deposit (cf. Scott *et al.*, 2008). North of the Hotailuh batholith, West Cirque Resource's (2011b) Tanzilla project comprises a ~7 km long trend of altered and mineralized rocks associated with possible Middle Jurassic (Gabrielse, 1998) porphyry dikes. Both the Gnat Pass and Tanzilla project, as well as the newly described mineral occurrences (this study), confirm the potential for intrusion-related magmatic-hydrothermal mineralization during at least two magmatic episodes of the Hotailuh batholith. The Early Jurassic McBride intrusion was not studied here, but abundant showings located south and east of the intrusion warrant additional investigation regarding the timing and mineralization style of these occurrences.

ACKNOWLEDGEMENTS

We would like to acknowledge financial support from Geoscience BC that covered field, analytical and salary costs associated with this project. Travis McCarron, Catie Young, Meagan Hogg and Olivia Iverson are thanked for their capable assistance during the field season. A warm thanks to Patricia McIntosh for opening her home for our use during the summer mapping project, to Jan Anderson and Dempsey Callison for the cooking, logistical support and help in setting up camp, and to Pacific Western Helicopters for safe flying. Special thanks to Fion Ma for her assistance in producing the accompanying 1:50,000 geology map.

REFERENCES

Aeroquest Airborne (2012): Report on a helicopter-borne magnetic survey (Aeroquest Job #11-046) for Geoscience BC; Geoscience BC, Report 2012-2, 11 pages.

Alldrick, D.J. (1991): Geology and ore deposits of the Stewart mining camp, British Columbia; University of British Columbia, Vancouver, Canada, unpublished Ph.D. thesis, 347 pages.

Anderson, R.G., Loveridge, W.D., and Sullivan, R.W. (1982): U-Pb isotopic ages of zircon from the Jurassic plutonic suite, Hotailuh batholith, north-central British Columbia; in Current Research, Part C, Geological Survey of Canada, Paper 22-1C, pages 133-137.

Anderson, R.G. (1983): Geology of the Hotailuh batholith and surrounding volcanic and sedimentary rocks, north-central British Columbia; Carleton University, Ottawa, Canada, unpublished Ph.D. dissertation, 669 pages.

Anderson, R.G. (1984): Late Triassic and Jurassic magmatism along the Stikine Arch and the geology of the Stikine batholith, north-central British Columbia; in Current Research, Part A, Geological Survey of Canada, Paper 84-1A, pages 67-73.

Anderson, R.G., and Bevier, M.L. (1990): A note on Mesozoic and Tertiary geochronometry of plutonic suites, Iskut River area, northwestern British Columbia; in Current Research, Part A, Geological Survey of Canada, Paper 90-1E, pages 141-147.

Anderson, R.G. and Bevier, M.L. (1992): New Late Triassic and Early Jurassic U-Pb zircon ages from the Hotailuh batholith, Cry Lake map area, north-central British Columbia; in Radiogenic Age and Isotope Studies (Report 6); Geological Survey of Canada, Paper 92-2, pages 145-152.

Asbury, D.W. (1967): Report of geological, magnetometer and geochemical soil surveys on Moss claims 53 to 71, Gnat Lake, B.C.; B.C. Ministry of Energy, Mines and Petroleum Resources, Assessment Report 1106, 10 pages.

Ash, C.H., Macdonald, R.W.J. and Friedman, R.M. (1997): Stratigraphy of the Tatogga Lake area, northwestern British Columbia (104H/12&13, 104G/9&16); B.C. Ministry of Energy, Mines and Petroleum Resources, Geological Fieldwork 1996, Paper 1997-1, pages 283-290.

Bartsch, R.D. (1993): Volcanic stratigraphy and lithochemistry of the Lower Jurassic Hazelton Gorup, host to the Eskay Creek precious and base metal volcanogenic deposit; The University of

British Columbia, Vancouver, Canada, unpublished M.Sc. thesis, 124 pages.

Boynton, W.V. (1984): Cosmochemistry of the rare earth elements; meteorite studies; in: Rare earth element geochemistry. Henderson, P. (Editors), Elsevier Sci. Publ. Co., Amsterdam, pages 63-114.

Bradford, J.A. and Brown, D.A. (1993): Geology of Bearskin Lake and southern Tatsamenie Lake map areas, Northwestern British Columbia; B.C. Ministry of Energy, Mines and Petroleum Resources, Geological Fieldwork 1992, Paper 1993-1, pages 159-176.

British Columbia Geological Survey (2012): MINFILE – British Columbia mineral deposits database; B.C. Ministry of Energy, Mines and Petroleum Resources (http://minfile.gov.bc.ca/).

Brown, D.A., Gunning, M.H. and Greig, C.J. (1996): The Stikine Project: Geology of western Telegraph Creek map area, Northwestern British Columbia; B.C. Ministry of Energy, Mines and Petroleum Resources, Bulletin 95, 175 pages.

Colpron, M. and Nelson, J.L., (2011): A digital atlas of terranes for the Northern Cordillera; B.C. Ministry of Energy and Mines, GeoFile 2011-11.

Currie, L.D. and Parrish, R.R. (1997): Paleozoic and Mesozoic rocks of Stikinia exposed in northwestern British Columbia: Implications for correlations in the northern Cordillera; Geological Society of America Bulletin, Volume 107, pages 1402-1420.

Dircks, N.J. (1974): Percussion drilling report for Railway property 104I/4W; B.C. Ministry of Energy, Mines and Petroleum Resources, Assessment Report 5298, 24 pages.

Duuring, P., Rowins, S.M., McKinley, B.S.M., Dickinson, J.M., Diakow, L.J., Kim, Y.-S. and Creaser, R.A. (2009): Magmatic and structural controls on porphyry-style Cu-Au-Mo mineralization at Kemess South, Toodoggone District of British Columbia, Canada; Mineralium Deposita, Volume 44, pages 435-462.

English, J.M. and Johnston, S.T. (2005): Collisional orogenesis in the northern Canadian Cordillera: Implications for Cordilleran crustal structure, ophiolite emplacement, continental growth, and the terrane hypothesis; Earth and Planetary Science Letters, Volume 232, pages 333-344.

Evenchick, C.A. and Thorkelson, D.J. (2005): Geology of the Spatsizi River map area, north-central British Columbia; Geological Survey of Canada, Bulletin 577, 189 pages.

Evenchick, C.A., Gabrielse, H. and Snyder, D. (2005): Crustal structure and lithology of the northern Canadian Cordillera: alternative interpretations of SNORCLE seismic reflection lines 21 and 2b; Canadian Journal of Earth Sciences, Volume 42, pages 1149-1161.

Faye, G.H., Bowman, W.S. and Sutarno, R. (1977): Zinc-copper ore RU-1: Its characterization and preparation for use as a certified reference material; Ministry of Energy, Mines and Resources Canada, Canada Centre for

Mineral and Energy Technology Report 77-7, 18 pages.

Friedman, R.M., and Ash, C.H. (1997): U-Pb ages of intrusions related to porphyry Cu-Au mineralization in the Tatogga Lake area, northwestern British Columbia (104H/12NW, 104G/9NE); B.C. Ministry of Energy, Mines and Petroleum Resources, Geological Fieldwork 1996, Paper 1997-1, pages 291-298.

Frost, B.R., Barnes, C.G., Collins, W.J., Arculus, R.J., Ellis, D.J., and Frost, C.D. (2001): A geochemical classification for granitic rocks; Journal of Petrology, Volume 42, pages 2033-2048.

Gabrielse, H. (1991): Late Paleozoic and Mesozoic terrane interactions in north-central British Columbia; Canadian Journal of Earth Sciences, Volume 28, pages 947-957.

Gabrielse, H. (1998): Geology of Cry Lake and Dease Lake map areas, north-central British Columbia; Geological Survey of Canada, Bulletin 504, 118 pages.

Geherels, G.E., (2001): Geology of the Chatham Sound region, southeast Alaska and coastal British Columbia; Canadian Journal of Earth Sciences, Volume 38, pages 1579–1599.

Geo Data Solutions Inc. (2012): Geoscience BC Aeromagnetic Survey, QUEST-Northwest Project Block 2 (Geo Data Solutions Project # P11026); Geoscience BC, Report 2012-3, 26 pages.

Gillespie, M.R. and Styles, M.T. (1999): Classification of igneous rocks; British Geological Survey, BGS Rock Classification Scheme, Volume 1, Research Report RR 99-06, 52 pages.

Govindaraju, (1994): 1994 compilation of working values and sample description for 383 geostandards; Geostandards Newsletter, Volume 18, pages 1-158.

Hallsworth, C.R. and Knox, R.W.O'B. (1999): Classification of sediments and sedimentary rocks; British Geological Survey, BGS Rock Classification Scheme, Volume 3, Research Report RR 99-03, 44 pages.

Henderson, C.M. and Perry, D.G. (1981): A Lower Jurassic heteroporid bryozoan and associated biota, Turnagain Lake, British Columbia; Canadian Journal of Earth Sciences, Volume 18, pages 457-468.

Hollis, L. (2011): Assessment report on the 2010 geological mapping, core re-logging, spectral and geophysical program at the GJ/Kinaskan Property, BC, Canada; B.C. Ministry of Energy, Mines and Petroleum Resources, Assessment Report 32303, 197 pages.

Hutchison, C.S. (1974): Laboratory handbook of petrographic techniques. John Wiley & Sons, New York, 527 pages.

International Commission on Stratigraphy (2010): International stratigraphic chart; Available online at http://www.stratigraphy.org/ics%20chart/09_2010/StratChart2010.pdf

Irvine, T.N., (1967): Chromian spinel as a petrogenetic indicator Part 2. Petrologic Applications; Canadian Journal of Earth Sciences, Volume 4, pages 71-103.

Irvine, T.N., 1974. Petrology of the Duke Island Ultra-mafic complex, Southeastern Alaska; Geological Society of America, Memoir 138, 240 pages.

Irvine, T. N. (1982): Terminology for layered intrusions; Journal of Petrology, Volume 23, pages 127-162.

Irvine, T.N. and Baragar, W.R. (1971): A Guide to the chemical classification of the common volcanic rocks; Canadian Journal of Earth Sciences, Volume 8, pages 523-548.

Ishihara, S. (1977): Ishihara,S (l977) The magnetite-series and ilmenite-series granitic rocks; Mining Geology, Volume 27, pages 293-305.

Ishihara, S. (1981): The granitoid series and mineralization; Economic Geology 75th Anniversary Volume, pages 458-484.

Ishihara, S., Hashimoto, M., Machida, M., (2000): Magnetite/ilmenite series classification and magnetic susceptibility of the Mesozoic–Cenozoic batholiths in Peru; Resource Geology 50, pages 123–129.

Iverson, O., (2012): Reassessment of Triassic and Jurassic volcanic strata in the Dease Lake region, northern British Columbia; University of Wisconsin-Eau Claire, Eau Claire (WI), U.S.A., unpublished B.Sc. thesis.

Iverson, O., Mahoney, J.B. and Logan, J.M. (2012): Dease Lake Geoscience Project, Part IV: Tsaybahe group: lithological and geochemical characterization of Middle Triassic volcanism in the Stikine Arch, North-central British Columbia. B.C. Ministry of Energy and Mines, Geological Fieldwork 2011, Paper 2012-1, pages 17-22.

Jackaman, W. (2012a): QUEST-Northwest Project: new regional geochemical survey and sample reanalysis data (NTS 104F, G, H, I, J & K), northern British Columbia; Geoscience BC, Summary of Activities 2011, Report 2012-1, pages 15-18.

Jackaman, W. (2012b): QUEST-Northwest sample reanalysis (ICP-MS) (NTS 104K); Geoscience BC, Report 2012-05, 9 pages.

Jackaman, W. (2012c): QUEST-Northwest sample reanalysis (INAA) (NTS 104F & G); Geoscience BC, Report 2012-06, 9 pages.

Jackaman, W. (2012d): QUEST-Northwest regional geochemical data (NTS 104G, H, I & J); Geoscience BC, Report 2012-07.

Kretz, R. (1983): Symbols for rock-forming minerals; American Mineralogist, Volume 68, pages 277-279.

Le Bas, M. J., Le Maitre, R. W., Streckeisen, A. and Zanettin, B. (1986): A chemical classification of volcanic rocks on the total alkali-silica diagram; Journal of Petrology, Volume 27, pages 745–750.

Logan, J.M., Drobe, J.R. and McClelland, W.C. (2000): Geology of the Forrest Kerr-Mess Creek area, northwestern British Columbia (NTS 104B/10, 15 & 104G/2 & 7W); B.C. Ministry of Energy and Mines, Bulletin 104, 132 pages.

Logan, J.M., Diakow, L.J., van Straaten, B.I., Moynihan, D.P. and Iverson, O.

(2012a): QUEST-Northwest Mapping, BC Geological Survey Dease Lake Geoscience Project, northern British Columbia; Geoscience BC, Summary of Activities 2011, Report 2012-1, pages 5-14.

Logan, J.M., Moynihan, D.P. and Diakow, L.J. (2012b): Dease Lake Geoscience Project, Part I: Geology and mineralization of the Dease Lake (104J/8) and east-half of the Little Tuya River (104J/7E) map sheets, northern British Columbia; B.C. Ministry of Energy and Mines, Geological Fieldwork 2011, Report 2012-1, pages 23-44.

Logan, J.M., Moynihan, D.P., Diakow, L.J. and van Straaten, B.I. (2012c): Dease Lake - Little Tuya River Geology, NTS 104J/ 08 & 07E; Geoscience BC, Map 2012-08-1 *and* B.C. Ministry of Energy and Mines, Open File 2012-04, 1 sheet.

MacIntyre, D.G., Villeneuve, M.E., and Schiarizza, P. (2001): Timing and tectonic setting of Stikine terrane magmatism, Babine-Takla lakes area, central British Columbia; Canadian Journal of Earth Sciences, Volume 38, pages 579–601.

Maniar, P.D. and Piccoli, P.M. (1989): Tectonic discriminations of granitoids; Geological Society of America Bulletin, 101, pages 635-643.

Marsden, H. and Thorkelson, D.J. (1992): Geology of the Hazelton volcanic belt in British Columbia: Implications for the Early to Middle Jurassic evolution of Stikinia; Tectonics, Volume 11, pages 1266-1287.

Massey, N.W.D., Alldrick, D.J. and Lefebure, D.V. (1999): Potential for subaqueous hot-spring (Eskay Creek) deposits in British Columbia; B.C. Ministry of Energy and Mines, Open File Report 1999-14, 54 pages.

Massey, N.W.D., MacIntyre, D.G., Desjardins, P.J. and Cooney, R.T. (2005): Digital geology map of British Columbia: Whole Province; B.C. Ministry of Energy, Mines and Petroleum Resources, Geofile 2005-1.

McAusland, J.H. (1971): Combined geochemical, geophysical, and geological report on mineral claims Mat 1 to Mat 26 inclusive; B.C. Ministry of Energy, Mines and Petroleum Resources, Assessment Report 3028, 9 pages.

Mihalynuk, M.G., Smith, M.T., Gabites, J.E. and Runkle, D. (1992): Age of emplacement and basement character of the Cache Creek terrane as constrained by new isotopic and geo-chemical data; Canadian Journal of Earth Sciences, Volume 29, pages 2463–2477.

Mihalynuk, M.G., Nelson, J., and Diakow, L.J. (1994a): Cache Creek Terrane entrapment; oroclinal paradox within the Canadian Cordillera: Tectonics, Volume 13, pages 575-595.

Mihalynuk, M.G., Erdmer, P., Ghent, E.D., Cordey, F., Archibald, D.A., Friedman R.M. and Johannson, G.G. (2004): Coherent French Range blueschist: Subduction to exhumation in <2.5 m.y.? Geological Society of America Bulletin Volume 116, pages 910-922.

Mortensen, J.K., Ghosh, D.K., and Ferri, F. (1995): U-Pb geochronology of

intrusive rocks associated with copper-gold porphyry deposits in the Canadian Cordillera, in Schroeter, T. G., ed., Porphyry Deposits of the north western Cordillera of North America, Canadian Institute of Mining, Metallurgy and Petroleum Special Volume 46, pages 142–158.

Moynihan, D.P. and Logan, J.M. (2012): Dease Lake Geoscience Project, Part III: Age, emplacement and mineralization of the Cretaceous Snow peak pluton; B.C. Ministry of Energy and Mines, Geological Fieldwork 2011, Report 2012-1, pages 69-74.

Nelson, J. and Mihalynuk, M. (1993): Cache Creek ocean: Closure or enclosure? Geology, Volume 21, pages 173-176.

Nixon, G.T., Ash, C.H., Connelly, J.N. and Case, G. (1989): Alaskan-type mafic-ultramafic rocks in British Columbia: The Gnat Lakes, Hickman, and Menard Creek complexes; B.C. Ministry of Energy, Mines and Petroleum Resources, Geological Fieldwork 1988, Paper 1989-1, pages 429-442.

Nixon, G.T., Hammack, J.L, Ash, C.H., Cabri, L.J., Case, G., Connelly, J.N., Heaman, L.M., Laflamme, J.H.G., Nuttall, C., Paterson, W.P.E. and Wong, R.H. (1997): Geology and platinum-group-element mineralization of Alaskan-type ultramafic-mafic complexes in British Columbia; B.C. Ministry of Energy and Mines, Bulletin 93, 132 pages.

Norris, J.R., Hart, C.J.R., Tosdal, R.M. and Rees, C. (2011): Magmatic evolution, mineralization and alteration of the Red Chris copper-gold porphyry deposit, northwestern British Columbia (NTS 104H/12W); Geoscience BC, Summary of Activities 2010, Report 2011-1, pages 33-44.

Page, J.W. (2006): Assessment report on Induced polarization and magnetometer surveys on the Gnat Pass property; B.C. Ministry of Energy, Mines and Petroleum Resources, Assessment Report 28518, 28 pages.

Pearce, J.A., Harris, N.B.W. and Tindle, A.G. (1984): Trace Element Discrimination Diagrams for the Tectonic Interpretation of Granitic Rocks; Journal of Petrology, Volume 25, Part 4, pages 956-983.

Read, P.B. (1983): Geology, Classy Creek (104J/2E) and Stikine Canyon (104J/1W), British Columbia; Geological Survey of Canada, Open File Map 940.

Read, P.B. (1984): Geology, Klastine River (104G/16E), Ealue Lake (104H/13W), Cake Hill (104I/4W) and Stikine Canyon (104J/1E), British Columbia; Geological Survey of Canada, Open File Map 1080.

Read, P.B. and Psutka, J.F. (1990): Geology, Ealue Lake east-half (104H/13E) and Cullivan Creek (104H/14) map areas, British Columbia; Geological Survey of Canada, Open File Map 2241.

Ricketts, B.D., Evenchick, C.A., Anderson, R.G. and Murphy, D.C. (1992): Bowser basin, northern British Columbia: Constraints on the timing of initial subsidence and Stikina-North America terrane interactions; Geology, Volume 20, pages 1119-1122.

Sadlier-Brown, T.L. and Chisholm, E.O. (1971): A geochemical report on the Pat

claims (1 to 24); B.C. Ministry of Energy, Mines and Petroleum Resources, Assessment Report 3963, 6 pages.

Sadlier-Brown, T.L. and Nevin, A.E. (1977): A report on geochemical and geophysical surveys of the Mac group; B.C. Ministry of Energy, Mines and Petroleum Resources, Assessment Report 6323, 33 pages.

Schiarizza, P. (2011): Geology of the Kutcho assemblage between Kutcho Creek and the Tucho River, northern British Columbia (NTS 104I/01); B.C. Ministry of Energy and Mines, Geological Fieldwork 2010, Paper 2011-1, pages 99-118.

Scott, J. E., Richards, J. P., Heaman, L. M., Creaser , R. A., and Salazar, G. S. (2008): The Schaft Creek porphyry Cu-Mo-(Au) deposit, northwestern British Columbia: Exploration and Mining Geology, Volume 17, pages 163-196.

Simpson, K.A. (2012): QUEST-Northwest: Geoscience BC's new minerals project in northwest British Columbia (104G, 104J, parts of NTS 104A,B,F,H,I,K, 103O,P); Geoscience BC, Summary of Activities 2011, Report 2012-1, pages 1-4.

Singer, D.A., Berger, V.I., Moring, B.C. (2008): Porphyry copper deposits of the world: database and grade and tonnage models; U.S. Geological Survey, Menlo Park, Open File Report 2008-1155.

Smith, G. and Garagan, T. (1990): Summary report on the 1989 exploration program on the Gnat Pass property; B.C. Ministry of Energy, Mines and Petroleum Resources, Assessment Report 20408, 156 pages.

Stevens, R.D., Delabio, R.N., and Lachance, G.R. (1982): Age determinations and geological studies, K-Ar isotopic ages, Report 15 and 16; Geological Survey of Canada, Paper 82-2, pages 3–11.

Sun, S.S., and McDonough, W.F. (1989): Chemical and isotopic systematics of oceanic basalts: Implications for mantle composition and processes; in: Magmatism in the Ocean Basins, Saunders, A.D., and Norry, M.J. (Eds.); Geological Society of London, Special Publication 42, pages 313-345.

van Straaten, B.I., Logan, J.M. and Diakow, L.J. (2012a): Dease Lake Geoscience Project, Part II: Preliminary report on the Mesozoic magmatic history and metallogeny of the Hotailuh batholith and surrounding volcanic and sedimentary rocks; B.C. Ministry of Energy and Mines, Geological Fieldwork 2011, Report 2012-1, pages 99-120.

van Straaten, B.I., Logan, J.M. and Diakow, L.J. (2012b): Mesozoic magmatic history and metallogeny of the Hotailuh batholith (NWBC); B.C. Ministry of Energy and Mines, Geofile 2012-08.

Wanless R.K., Stevens, R.D., Lachance, G.R., and Delabio, R.N. (1972): Age determinations and geological studies, K-Ar isotopic ages, Report 15; Geological Survey of Canada, Paper 71-2, pages 20–21.

West Cirque Resources Ltd. (2011a): West Cirque discovers new copper-gold zone; stakes Pliny property; West Cirque

Resources, Press Release, Aug. 11, 2011.

West Cirque Resources Ltd. (2011b): West Cirque identifies IP anomaly associated with Tanzilla alteration zone; West Cirque Resources, Press Release, Sept. 28, 2011.

Wetherill, J.F. (1989): Geological report on the Pass 40 claim; B.C. Ministry of Energy, Mines and Petroleum Resources, Assessment Report 19177, 23 pages.

Wetherill, J.F. (1990): Geological, geochemical and geophysical report on the Gnat Pass property; Equity Silver Mines Limited, B.C. Ministry of Energy, Mines and Petroleum Resources, Assessment Report 19885, 176 pages.

Woodsworth, G.J., Anderson, R.G. and Armstrong, R.L. (1991): Plutonic regimes; in Geology of the Cordilleran orogen in Canada, Gabrielse, H. and Yorath, C.J. (eds.); Geological Survey of Canada, Geology of Canada, no. 4, pages 491-531.

Zagorevski, A., Joyce, N., Mihalynuk, M. and Logan, J. (2011): Regional U/Pb zircon and Ar/Ar geochronology of Carboniferous to Early Jurassic Stikinia; AME BC Mineral Exploration Roundup, January 2011, poster presentation.

APPENDICES

Appendix 1: Location, rock type, alteration and modal mineralogy of lithogeochemistry samples

Sample no.		Sample location			Sample description*	Alteration**		Mafic mineral vol. %					Texture
Geochem.	Original	UTM E	UTM N	Unit	Rock type	Feldspar	Mafic minerals	M	Hbl	Bt	Cpx	Opx	
62187	11BVA-04-24a	449,423	6,446,393	MJ TSp	Bt-bearing Hbl S	+/- Turbid	-	15	13	2			
62188	11BVA-05-34b	448,764	6,444,221	MJ TSp	Bt-bearing SGr	+/- Turbid	-	5	1	3.5			
62189	11BVA-06-39	450,377	6,454,968	LT CH	Hbl-Cpx QMz	+/- Turbid	- (Cpx -> Hbl)	15	6		9		Foliated
62190	11BVA-09-52	448,964	6,450,050	LT GL	Plag-bearing hornblendite	+ Ser, turbid	+/- Locally Chl	80	80				Cumulate
62191	11BVA-11-60a	449,254	6,449,987	LT GL	Plag-bearing hornblendite	+ Ser, turbid	+/- Partly Chl	87	87				Cumulate
62192	11BVA-12-68a	465,787	6,447,921	MJ TSm	Bt=Cpx=Hbl QD	-	-	30	10	10	10		
62193	11BVA-14-83	467,589	6,447,538	MJ TSc	Bt-Hbl QMd	+ Ser, turbid	+ Chl	18	10	8			
62194	11BVA-15-84	466,882	6,449,220	LT CH	Hbl QMd	+/- Turbid	-	12	12				
62195	11BVA-15-89b	466,278	6,448,139	MJ TSp	Bt-bearing SGr	+/- Turbid	+/- Minor Chl	6	1	5			
62196	11BVA-16-97	470,019	6,448,963	MJ TSp	Bt-bearing SGr dike (cuts LT CH)	+/- Turbid	+/- Partly Chl	3		3			
62198	11BVA-16-97b	470,019	6,448,963	MJ TSm?	Bt-Cpx Hbl-rich QD	+/- Turbid	+/- Partly Chl	40	20	8	12		
62199	11BVA-16-97c	470,019	6,448,963	LT CH	Bt-bearing Hbl QMd-Md	+ Minor Ser, turbid	+ Chl, some Ep	12	9	3			
62200	11BVA-17-105	470,972	6,448,720	LT CH	Bt-Hbl QMd	+ Ser, turbid	+ Chl	20	14	6			
62201	11BVA-18-112	464,327	6,444,251	≤LT AP dike	Cpx Hbl-rich diabase dike (cuts LT CH)	+/- Turbid	- (Cpx -> Hbl)	40	30		10		Cpx-Plag porph.
62202	11BVA-18-114	464,615	6,444,138	LT CH	Hbl QMz	+/- Turbid	-	17	17				
62203	11BVA-18-117	465,432	6,442,450	MJ TSp	Pink Bt-Fsp porph. dike (cuts LT CH)	++ Turbid	+ Chl	1		1			
62204	11BVA-20-130b	471,886	6,438,030	LT CH	Bt-bearing Hbl QMd	+/- Turbid	+/- Bt partly Chl, Hbl fresh	18	16	2			
62205	11BVA-20-131	471,861	6,438,215	MJ TSm	Bt Hbl-rich QD	+ Ser, turbid	-	38	30	8			
62206	11BVA-21-134	472,659	6,436,308	MJ TSc	Cpx-Hbl-bearing Bt QD	+/- Minor Ser, turbid	-	16	4	8	4		
62207	11BVA-22-142	473,559	6,436,426	MJ TSc	Bt-Hbl QMd	-	+/- Bt mostly Chl, Hbl fresh	20	14	6			
62208,9	11BVA-23-152	472,774	6,435,676	MJ TSp	Hbl-bearing Bt QMz-MGr	+/- Turbid	+/- Bt partly Chl, Hbl fresh	15	5	10			
62210	11BVA-24-163	462,745	6,428,368	LT BCc	Plag-bearing clinopyroxenite	+ Ser	+/- Minor Chl	95			95		Cumulate
62211	11BVA-26-182	462,425	6,428,895	LT BC	Hbl Cpx-rich gabbro	+ Ser	+ Partly Chl	55	10	5	40		
62212	11BVA-27-193	460,851	6,429,233	LT BCw	Websterite		++ Opx completely Serp	100			50	50	Cumulate
62213	11BVA-29-205	454,926	6,455,096	LT CH	Hbl QMz-MGr	+/- Turbid	-	12	12				
62214	11BVA-30-215	480,345	6,438,923	MJ TSc	Hbl=Bt QMz	+/- Turbid	+/- Bt partly Chl, Hbl fresh	18	9	9			
62215	11BVA-30-220	480,067	6,437,062	MJ TSc	Hbl-bearing Bt MGr	+/- Turbid	-	12	5	7			
62216	11BVA-31-232	478,755	6,434,626	MJ TSp	Hbl-Bt-bearing MGr	+/- Turbid	+/- Bt partly Chl	7	3	4			
62217	11BVA-32-242	480,361	6,435,736	MJ TSf	Hbl-Bt QD	+/- Turbid	-	22	10	12			
62218	11BVA-32-244-a1	481,062	6,435,808	MJ TSf	Hbl-Bt QD	+ Ser, turbid	+ Bt partly Chl	18	6	12			
62220	11BVA-34-263	480,909	6,434,221	LT CHl	Bt=Hbl MGr	+/- Turbid	+/- Bt partly Chl, minor Ep	8	4	4			Fsp porph.
62221	11BVA-34-264	480,833	6,433,125	LT CHl	Hbl QMd-Gd	+/- Turbid	- Fresh Hbl	12	12				
62222	11BVA-35-276	480,640	6,439,273	MJ TSc	Hbl-bearing Bt QMz-MGr	+ Turbid	- Trace Chl	16	5	11			
62223	11BVA-35-283	482,014	6,439,937	LT CHq	Hbl(?)-bearing Gd	+ Turbid	++	5	5?				
62224	11BVA-38-304	481,362	6,439,991	LT CHq	Hbl-bearing Gd-MGr	+/- Turbid	-	5	5				
62225	11BVA-38-305	482,467	6,438,806	LT CHq	Hbl Gd-MGr	+/- Turbid	-	7	7				
62226	11BVA-40-317-a1	450,388	6,455,942	LT GL	Cpx Hbl-rich gabbro	++ Ser, turbid	- (Cpx -> Hbl)	60	45		15		
62227,8	11BVA-40-317-a2	450,388	6,455,942	LT GLm	Cpx Hbl-rich gabbro	++ Ser, turbid	+/- Chl (Cpx -> Hbl)	50	42		8		
62229	11BVA-27-199	462,983	6,427,463	LT BC	Cpx-bearing Hbl-rich gabbro	++ Ser, turbid, Ep?	+/- Chl, Ep present (Cpx -> Hbl)	40	35		5		
62230	11BVA-42-327	466,259	6,447,899	MJ TSc	Hbl-bearing Cpx-Bt QMd	+/- Turbid	- (Cpx -> Hbl)	30	5	15	10		
62231	11BVA-42-328	466,358	6,447,975	MJ TSp	Bt-bearing SGr	+/- Turbid	+/- Bt partly Chl	5		5			
62232	11BVA-42-329	466,997	6,448,398	MJ TSm	Hbl-rich QD	+/- Minor Ser	-	60	60				
62233	11BVA-42-330	473,470	6,438,370	MJ TSm	Hbl-rich D	+/- Minor Ser	-	60	60				
62234	11BVA-42-331	473,504	6,438,444	MJ TSp	Bt-bearing SGr	+ Some Ser, turbid	+/- Bt partly Chl	4		4			
62235	11BVA-42-332	479,794	6,436,014	MJ TSf	Hbl=Bt QD	+/- Turbid, minor Ser	+/- Bt mostly Chl	24	12	12			
62236	11BVA-42-333	463,692	6,431,161	LT CH	Hbl QMz	+/- Turbid	-	15	15				

* Abbreviations: D = Diorite, QD = Qtz-Diorite, T = Tonalite, Md = Monzodiorite, QMd = Qtz-Monzodiorite, Gd = Granodiorite, Mz = Monzonite, QMz = Qtz-Monzonite, MGr = Monzogranite, S = Syenite, QS = Qtz-Syenite, SGr = Syenogranite, porph. = porphyritic, -> = partly replaced by, mineral abbreviations after Kretz (1983)

** Alteration: - unaltered, +/- weakly, + moderately, ++ significantly altered; Turbid = turbid appearance of Fsp in PPL, Ser = Sericitized, Chl = Chloritized, Serp = Serpentinized, Ep = contains epidote

Appendix 2: Major, minor and trace element data of lithogeochemistry samples

Analyte symbol		SiO_2	Al_2O_3	Fe_2O_3[(T)]	MnO	MgO	CaO	Na_2O	K_2O	TiO_2	P_2O_5	LOI	Total
Unit		%	%	%	%	%	%	%	%	%	%	%	%
Detection limit		0.01	0.01	0.01	0.001	0.01	0.01	0.01	0.01	0.001	0.01		0.01
Analytical method*		F-ICP	F-ICP	F-ICP	F-ICP	F-ICP	F-ICP	F-ICP	F-ICP	F-ICP	F-ICP	F-ICP	F-ICP
Sample no.	**Unit**												
62187	MJ TSp	61.58	16.77	4.91	0.08	0.73	2.14	4.73	5.69	0.45	0.11	0.66	97.85
62188	MJ TSp	74.71	13.41	1.78	0.03	0.34	1.13	3.81	4.77	0.20	0.06	0.40	100.60
62189	LT CH	62.08	18.84	3.40	0.08	0.84	3.75	6.05	3.58	0.36	0.15	0.40	99.55
62190	LT GL	37.87	10.75	20.64	0.21	9.94	12.48	1.76	1.03	2.23	1.58	1.56	100.00
62191	LT GL	40.50	9.17	19.57	0.26	10.93	13.51	1.51	0.86	2.07	0.96	0.86	100.20
62192	MJ TSm	55.84	17.37	8.20	0.19	3.33	7.14	3.48	2.20	0.75	0.24	0.70	99.43
62193	MJ TSc	57.02	15.31	7.64	0.17	2.94	5.57	3.31	2.99	0.75	0.26	1.77	97.74
62194	LT CH	65.34	17.26	3.40	0.07	1.21	3.18	5.92	2.43	0.40	0.17	0.50	99.88
62195	MJ TSp	69.98	14.22	2.53	0.03	0.53	1.78	3.79	4.15	0.23	0.09	0.56	97.90
62196	MJ TSp	72.84	14.16	1.83	0.03	0.27	1.76	3.18	4.78	0.19	0.04	0.45	99.54
62198	MJ TSm?	49.50	18.24	11.47	0.22	4.67	9.62	3.49	0.90	0.85	0.14	0.67	99.77
62199	LT CH	57.12	19.39	5.01	0.11	1.50	5.94	4.60	3.02	0.58	0.30	1.19	98.75
62200 #	LT CH	58.75	16.61	6.64	0.13	2.31	5.71	3.68	3.12	0.62	0.22	0.76	98.55
62201	≤LT AP dike	48.86	16.01	11.28	0.21	5.48	10.78	2.60	1.37	0.88	0.20	1.06	98.73
62202	LT CH	64.26	15.99	4.46	0.09	1.68	3.97	4.78	3.21	0.51	0.23	0.56	99.73
62203	MJ TSp	70.80	15.55	2.33	0.04	0.33	0.64	4.71	5.02	0.27	0.06	0.53	100.30
62204	LT CH	60.67	17.01	6.92	0.14	2.15	5.57	3.93	2.72	0.53	0.24	0.58	100.50
62205	MJ TSm	53.99	17.08	8.56	0.15	3.51	7.16	3.20	2.33	0.80	0.24	1.11	98.14
62206 #	MJ TSc	60.11	17.28	6.04	0.15	1.98	4.71	4.13	3.56	0.65	0.29	0.53	99.44
62207	MJ TSc	56.08	18.76	7.64	0.15	2.92	6.09	4.04	2.52	0.71	0.29	1.55	100.80
62208,9 ##	MJ TSp	65.41	16.36	4.53	0.09	1.07	2.59	3.57	5.27	0.53	0.21	1.08	100.70
62210	LT BCc	42.79	7.59	17.93	0.21	10.47	15.46	1.12	0.95	1.10	0.23	1.14	98.99
62211	LT BC	48.99	13.60	10.94	0.21	6.42	10.95	2.59	3.68	0.76	0.71	1.25	100.10
62212	LT BCw	45.14	1.11	8.26	0.13	26.50	11.88	0.09	0.03	0.15	0.03	6.30	99.61
62213	LT CH	67.64	15.70	2.96	0.07	1.08	2.77	4.86	3.50	0.34	0.14	0.45	99.52
62214	MJ TSc	62.05	16.28	5.80	0.12	1.29	3.25	4.11	4.69	0.60	0.29	0.72	99.20
62215	MJ TSc	70.29	14.64	2.76	0.08	0.73	2.35	3.89	4.18	0.28	0.10	0.51	99.81
62216	MJ TSp	70.12	14.49	2.76	0.07	0.62	2.02	3.92	4.01	0.26	0.08	0.60	98.95
62217 #	MJ TSf	62.28	16.32	5.87	0.15	1.95	4.56	4.12	2.96	0.61	0.22	0.80	99.84
62218	MJ TSf	63.57	16.95	5.46	0.14	1.76	4.13	4.09	2.97	0.59	0.22	1.00	100.90
62220	LT CHl	71.21	14.64	2.26	0.03	0.67	2.49	3.57	4.04	0.26	0.09	0.53	99.81
62221 #	LT CHl	64.43	16.77	3.77	0.06	1.29	3.27	5.73	2.76	0.35	0.18	0.61	99.23
62222	MJ TSc	67.33	15.18	4.04	0.09	0.73	2.26	3.96	4.97	0.41	0.14	0.60	99.71
62223	LT CHq	69.26	15.95	2.21	0.03	0.31	1.89	5.76	3.20	0.27	0.10	0.45	99.44
62224	LT CHq	70.77	15.86	2.05	0.04	0.53	1.72	5.94	3.01	0.22	0.08	0.27	100.50
62225	LT CHq	69.38	15.75	2.50	0.04	0.65	2.02	5.59	3.23	0.26	0.10	0.44	99.96
62226	LT GL	40.55	15.53	15.31	0.25	6.62	12.93	2.16	1.72	1.47	1.23	1.96	99.72
62227,8 ##	LT GLm	40.98	16.30	14.20	0.24	6.18	13.10	2.23	1.65	1.38	1.18	1.68	99.11
62229	LT BC	49.08	18.66	9.30	0.24	3.62	8.74	3.09	3.68	0.78	0.80	2.00	99.97
62230	MJ TSc	54.01	16.59	9.17	0.19	3.81	8.16	3.45	1.66	0.88	0.16	0.56	98.64
62231	MJ TSp	70.84	14.00	2.70	0.03	0.50	1.77	3.66	4.08	0.24	0.07	0.54	98.42
62232	MJ TSm	50.00	16.96	11.81	0.24	5.15	9.81	2.91	1.47	0.99	0.16	0.87	100.40
62233 #	MJ TSm	45.94	16.30	15.38	0.17	5.46	9.82	2.92	0.43	1.25	0.15	1.48	99.30
62234	MJ TSp	73.27	14.13	1.93	0.02	0.33	1.35	3.59	5.13	0.19	0.04	0.23	100.20
62235	MJ TSf	60.36	17.07	6.21	0.14	2.19	4.75	4.27	3.06	0.64	0.24	0.49	99.42
62236	LT CH	64.14	16.87	4.51	0.11	1.77	3.83	5.10	3.24	0.51	0.23	0.61	100.90

* Analytical methods: F-ICP = Fusion ICP; F-MS = Fusion ICP-MS; INAA; TD-ICP = "Total" Digestion ICP

#, ## Average value of Activation Labs' duplicate analysis of powdered material, or average value of blind duplicate analysis of jaw crushed material, respectively.

Analyte symbol	Be	Sc	V	Cr	Cr	Mass	Co	Ni	Ni	Cu	Zn	Ga	Ge	As	Rb	Sr	Y	Zr	Nb	Mo	Ag	In	Sn	Sb	Cs
Unit	ppm	ppm	ppm	ppm	ppm	g	ppm	ppm	ppm	ppm	ppm	ppm	ppm	ppm	ppm	ppm	ppm	ppm	ppm	ppm	ppm	ppm	ppm	ppm	ppm
Detection limit	1	1	5	20	5		1	20	1	10	30	1	0.5	5	1	2	0.5	1	0.2	2	0.5	0.1	1	0.2	0.1
Analyt. method*	F-ICP	F-ICP	F-ICP	F-MS	INAA	INAA	F-MS	F-MS	TD-ICP	F-MS	F-MS	F-MS	F-MS	F-MS	F-MS	F-ICP	F-MS	F-MS	F-MS	F-MS	F-MS	F-MS	F-MS	F-MS	F-MS
Sample no.																									
62187	4	12	36	<20	<5	1.46	3	<20	4	20	40	20	1.5	<5	146	175	52.9	653	40.0	18	5.8	<0.1	2	0.8	1.8
62188	3	2	18	<20	<5	1.61	1	<20	2	<10	<30	14	1.7	<5	118	184	15.7	150	23.2	2	1.4	<0.1	<1	<0.2	0.7
62189	2	3	83	<20	9	1.60	4	<20	4	<10	50	21	1.3	<5	67	1504	9.0	89	3.9	<2	0.9	<0.1	<1	0.6	0.7
62190	<1	60	706	40	39	2.02	61	40	43	310	120	19	1.4	<5	9	375	27.3	50	2.1	<2	<0.5	<0.1	2	0.3	0.2
62191	1	68	668	30	37	2.00	62	60	50	130	120	18	1.9	<5	6	355	25.5	51	2.4	<2	<0.5	<0.1	2	1.6	0.2
62192	<1	22	199	<20	10	1.78	16	<20	4	10	70	19	2.0	<5	36	813	17.8	81	2.9	<2	0.7	<0.1	<1	<0.2	0.8
62193	1	21	194	<20	<5	1.79	17	<20	6	100	70	18	2.1	<5	59	577	24.8	186	5.2	<2	1.4	<0.1	1	0.6	0.6
62194	2	5	72	<20	13	1.58	5	<20	7	<10	50	22	1.4	<5	34	1222	14.1	132	5.6	<2	1.0	<0.1	<1	0.6	0.6
62195	2	3	26	<20	<5	1.68	2	<20	2	10	<30	16	1.7	<5	94	358	18.6	168	5.4	<2	1.3	<0.1	1	<0.2	0.6
62196	1	1	26	<20	<5	1.70	2	<20	2	<10	<30	15	1.3	<5	90	520	11.0	109	4.4	<2	0.8	<0.1	<1	0.4	0.9
62198	<1	30	292	<20	<5	1.81	29	<20	8	130	100	20	1.6	<5	15	956	16.6	39	1.1	<2	<0.5	<0.1	<1	<0.2	0.3
62199	1	9	72	<20	<5	1.60	6	<20	2	20	30	19	1.5	<5	47	939	23.0	222	5.0	<2	1.7	<0.1	1	0.4	0.5
62200 #	1	15	150	<20	<5	1.72	15	<20	4	20	50	18	1.8	<5	62	640	19.2	184	4.2	<2	1.5	<0.1	<1	0.4	0.8
62201	<1	34	331	50	39	1.81	36	20	25	110	110	19	1.8	<5	29	871	18.3	60	1.8	<2	<0.5	<0.1	<1	2.2	1.3
62202	2	7	92	<20	14	1.69	8	<20	8	20	60	20	1.6	<5	68	919	15.0	165	4.2	<2	1.3	<0.1	<1	0.9	0.7
62203	2	5	12	<20	<5	1.72	2	<20	2	<10	50	17	1.8	<5	98	200	27.2	231	7.4	<2	1.8	<0.1	1	1.5	0.5
62204	2	15	134	<20	<5	1.65	11	<20	3	20	50	18	1.9	<5	45	659	23.4	238	5.5	<2	1.9	<0.1	1	0.3	0.6
62205	1	22	242	<20	<5	1.75	20	<20	9	30	60	18	1.7	<5	47	732	21.0	175	3.8	<2	1.6	<0.1	<1	0.3	1.3
62206 #	2	15	121	<20	<5	1.49	11	<20	4	40	70	19	1.7	<5	78	578	26.0	168	6.0	<2	1.4	<0.1	1	0.4	1.1
62207	1	19	183	<20	<5	1.78	18	<20	6	60	70	20	1.5	<5	45	798	19.9	121	3.9	<2	1.0	<0.1	<1	0.4	0.7
62208,9 ##	2	9	71	<20	<5	1.61	8	<20	2	45	30	17	1.6	<5	124	384	25.3	300	8.9	<2	2.5	<0.1	1	0.4	1.4
62210	1	71	540	70	68	2.19	64	80	73	40	110	16	2.1	<5	18	280	14.1	46	1.3	<2	<0.5	<0.1	1	0.4	0.2
62211	2	32	307	160	140	2.02	37	40	33	230	110	16	1.8	<5	64	1056	15.7	57	2.8	<2	<0.5	<0.1	<1	0.5	0.4
62212	<1	52	75	1320	1080	1.84	84	690	666	60	40	2	2.2	<5	<1	42	2.5	3	<0.2	<2	<0.5	<0.1	<1	0.3	<0.1
62213	2	4	59	<20	10	1.66	6	<20	7	10	50	21	1.4	<5	98	891	11.8	132	6.3	<2	1.0	<0.1	<1	0.8	1.1
62214	3	11	65	<20	<5	1.63	8	<20	4	40	50	20	1.8	<5	114	435	33.3	372	9.6	<2	2.9	<0.1	2	0.7	1.4
62215	2	5	42	<20	<5	1.84	5	<20	2	70	<30	15	1.7	<5	94	341	18.2	136	5.4	<2	1.2	<0.1	<1	0.2	0.7
62216	2	4	34	<20	<5	1.70	3	<20	2	<10	<30	15	1.8	<5	93	322	15.4	159	4.8	<2	1.3	<0.1	<1	0.3	0.6
62217 #	1	12	123	<20	<5	1.57	11	<20	4	30	70	18	1.9	<5	60	561	20.2	132	4.6	<2	1.2	<0.1	<1	0.6	1.0
62218	2	12	114	<20	6	1.69	9	<20	3	30	60	18	1.7	<5	53	557	20.2	140	4.7	<2	1.0	<0.1	<1	0.7	0.7
62220	1	3	37	<20	6	1.66	2	<20	2	<10	<30	15	1.5	<5	69	416	12.5	158	5.4	<2	1.3	<0.1	<1	0.4	0.4
62221 #	1	5	75	<20	11	1.64	5	<20	7	<10	<30	21	1.3	<5	35	1152	10.5	146	3.5	<2	1.0	<0.1	<1	0.3	0.3
62222	4	7	36	<20	<5	1.84	5	<20	3	10	60	19	1.8	<5	154	241	37.9	341	11.9	<2	2.5	<0.1	1	0.9	2.0
62223	2	3	43	<20	6	1.53	1	<20	3	<10	<30	21	1.4	<5	64	999	7.8	103	3.7	<2	0.7	<0.1	<1	0.8	0.7
62224	2	2	37	<20	7	1.67	2	<20	4	<10	<30	22	0.9	<5	56	986	7.5	109	2.9	<2	0.9	<0.1	<1	0.6	0.5
62225	2	3	44	<20	<5	1.64	3	<20	4	<10	<30	21	1.4	<5	71	888	8.4	118	3.7	<2	0.8	<0.1	<1	0.6	0.6
62226	1	26	423	20	23	2.10	39	20	22	30	140	24	1.7	12	31	1148	25.1	52	3.1	<2	<0.5	<0.1	2	1.7	0.4
62227,8 ##	1	24	392	20	18	1.98	38	20	21	155	145	24	1.7	17	29	1463	23.8	51	3.0	<2	0.6	<0.1	2	0.9	0.6
62229	2	15	281	<20	<5	1.87	28	<20	7	290	120	19	1.5	<5	86	1289	19.3	53	2.4	<2	<0.5	<0.1	<1	0.5	0.7
62230	<1	24	266	<20	9	1.95	24	<20	8	80	90	20	1.8	<5	43	786	16.5	90	3.0	<2	0.7	<0.1	<1	0.5	0.8
62231	2	3	27	<20	<5	1.83	<1	<20	2	<10	<30	15	1.7	<5	88	380	21.7	131	6.7	<2	0.9	<0.1	<1	<0.2	0.7
62232	<1	40	365	<20	<5	1.85	31	<20	7	90	100	19	1.9	<5	23	705	18.5	48	1.3	<2	<0.5	<0.1	<1	0.3	0.4
62233 #	<1	53	628	<20	<5	1.93	39	30	24	320	40	19	1.7	<5	8	660	13.8	40	1.6	<2	<0.5	<0.1	1	0.4	0.2
62234	1	3	18	<20	<5	1.77	2	<20	2	<10	<30	12	1.6	<5	87	230	10.7	130	3.3	<2	1.1	<0.1	<1	<0.2	0.6
62235	1	14	142	<20	<5	1.65	12	<20	5	50	90	17	1.5	<5	53	598	19.3	118	4.4	<2	1.2	<0.1	<1	<0.2	0.9
62236	2	8	95	<20	15	1.76	8	<20	10	10	70	20	1.4	<5	70	862	19.8	161	6.7	<2	1.2	<0.1	1	0.4	1.0

Analyte symbol	Ba	La	Ce	Pr	Nd	Sm	Eu	Gd	Tb	Dy	Ho	Er	Tm	Yb	Lu	Hf	Ta	W	Tl	Pb	Bi	Th	U
Unit	ppm	ppm	ppm	ppm	ppm	ppm	ppm	ppm	ppm	ppm	ppm	ppm	ppm	ppm	ppm	ppm	ppm	ppm	ppm	ppm	ppm	ppm	ppm
Detection limit	3	0.05	0.05	0.01	0.05	0.01	0.005	0.01	0.01	0.01	0.01	0.01	0.005	0.01	0.002	0.1	0.01	0.5	0.05	5	0.1	0.05	0.01
Analyt. method*	F-ICP	F-MS	F-MS	F-MS	F-MS	F-MS	F-MS	F-MS	F-MS	F-MS	F-MS	F-MS	F-MS	F-MS	F-MS	F-MS	F-MS	F-MS	F-MS	F-MS	F-MS	F-MS	F-MS
Sample no.																							
62187	471	99.0	196.0	22.30	86.7	15.90	0.870	12.50	1.87	10.50	1.98	5.71	0.841	5.77	0.912	16.6	1.97	<0.5	0.17	15	<0.1	98.60	25.20
62188	530	37.1	64.4	6.15	20.5	3.31	0.587	2.78	0.42	2.37	0.48	1.56	0.280	2.12	0.393	3.7	2.33	<0.5	0.28	10	<0.1	17.20	3.19
62189	1995	12.2	23.7	2.72	10.3	1.81	0.714	1.55	0.23	1.41	0.29	0.92	0.153	1.15	0.182	2.2	0.26	<0.5	0.14	13	<0.1	2.10	0.98
62190	390	10.5	28.1	4.39	22.9	6.42	1.930	6.69	1.07	5.71	1.08	2.85	0.384	2.45	0.361	1.9	0.10	<0.5	<0.05	<5	<0.1	0.69	0.46
62191	268	10.1	25.8	3.74	19.1	5.34	1.720	6.29	0.92	5.18	0.99	2.68	0.372	2.39	0.366	2.0	0.10	<0.5	<0.05	<5	<0.1	0.91	0.58
62192	915	13.1	27.0	3.30	14.2	3.40	1.080	3.33	0.53	3.09	0.62	1.92	0.296	1.96	0.311	2.4	0.22	<0.5	0.13	<5	<0.1	3.26	1.48
62193	880	20.5	43.0	5.06	20.6	4.65	1.060	4.44	0.66	4.27	0.88	2.57	0.418	2.91	0.502	5.1	0.40	<0.5	0.17	7	<0.1	6.68	3.28
62194	1979	18.4	38.7	4.65	19.0	3.62	1.000	2.89	0.41	2.32	0.48	1.38	0.213	1.60	0.273	3.6	0.59	<0.5	0.16	14	<0.1	1.66	1.01
62195	1128	19.9	36.8	4.11	14.3	3.09	0.692	2.84	0.47	2.70	0.60	1.88	0.317	2.36	0.445	4.4	0.57	<0.5	0.21	<5	<0.1	9.06	2.57
62196	1988	10.8	22.6	2.64	9.4	1.98	0.567	1.57	0.29	1.67	0.34	1.12	0.202	1.58	0.270	3.4	0.72	<0.5	0.25	7	<0.1	13.30	3.80
62198	578	7.6	16.6	2.32	10.8	3.23	1.020	3.24	0.54	3.16	0.64	1.87	0.256	1.80	0.307	1.3	0.02	<0.5	0.05	<5	<0.1	0.51	0.35
62199	1481	26.1	55.9	6.87	29.2	5.71	1.920	4.95	0.71	4.14	0.86	2.45	0.388	2.64	0.427	5.4	0.31	<0.5	0.13	6	<0.1	4.64	3.13
62200 #	988	17.4	35.0	4.10	17.2	3.72	1.100	3.44	0.58	3.23	0.68	2.03	0.317	2.23	0.365	4.5	0.31	<0.5	0.18	7	<0.1	5.61	2.93
62201	467	11.5	24.4	3.21	14.4	3.60	1.260	3.88	0.56	3.41	0.66	1.94	0.299	1.87	0.301	1.8	0.15	<0.5	0.14	6	0.2	1.83	0.87
62202	1391	17.5	34.9	4.26	17.5	3.94	1.100	3.30	0.47	2.58	0.51	1.56	0.234	1.57	0.253	4.4	0.26	<0.5	0.27	12	<0.1	3.86	2.99
62203	1504	34.5	63.6	7.23	27.0	5.58	1.070	4.86	0.80	4.32	0.94	2.88	0.468	3.51	0.608	5.6	0.70	<0.5	0.32	18	0.2	12.30	5.26
62204	832	21.1	43.8	5.09	20.6	4.49	1.290	3.92	0.66	3.86	0.84	2.52	0.409	2.89	0.483	5.5	0.65	<0.5	0.14	7	<0.1	4.93	2.47
62205	822	15.5	33.7	4.29	18.1	4.43	1.230	4.30	0.64	3.55	0.72	2.17	0.321	2.26	0.389	4.0	0.30	<0.5	0.20	<5	<0.1	3.52	1.82
62206 #	1206	22.7	47.6	5.72	23.6	5.53	1.340	4.92	0.77	4.31	0.85	2.62	0.400	2.84	0.487	4.6	0.46	<0.5	0.20	10	<0.1	7.79	2.74
62207	1037	17.4	34.6	4.30	18.7	3.93	1.210	3.46	0.60	3.45	0.75	2.23	0.336	2.21	0.379	3.3	0.27	<0.5	0.14	11	<0.1	3.66	1.79
62208,9 ##	1148	25.9	50.7	5.86	22.9	4.95	0.956	4.26	0.67	4.01	0.85	2.68	0.414	3.05	0.537	7.7	0.78	<0.5	0.32	10	<0.1	15.35	7.77
62210	273	8.2	19.0	2.56	12.0	3.53	0.964	3.40	0.54	2.78	0.53	1.44	0.203	1.28	0.202	1.7	0.05	<0.5	<0.05	<5	<0.1	1.17	0.61
62211	675	16.6	33.5	4.28	17.8	4.29	1.210	4.20	0.58	3.00	0.57	1.52	0.216	1.42	0.217	1.4	0.19	<0.5	<0.05	10	<0.1	2.68	1.25
62212	56	0.6	1.9	0.32	1.6	0.56	0.148	0.57	0.10	0.52	0.10	0.29	0.040	0.23	0.034	0.1	<0.01	<0.5	<0.05	<5	<0.1	<0.05	0.01
62213	1408	22.6	36.9	4.25	16.7	3.02	0.846	2.71	0.36	1.92	0.39	1.14	0.172	1.19	0.198	3.4	0.64	<0.5	0.35	14	<0.1	6.09	1.84
62214	1149	37.6	73.1	8.35	32.7	6.92	1.520	6.05	0.95	5.70	1.13	3.68	0.576	4.03	0.729	9.3	0.77	<0.5	0.16	11	<0.1	13.10	3.95
62215	934	20.2	39.0	4.25	16.8	3.33	0.761	2.99	0.48	2.70	0.58	1.92	0.332	2.48	0.396	3.5	0.54	<0.5	0.23	8	<0.1	9.66	3.80
62216	1118	16.6	31.4	3.38	13.0	2.68	0.655	2.42	0.39	2.27	0.52	1.73	0.279	1.93	0.340	4.2	0.47	<0.5	0.22	6	<0.1	10.90	4.11
62217 #	1018	21.5	42.1	4.85	20.1	4.37	1.200	3.70	0.61	3.26	0.72	2.06	0.317	2.37	0.406	3.3	0.38	<0.5	0.20	10	<0.1	6.07	2.62
62218	1151	21.8	42.5	4.95	19.1	3.86	1.140	3.92	0.60	3.35	0.71	2.06	0.331	2.37	0.399	3.8	0.43	<0.5	0.15	9	<0.1	6.46	2.44
62220	1382	21.1	36.9	3.72	12.7	2.53	0.636	1.84	0.31	1.90	0.41	1.34	0.228	1.63	0.303	3.8	0.61	<0.5	0.15	<5	<0.1	11.20	3.49
62221 #	1774	15.6	31.7	3.78	15.0	3.12	0.920	2.41	0.34	1.75	0.35	1.00	0.150	1.05	0.180	3.6	0.28	<0.5	0.11	9	<0.1	1.53	0.69
62222	727	35.0	70.7	8.02	30.4	6.56	0.868	5.94	0.98	5.93	1.28	4.10	0.678	4.79	0.781	9.0	1.00	<0.5	0.20	16	<0.1	18.40	4.94
62223	1639	11.9	21.8	2.46	9.8	2.26	0.589	1.69	0.20	1.29	0.25	0.73	0.118	0.90	0.168	2.9	0.32	<0.5	0.20	13	<0.1	3.56	1.16
62224	1654	10.2	19.9	2.25	8.6	1.84	0.448	1.65	0.20	1.28	0.25	0.71	0.114	0.85	0.155	3.2	0.25	<0.5	0.18	9	<0.1	2.29	1.15
62225	1624	13.4	25.5	2.88	11.1	2.14	0.677	1.79	0.25	1.48	0.29	0.88	0.143	1.06	0.185	3.3	0.33	<0.5	0.17	10	<0.1	3.69	1.62
62226	656	14.2	37.4	5.57	28.6	6.81	1.980	6.88	0.94	4.89	0.94	2.56	0.337	2.15	0.359	2.3	0.13	<0.5	0.10	<5	<0.1	0.58	0.26
62227,8 ##	783	13.4	35.6	5.12	26.4	6.67	1.910	6.48	0.94	4.60	0.89	2.44	0.343	2.19	0.355	2.3	0.12	<0.5	0.08	<5	<0.1	0.58	0.23
62229	894	20.1	41.3	5.26	23.0	4.98	1.610	4.76	0.70	3.62	0.69	1.89	0.268	1.72	0.287	1.6	0.17	<0.5	0.08	8	<0.1	2.31	1.12
62230	667	11.4	22.8	2.83	12.8	2.84	1.020	3.06	0.49	2.85	0.58	1.74	0.275	1.87	0.316	2.4	0.26	<0.5	0.17	5	<0.1	3.67	1.65
62231	1153	25.7	46.7	5.22	19.7	3.83	0.645	3.16	0.51	3.20	0.71	2.25	0.389	2.82	0.491	3.7	0.82	<0.5	0.21	<5	<0.1	13.80	3.71
62232	549	8.3	17.8	2.35	11.7	2.99	1.010	3.20	0.54	3.05	0.62	1.87	0.295	1.95	0.324	1.5	0.08	<0.5	0.09	<5	<0.1	1.60	0.81
62233 #	211	11.0	21.2	2.59	12.1	2.71	1.030	3.18	0.48	2.63	0.53	1.50	0.216	1.39	0.213	1.4	0.12	1.4	<0.05	<5	0.1	1.32	1.65
62234	941	27.7	50.0	5.08	17.1	2.86	0.606	1.96	0.33	1.88	0.39	1.12	0.181	1.33	0.238	3.5	0.17	<0.5	0.27	5	<0.1	6.67	1.64
62235	1007	20.0	39.4	4.73	19.9	4.18	1.090	3.51	0.55	3.27	0.67	1.97	0.301	1.98	0.343	3.0	0.35	<0.5	0.16	8	<0.1	5.35	2.28
62236	1117	19.4	41.9	5.14	21.9	4.56	1.160	4.16	0.56	3.19	0.65	1.89	0.290	2.05	0.341	4.1	0.39	<0.5	0.24	13	0.1	4.63	2.44

Appendix 3: Quality control data of lithogeochemistry samples

	Analyte symbol		SiO_2	Al_2O_3	$Fe_2O_3^{(T)}$	MnO	MgO	CaO	Na_2O	K_2O	TiO_2	P_2O_5	LOI	Total
	Unit		%	%	%	%	%	%	%	%	%	%	%	%
	Detection limit		0.01	0.01	0.01	0.001	0.01	0.01	0.01	0.01	0.001	0.01		0.01
	Analytical method*		F-ICP	F-ICP	F-ICP	F-ICP	F-ICP	F-ICP	F-ICP	F-ICP	F-ICP	F-ICP	F-ICP	F-ICP
Sample no.#	**Orig. sample no.**	**Unit**												
62200 Dup	11BVA-17-105	LT CH	58.56	16.68	6.66	0.13	2.30	5.73	3.66	3.11	0.61	0.22	0.76	98.42
62200 Orig	11BVA-17-105	LT CH	58.93	16.55	6.62	0.13	2.32	5.70	3.69	3.14	0.62	0.22	0.76	98.67
*Difference**	*11BVA-17-105*	*LT CH*	*0.16*	*0.20*	*0.15*	*0.00*	*0.22*	*0.13*	*0.20*	*0.24*	*0.33*	*0.00*	*0.00*	*0.06*
62206 Dup	11BVA-21-134	MJ TSc												
62206 Orig	11BVA-21-134	MJ TSc												
*Difference**	*11BVA-21-134*	*MJ TSc*												
62208	11BVA-23-152	MJ TSp	64.79	16.47	4.74	0.09	1.10	2.73	3.49	5.16	0.54	0.21	1.13	100.50
62209	11BVA-23-152-2dupl	MJ TSp	66.03	16.25	4.32	0.08	1.03	2.45	3.65	5.38	0.52	0.20	1.02	100.90
*Difference**	*11BVA-23-152-2dupl*	*MJ TSp*	*0.47*	*0.34*	*2.32*	*2.27*	*1.64*	*2.70*	*1.12*	*1.04*	*0.90*	*1.22*	*2.56*	*0.10*
62217 Dup	11BVA-32-242	MJ TSf	62.50	16.44	5.86	0.15	1.95	4.52	4.17	2.99	0.61	0.22	0.80	100.20
62217 Orig	11BVA-32-242	MJ TSf	62.06	16.19	5.87	0.15	1.94	4.60	4.07	2.93	0.61	0.23	0.80	99.46
*Difference**	*11BVA-32-242*	*MJ TSf*	*0.18*	*0.38*	*0.04*	*0.33*	*0.13*	*0.44*	*0.61*	*0.51*	*0.12*	*1.11*	*0.00*	*0.19*
62221 Dup	11BVA-34-264	LT CHl												
62221 Orig	11BVA-34-264	LT CHl												
*Difference**	*11BVA-34-264*	*LT CHl*												
62227	11BVA-40-317-a2	LT GLm	40.83	16.08	14.22	0.24	6.18	13.18	2.20	1.63	1.37	1.17	1.72	98.81
62228	11BVA-40-317-a2-2dupl	LT GLm	41.13	16.51	14.17	0.24	6.18	13.02	2.26	1.66	1.39	1.19	1.64	99.40
*Difference**	*11BVA-40-317-a2*	*LT GLm*	*0.18*	*0.66*	*0.09*	*0.21*	*0.00*	*0.31*	*0.67*	*0.46*	*0.40*	*0.42*	*1.19*	*0.15*
62233 Dup	11BVA-42-330	MJ TSm	45.69	16.32	15.41	0.17	5.49	9.82	2.90	0.42	1.25	0.15	1.48	99.09
62233 Orig	11BVA-42-330	MJ TSm	46.18	16.29	15.36	0.17	5.44	9.82	2.95	0.44	1.25	0.15	1.48	99.51
*Difference**	*11BVA-42-330*	*MJ TSm*	*0.27*	*0.05*	*0.08*	*0.00*	*0.23*	*0.00*	*0.43*	*1.16*	*0.12*	*0.00*	*0.00*	*0.11*
62197	11BVA-50-503blank	Blank	99.78	0.04	0.47	0.00	<0.01	0.01	0.01	<0.01	<0.001	<0.01	0.19	100.50
62250	11DMO50-505blank	Blank	99.89	0.06	0.40	0.00	0.01	0.02	0.02	<0.01	0.00	<0.01	0.08	100.50
*Difference**	*Blank*	*Blank*	*0.03*	*10.00*	*4.02*	*0.00*		*16.67*	*16.67*				*20.37*	*0.00*
62274	MRG1standard	Standard	39.63	8.40	17.32	0.17	13.65	14.77	0.71	0.18	3.79	0.06	1.38	100.10
Expected##	MRG1standard	Standard	**39.12**	**8.47**	**17.94**	**0.17**	**13.55**	**14.70**	**0.74**	**0.18**	**3.77**	**0.08**	**2.23**	100.95
*Difference**	*MRG1standard*	*Standard*	*0.32*	*-0.21*	*-0.88*	*-0.45*	*0.18*	*0.12*	*-1.03*	*0.00*	*0.16*	*-7.14*	*-11.77*	*-0.21*
62275 Dup	SY3standard	Standard	59.24	11.47	6.53	0.32	2.61	8.14	3.98	4.27	0.15	0.55	1.19	98.45
62275 Orig	SY3standard	Standard	59.85	11.67	6.46	0.32	2.61	8.03	4.07	4.39	0.15	0.55	1.19	99.28
Expected##	SY3standard	Standard	**59.68**	**11.76**	**6.49**	**0.32**	**2.67**	**8.25**	**4.12**	**4.23**	**0.15**	**0.54**	**1.31**	99.52
*Difference**	*SY3standard*	*Standard*	*-0.18*	*-0.62*	*0.15*	*0.23*	*-0.57*	*-0.34*	*-0.86*	*0.24*	*-0.68*	*0.46*	*-2.40*	*-0.27*
*Difference**	*SY3standard*	*Standard*	*0.07*	*-0.19*	*-0.12*	*0.00*	*-0.57*	*-0.68*	*-0.31*	*0.93*	*-0.17*	*0.46*	*-2.40*	*-0.06*

* Difference calculated as follows: |0.5*100*{(x1-x2)/(x1+x2)}|

** Analytical methods: F-ICP = Fusion ICP; F-MS = Fusion ICP-MS; INAA = Instrumental Neutron Activation Analysis; TD-ICP = "Total" Digestion ICP

Analyses with the same sample number are Activation Labs' duplicates of powdered material. Analyses with a different sample number are blind duplicates of jaw crushed material

Recommended values for CANMET standards (Govindaraju, 1994) in bold, proposed values underlined, informational values in normal font

Analyte symbol	Be	Sc	V	Cr	Cr	Mass	Co	Ni	Ni	Cu	Zn	Ga	Ge	As	Rb	Sr	Y	Zr	Nb	Mo	Ag	In	Sn	Sb	Cs
Unit	ppm	ppm	ppm	ppm	ppm	g	ppm	ppm	ppm	ppm	ppm	ppm	ppm	ppm	ppm	ppm	ppm	ppm	ppm	ppm	ppm	ppm	ppm	ppm	ppm
Detection limit	1	1	5	20	5		1	20	1	10	30	1	0.5	5	1	2	0.5	1	0.2	2	0.5	0.1	1	0.2	0.1
Analyt. method*	F-ICP	F-ICP	F-ICP	F-MS	INAA	INAA	F-MS	F-MS	TD-ICP	F-MS	F-MS	F-MS	F-MS	F-MS	F-MS	F-ICP	F-MS	F-MS	F-MS	F-MS	F-MS	F-MS	F-MS	F-MS	F-MS
Sample no.																									
62200 Dup	1	15	151	<20			16	<20		20	50	18	1.8	<5	62	639	19.1	179	4.1	<2	1.5	<0.1	1	0.4	0.8
62200 Orig	1	15	150	<20			14	<20		20	50	18	1.8	<5	62	640	19.4	189	4.3	<2	1.5	<0.1	<1	0.4	0.8
*Difference**	*0*	*0*	*0*				*3*			*0*	*0*	*0*	*0.0*		*0*	*0*	*0.4*	*1*	*1.2*		*0.0*			*0.0*	*0.0*
62206 Dup									4																
62206 Orig									3																
*Difference**									*7*																
62208	2	9	73	<20	<5	1.63	7	<20	2	40	30	17	1.5	<5	120	392	25.9	294	8.9	<2	2.5	<0.1	1	0.4	1.3
62209	2	8	68	<20	<5	1.59	8	<20	2	50	<30	17	1.7	<5	127	375	24.6	305	8.9	<2	2.5	<0.1	1	0.4	1.5
*Difference**	*0*	*3*	*2*			*0.62*	*3*		*0*	*6*		*0*	*3.1*		*1*	*1*	*1.3*	*1*	*0.0*		*0.0*		*0*	*0.0*	*3.6*
62217 Dup	1	12	124	<20			10	<20		30	70	17	2.0	<5	60	560	20.0	136	4.4	<2	1.1	<0.1	<1	0.6	1.0
62217 Orig	1	12	123	<20			11	<20		30	70	18	1.8	<5	61	561	20.4	128	4.7	<2	1.2	<0.1	<1	0.6	1.0
*Difference**	*0*	*0*	*0*				*2*			*0*	*0*	*1*	*2.6*		*0*	*0*	*0.5*	*2*	*1.6*		*2.2*			*0.0*	*0.0*
62221 Dup									7																
62221 Orig									7																
*Difference**									*0*																
62227	1	24	392	20	21	1.87	37	<20	21	150	150	24	1.5	17	29	1452	23.5	53	3.0	<2	0.6	<0.1	2	0.9	0.6
62228	1	24	392	20	15	2.09	38	20	21	160	140	24	1.9	16	29	1473	24.0	48	3.0	<2	<0.5	<0.1	2	0.9	0.6
*Difference**	*0*	*0*	*0*	*0*	*8*	*2.78*	*1*		*0*	*2*	*2*	*0*	*5.9*	*2*	*0*	*0*	*0.5*	*2*	*0.0*				*0*	*0.0*	*0.0*
62233 Dup	<1	53	626	<20			39	30		310	40	19	1.7	<5	8	660	13.6	38	1.6	<2	<0.5	<0.1	1	0.2	0.3
62233 Orig	<1	53	629	<20			38	30		320	40	19	1.7	<5	8	661	13.9	41	1.6	<2	<0.5	<0.1	1	0.6	0.2
*Difference**		*0*	*0*				*1*	*0*		*1*	*0*	*0*	*0.0*		*0*	*0*	*0.5*	*2*	*0.0*				*0*	*25.0*	*10.0*
62197	<1	<1	<5	<20	10	1.63	<1	<20	2	<10	<30	<1	2.1	<5	<1	<2	<0.5	<1	<0.2	<2	<0.5	<0.1	<1	<0.2	<0.1
62250	<1	<1	<5	<20	11	1.93	<1	<20	<1	<10	<30	<1	1.5	<5	<1	<2	<0.5	<1	<0.2	<2	<0.5	<0.1	<1	<0.2	<0.1
*Difference**					*2*	*4.21*							*8.3*												
62274	<1	54	541	430	440	1.67	79	170	179	130	220	19	1.4	<5	7	270	12.1	99	18.1	<2	1.2	<0.1	6	0.7	0.6
Expected#	1	**55**	**526**	430	430		**87**	**193**	**193**	**134**	**191**	17		1	9	**266**	14.0	**108**	20.0	1	0.1		4	0.9	0.6
*Difference**		*0*	*1*	*0*	*1*		*-2*	*-3*	*-2*	*-1*	*4*	*3*			*-5*	*0*	*-3.6*	*-2*	*-2.5*		*41.6*		*13*	*-5.1*	*1.3*
62275 Dup	24	8	55	<20			7	<20		20	250	33	2.2	18	195	301	675.0	357	183.0	<2	2.3	<0.1	8	0.2	2.6
62275 Orig	24	8	55	<20			8	<20		10	250	32	2.6	19	198	303	674.0	345	180.0	<2	2.4	<0.1	7	6.4	2.7
Expected#	20	7	50	11	11		9	11	11	17	**244**	**27**	1.4	19	**206**	**302**	**718.0**	320	148.0	1	1.5		7	0.3	2.5
*Difference**	*5*	*4*	*2*				*-6*			*4*	*1*	*5*	*11.1*	*-1*	*-1*	*0*	*-1.5*	*3*	*5.3*		*10.5*		*5*	*-10.8*	*1.0*
*Difference**	*5*	*4*	*2*				*-2*			*-13*	*1*	*4*	*15.0*	*0*	*-1*	*0*	*-1.6*	*2*	*4.9*		*11.5*		*2*	*45.4*	*1.9*

Analyte symbol	Ba	La	Ce	Pr	Nd	Sm	Eu	Gd	Tb	Dy	Ho	Er	Tm	Yb	Lu	Hf	Ta	W	Tl	Pb	Bi	Th	U
Unit	ppm	ppm	ppm	ppm	ppm	ppm	ppm	ppm	ppm	ppm	ppm	ppm	ppm	ppm	ppm	ppm	ppm	ppm	ppm	ppm	ppm	ppm	ppm
Detection limit	3	0.05	0.05	0.01	0.05	0.01	0.005	0.01	0.01	0.01	0.01	0.01	0.005	0.01	0.002	0.1	0.01	0.5	0.05	5	0.1	0.05	0.01
Analyt. method*	F-ICP	F-MS	F-MS	F-MS	F-MS	F-MS	F-MS	F-MS	F-MS	F-MS	F-MS	F-MS	F-MS	F-MS	F-MS	F-MS	F-MS	F-MS	F-MS	F-MS	F-MS	F-MS	F-MS
Sample no.																							
62200 Dup	984	16.80	34.50	4.02	16.60	3.60	1.100	3.39	0.56	3.21	0.67	1.98	0.306	2.16	0.357	4.5	0.31	<0.5	0.20	8	<0.1	5.61	2.91
62200 Orig	992	18.00	35.60	4.18	17.80	3.84	1.100	3.50	0.60	3.25	0.70	2.08	0.328	2.30	0.372	4.5	0.31	<0.5	0.16	7	<0.1	5.62	2.96
*Difference**	*0*	*1.72*	*0.78*	*0.98*	*1.74*	*1.61*	*0.000*	*0.80*	*1.72*	*0.31*	*1.09*	*1.23*	*1.735*	*1.57*	*1.0*	*0.0*	*0.00*		*5.56*	*3*		*0.04*	*0.43*
62206 Dup																							
62206 Orig																							
*Difference**																							
62208	1143	26.10	51.50	5.93	23.00	5.08	0.944	4.33	0.66	4.11	0.85	2.67	0.409	3.07	0.529	7.5	0.76	<0.5	0.33	10	<0.1	14.20	7.36
62209	1152	25.70	49.80	5.79	22.80	4.82	0.968	4.18	0.67	3.91	0.85	2.69	0.418	3.03	0.545	7.8	0.80	<0.5	0.30	10	<0.1	16.50	8.17
*Difference**	*0*	*0.39*	*0.84*	*0.60*	*0.22*	*1.31*	*0.628*	*0.88*	*0.38*	*1.25*	*0.00*	*0.19*	*0.544*	*0.33*	*0.7*	*1.0*	*1.28*		*2.38*	*0*		*3.75*	*2.61*
62217 Dup	1021	21.40	41.80	4.79	19.40	4.19	1.140	3.74	0.64	3.28	0.72	2.07	0.316	2.40	0.407	3.4	0.37	<0.5	0.20	10	<0.1	6.06	2.58
62217 Orig	1015	21.60	42.40	4.92	20.70	4.55	1.260	3.66	0.58	3.25	0.73	2.04	0.318	2.35	0.405	3.3	0.39	<0.5	0.21	10	<0.1	6.08	2.67
*Difference**	*0*	*0.23*	*0.36*	*0.67*	*1.62*	*2.06*	*2.500*	*0.54*	*2.46*	*0.23*	*0.34*	*0.36*	*0.158*	*0.53*	*0.1*	*0.7*	*1.32*		*1.22*	*0*		*0.08*	*0.86*
62221 Dup																							
62221 Orig																							
*Difference**																							
62227	779	13.30	35.40	5.01	26.70	6.62	1.970	6.78	0.93	4.57	0.90	2.45	0.332	2.09	0.338	2.3	0.14	<0.5	0.07	<5	<0.1	0.55	0.23
62228	787	13.50	35.70	5.22	26.10	6.72	1.850	6.18	0.94	4.62	0.87	2.43	0.353	2.28	0.372	2.3	0.10	<0.5	0.08	<5	<0.1	0.61	0.22
*Difference**	*0*	*0.37*	*0.21*	*1.03*	*0.57*	*0.37*	*1.571*	*2.31*	*0.27*	*0.27*	*0.85*	*0.20*	*1.533*	*2.17*	*2.4*	*0.0*	*8.33*		*3.33*			*2.59*	*1.11*
62233 Dup	210	11.10	21.60	2.55	12.00	2.82	1.040	3.22	0.48	2.65	0.52	1.49	0.218	1.39	0.216	1.5	0.12	1.3	<0.05	<5	0.1	1.34	1.64
62233 Orig	211	11.00	20.80	2.63	12.10	2.60	1.020	3.14	0.48	2.60	0.53	1.50	0.213	1.39	0.21	1.4	0.12	1.5	0.05	<5	0.1	1.30	1.66
*Difference**	*0*	*0.23*	*0.94*	*0.77*	*0.21*	*2.03*	*0.485*	*0.63*	*0.00*	*0.48*	*0.48*	*0.17*	*0.580*	*0.00*	*0.7*	*1.7*	*0.00*	*3.6*			*0.0*	*0.76*	*0.30*
62197	3	0.16	0.35	0.04	<0.05	0.02	<0.005	0.01	<0.01	<0.01	<0.01	<0.01	<0.005	<0.01	<0.002	<0.1	<0.01	<0.5	<0.05	<5	<0.1	<0.05	<0.01
62250	3	0.34	0.76	0.08	0.32	0.08	0.011	0.06	<0.01	0.02	<0.01	<0.01	<0.005	0.01	0.004	<0.1	<0.01	<0.5	<0.05	<5	<0.1	0.09	0.01
*Difference**	*0*	*18.00*	*18.47*	*16.67*		*30.00*		*35.71*															
62274	52	9.21	25.70	3.63	17.20	4.28	1.500	4.13	0.55	2.80	0.51	1.20	0.133	0.77	0.12	3.8	0.87	<0.5	<0.05	9	0.2	0.83	0.30
Expected#	61	**9.80**	26.00	3.40	**19.20**	**4.50**	**1.390**	4.00	**0.51**	2.90	**0.49**	1.12	0.110	0.60	0.12	**3.76**	**0.80**	0.3	0.06	10	0.13	0.93	0.24
*Difference**	*-4*	*-1.55*	*-0.29*	*1.64*	*-2.75*	*-1.25*	*1.903*	*0.80*	*1.89*	*-0.88*	*1.00*	*1.72*	*4.733*	*6.20*	*0.0*	*0.3*	*2.10*			*-3*	*10.6*	*-2.84*	*5.56*
62275 Dup	448	1210	2150	208	688	118	17.000	106.00	19.20	118.00	24.80	77.10	11.300	63.60	8.54	9.8	24.90	<0.5	1.27	372	0.3	984	670
62275 Orig	452	1220	2150	209	691	119	17.000	102.00	19.30	117.00	26.10	78.30	11.300	64.30	8.47	10.6	24.40	<0.5	1.34	415	0.4	999	663
Expected#	450	**1340**	**2230**	**223**	670	109	**17.000**	**105.00**	18.00	118.00	**29.50**	68.00	**11.600**	62.00	7.9	9.7	**30.00**	**1.1**	1.50	**133**	0.8	**1003**	**650**
*Difference**	*0*	*-2.55*	*-0.91*	*-1.74*	*0.66*	*1.98*	*0.000*	*0.24*	*1.61*	*0.00*	*-4.33*	*3.14*	*-0.655*	*0.64*	*1.9*	*0.3*	*-4.64*		*-4.15*	*24*	*-22.7*	*-0.48*	*0.76*
*Difference**	*0*	*-2.34*	*-0.91*	*-1.62*	*0.77*	*2.19*	*0.000*	*-0.72*	*1.74*	*-0.21*	*-3.06*	*3.52*	*-0.655*	*0.91*	*1.7*	*2.2*	*-5.15*		*-2.82*	*26*	*-16.7*	*-0.10*	*0.50*

APPENDIX 4: GEOCHRONOLOGY METHODOLOGIES

Zircon U-Pb LA-ICP-MS

Zircons were extracted using standard mineral separation techniques at the laboratories of Apatite To Zircon Inc. (Viola, Idaho, USA). Zircons (both standards and unknowns) were mounted in 1 cm^2 epoxy wafers, and ground down to expose internal grain surfaces prior to final polishing. The wafers were etched in 5.5N HNO_3 for 20 seconds at 21°C to thoroughly clean the surface of the grains prior to analysis. A representative suite of grains of all sizes and morphologies, and the locations for laser spots on these grains, were selected using transmitted light with an optical microscope at a magnification of 2000x.

Isotopic analyses were performed with a New Wave UP-213 laser ablation system in conjunction with a ThermoFinnigan Element2 single collector double-focusing magnetic sector inductively coupled plasma mass spectrometer (LA-ICP-MS) in the GeoAnalytical Lab at Washington State University (Pullman, WA, USA). For all analyses (both standard and unknown), the diameter of the laser-beam was set at 20 μm and the laser frequency was set at 5 Hz, yielding ablation pits approximately 10-15 μm deep. He and Ar gas were used to deliver the ablated material into the plasma source of the mass spectrometer. Each analysis of 250 cycles took approximately 30 seconds to complete, and consisted of a 6 second integration on peaks with the laser turned off (for background measurements), followed by a 25 second integration with the laser firing. A delay of up to 30 seconds occurred between analyses in order to purge the previous analysis and prepare for the next. The isotopes measured included ^{202}Hg, $^{204}(Hg + Pb)$, ^{206}Pb, ^{207}Pb, ^{208}Pb, ^{232}Th, ^{235}U, and ^{238}U. The Element2 detector was set at analog mode for ^{232}Th and ^{238}U, and at pulse counting mode for all other isotopes. Common Pb correction was made by using the measured ^{204}Pb content and assuming an initial Pb composition from Stacey and Kramers (1975).

Interelement fractionation of Pb/U is generally <20%, whereas fractionation of Pb isotopes is generally <5%. At the beginning of each LA-ICP-MS session, zircon standards Tardree (61.23±0.11 Ma) and FC1 (1099±0.6 Ma) were analyzed until fractionation was stable and the variance in the measured $^{206}Pb/^{238}U$ and $^{207}Pb/^{206}Pb$ ratios was at or near 1 percent. In order to monitor interelement fractionation during the session, these standards were generally reanalyzed each 15-25 unknowns. Fractionation also increases with depth into the laser pit. The accepted isotopic ratios were accordingly determined by least-squares projection through the measured values back to the initial determination.

For each spot, fractionation factor-corrected isotopic ratios and ages were calculated using data collected during scans 70-250 for each analysis. The laser is blocked during the first ca. 50 scans and the laser is fired during the remaining ca. 200 scans. Using the fitted polynomials routine LFIT from Press et al. (1992), the calculated values at the last scan (at scan 40 for a scan range of 20-40) are used as the background values. Fits to individual isotopic signal intensities versus scan number for each spot analyzed (scan number correlating with depth within the ablation pit from which material is derived for ICP analysis) is performed using the sum of multiple Gaussian equations. This approach was adopted because it

permits the accurate description of complicated signal intensity versus scan profiles. Complicated isotopic signal profiles are the rule, not the exception for natural zircon crystals due to chemical zoning. Fitting is performed using the Levenberg-Marquardt method (routine MRQMIN from Press et al., 1992) by chi-squared minimization. The standard deviation of each isotopic signal intensity is calculated using routine STEYX from Excel® and the quality of fit is assessed by determining the probability of a greater chi-squared using routine GAMMQ from Press et al. (1992). Up to 181 individual scans, each yielding isotopic ratios and ages, are used for calculation of isotopic ratios and ages.

Errors for the isotopic ratios and ages are based on the fitting errors of the respective isotopes. Errors are reported at 2σ and using the method outlined above include all analytical and machine errors.

Detailed review of the LA-ICP-MS data identified several issues that caused some spurious age results. This affected a subset of the preliminary age dates reported in van Straaten et al. (2012). Revised age dates are presented here. Two issues that were apparent in the data include 1) switch from pulse to analog mode counting for ^{238}U during analyses of some samples, causing apparent bimodal age distributions. This has been recovered using the well-measured ^{235}U to calculate ^{238}U, using the accepted value for the $^{238}U/^{235}U$ ratio of 137.88. 2) A marked shift in background signal for ^{202}Hg, $^{204}(Hg+Pb)$, and to a lesser extent also ^{206}Pb and ^{207}Pb, after sample 1226-8 was analyzed. Generally, a continuous polynomial function is fitted through the background data of one session (samples 1226-1, 2, 3, 4, 5, 7, 8, 9, 10). The drop in background values during analysis of samples 1226-9 and 1226-10 caused a significant misfit with age standards analyzed near the end of the session. The data has been improved by fitting a separate polynomial function to the background data for the first (samples 1226-1, 2, 3, 4, 5, 7, 8) and last (samples 1226-9, 10) parts of the session.

The weighted average age of a sample is calculated by weighting the selected data points by the inverse-square of their assigned 2 sigma errors. The 2 sigma internal error of the age of a sample is the error propagated from the assigned data point errors alone. Both parameters were calculated using the 'weighted average' subroutine in Isoplot 3.6 (developed by K.R. Ludwig, 2008). In all cases, the 'probability of fit' (the probability that the assigned errors will yield at least the amount of scatter actually observed) was greater than 0.15, validating the use of the 2 sigma internal error.

Hornblende/biotite Ar-Ar

Methodology

The samples were crushed in a ring mill, washed in distilled water and ethanol, and sieved when dry to -40+60mesh. Appropriate mineral grains were picked out of the bulk fraction. Mineral separates were wrapped in aluminum foil and stacked in an irradiation capsule with similar-aged samples and neutron flux monitors (Fish Canyon Tuff sanidine (FCs), 28.03 Ma (Renne et al., 1998).

The samples were irradiated on October 25-26, 2011 at the McMaster Nuclear Reactor in Hamilton, Ontario, Canada, for 45 MWH, with a neutron flux of approximately $6 \cdot 10^{13}$ neutrons/cm^2/s. Analyses (n=30) of 10 neutron flux monitor positions produced errors of <0.5% in the J value.

The samples were analyzed during November and December 2011 at the Noble Gas Laboratory, Pacific Centre for Isotopic and Geochemical Research, University of British Columbia, Vancouver, BC, Canada. The mineral separates were step-heated at incrementally higher powers in the defocused beam of a 10 W CO_2 laser (New Wave Research MIR10) until fused. The gas evolved from each step was analyzed by a VG5400 mass spectrometer equipped with an ion-counting electron multiplier. All measurements were corrected for total system blank, mass spectrometer sensitivity, mass discrimination, radioactive decay during and subsequent to irradiation, as well as interfering Ar from atmospheric contamination and the irradiation of Ca, Cl and K (Isotope production ratios: $(^{40}Ar/^{39}Ar)K = 0.0302 \pm 0.00006$, $(^{37}Ar/^{39}Ar)Ca = 1416.4 \pm 0.5$, $(^{36}Ar/^{39}Ar)Ca = 0.3952 \pm 0.0004$, $Ca/K = 1.83 \pm 0.01(^{37}ArCa/^{39}ArK)$).

Data processing

Details of the analyses, including plateau (spectrum) and inverse correlation ages, are presented in Appendix 6. Initial data entry and calculations were carried out using the software ArArCalc (Koppers, 2002). The plateau and correlation ages were calculated using Isoplot ver.3.09 (Ludwig, 2003). Errors are quoted at the 2-sigma (95% confidence) level and are propagated from all sources except mass spectrometer sensitivity and age of the flux monitor. The best statistically-justified plateau and plateau age were picked based on the following criteria:

- Three or more contiguous steps comprising more than 60% of the ^{39}Ar;
- Probability of fit of the weighted mean age greater than 5%;
- Slope of the error-weighted line through the plateau ages equals zero at 5% confidence;
- Ages of the two outermost steps on a plateau are not significantly different from the weighted-mean plateau age (at 1.8σ six or more steps only);
- Outermost two steps on either side of a plateau must not have nonzero slopes with the same sign (at 1.8σ nine or more steps only)

The two standard deviation error on all plateau ages includes a J-error of 0.6%.

REFERENCES

Koppers, A.A.P. (2002). ArArCALC – software for $^{40}Ar/^{39}Ar$ age calculations. Computers and Geosciences 28 (2002) 605-619.

Ludwig, K.R. (2003). Isoplot 3.09 A Geochronological Toolkit for Microsoft Excel. Berkeley Geochronology Center, Special Publication No. 4

Renne, P.R., C.Swisher, C.C., III, Deino, A.L., Karner, D.B., Owens, T. and DePaolo, D.J., (1998). Intercalibration of standards, absolute ages and uncertainties in $^{40}Ar/^{39}Ar$ dating. Chemical Geology, 145(1-2): 117-152.

van Straaten, B.I., Logan, J.M., Diakow, L.J. (2012). Dease Lake Geoscience Project, Part II: Preliminary report on the Mesozoic magmatic history and metallogeny of the Hotailuh batholith and surrounding volcanic and sedimentary rocks. BC Ministry of Energy and Mines, Geological Fieldwork 2011, Report 2012-1, pages 99-120.

Appendix 5: Zircon U-Pb LA-ICP-MS geochronology data

Zircon U-Pb LA-ICP-MS data for sample 11JLO32-319

Analysis	Isotopic ratios[1]					Age (Ma)[2]	
	$^{238}U/^{206}Pb$	±2σ abs	$^{207}Pb/^{206}Pb$	±2σ abs	Rho	$^{206}Pb/^{238}U$	±2σ abs
12265AZ1_1	28.737	0.469	0.05281	0.00356	0.04	220.51	9.29
12265AZ1_2	21.264	0.286	0.05351	0.00291	0.09	296.25	12.24
12265AZ1_3	20.931	0.966	0.23190	0.04177	0.29	251.26	-30.74 +42.23
12265AZ1_4	29.199	0.582	0.05163	0.00186	0.24	217.08	9.70
12265AZ1_5	29.123	0.649	0.05216	0.00336	0.10	217.63	9.77
12265AZ1_6	28.194	0.577	0.05351	0.00380	0.09	224.68	10.08
12265AZ1_7	29.151	0.659	0.05364	0.00399	0.07	217.43	9.76
12265AZ1_8	29.530	0.507	0.05002	0.00206	0.13	214.69	9.19
12265AZ1_9	26.394	0.641	0.05430	0.00405	0.06	239.72	10.90
12265AZ1_10	29.317	0.374	0.05027	0.00162	0.15	216.22	9.19
12265AZ1_11	29.153	0.355	0.05133	0.00163	0.15	217.42	9.18
12265AZ1_12	29.407	2.132	0.05096	0.00491	0.37	215.57	17.59
12265AZ1_13	28.959	1.608	0.05339	0.00397	0.36	218.85	14.69
12265AZ1_15	22.575	1.063	0.05964	0.02906	0.02	279.41	16.69
12265AZ1_16	29.235	0.324	0.05057	0.00154	0.13	216.81	8.92
12265AZ1_17	17.087	0.660	0.32438	0.06790	0.25	230.88	-31.74 +47.00
12265AZ1_18	29.102	0.574	0.05254	0.00426	0.03	217.79	9.57
12265AZ1_19	29.175	0.547	0.05467	0.00395	0.04	217.26	9.64
12265AZ1_20	27.609	0.549	0.05159	0.00213	0.16	229.36	10.26
12265AZ1_21	29.756	0.744	0.05266	0.00369	0.11	213.08	9.94
12265AZ1_22	29.865	1.961	0.05242	0.00409	0.48	212.31	15.99
12265AZ1_23	29.203	0.598	0.05201	0.00344	0.10	217.05	9.57
12265AZ1_24	28.817	0.374	0.05167	0.00249	0.11	219.91	9.16
12265AZ1_25	28.721	0.398	0.05065	0.00219	0.09	220.63	9.32
12265AZ1_26	28.847	0.342	0.05084	0.00214	0.07	219.68	7.53
12265AZ1_27	28.346	0.400	0.05177	0.00248	0.09	223.50	7.90
12265AZ1_28	29.060	0.736	0.05131	0.00251	0.24	218.10	8.96
12265AZ1_29	28.434	0.494	0.05135	0.00175	0.26	222.82	8.30
12265AZ1_30	29.603	0.545	0.05106	0.00255	0.14	214.16	7.89
12265AZ1_31	29.334	0.430	0.04979	0.00183	0.13	216.10	7.61
12265AZ1_32	30.275	0.384	0.05030	0.00153	0.19	209.49	7.33
12265AZ1_33	30.086	0.376	0.05121	0.00181	0.14	210.78	7.44
12265AZ1_34	29.836	0.445	0.05251	0.00334	0.04	212.52	7.50
12265AZ1_35	29.703	0.856	0.05163	0.00177	0.57	213.46	9.19
12265AZ1_36	29.207	0.756	0.05088	0.00263	0.25	217.02	8.85
12265AZ1_37	29.533	1.744	0.05203	0.00362	0.43	214.66	14.30
12265AZ1_38	28.091	1.761	0.05048	0.00424	0.35	225.49	15.63
12265AZ1_39	29.719	0.853	0.05322	0.00346	0.16	213.34	9.05
12265AZ1_40	29.717	0.594	0.05180	0.00320	0.11	213.36	8.13
12265AZ1_41	29.666	0.655	0.05160	0.00417	0.06	213.72	8.24
12265AZ1_42	29.496	0.348	0.05194	0.00225	0.08	214.93	7.50
12265AZ1_43	29.144	0.383	0.05098	0.00180	0.16	217.48	7.61
12265AZ1_44	29.976	0.595	0.05343	0.00360	0.07	211.54	8.09
12265AZ1_45	29.175	0.708	0.05149	0.00305	0.18	217.26	8.72
12265AZ1_46	30.003	0.860	0.05320	0.00303	0.21	211.35	9.03
12265AZ1_47	29.355	1.132	0.05714	0.00564	0.14	215.95	10.65
12265AZ1_48	29.733	0.712	0.05460	0.00462	0.10	213.25	8.51
12265AZ1_49	29.292	0.483	0.05385	0.00332	0.04	216.40	7.88
12265AZ1_50	28.968	0.347	0.05000	0.00215	0.09	218.78	7.60

[1] Data not corrected for common lead

[2] Data not corrected for common lead, except underlined values

Zircon U-Pb LA-ICP-MS data for sample 11BVA31-232

Analysis	Isotopic ratios[1]					Age (Ma)[1]	
	$^{238}U/^{206}Pb$	±2σ abs	$^{207}Pb/^{206}Pb$	±2σ abs	Rho	$^{206}Pb/^{238}U$	±2σ abs
12267AZ1_1	38.615	0.495	0.04969	0.00219	0.06	164.82	4.92
12267AZ1_2	37.788	0.482	0.04990	0.00221	0.09	168.38	4.88
12267AZ1_3	37.840	0.456	0.05213	0.00284	0.06	168.15	4.84
12267AZ1_4	37.555	0.644	0.04913	0.00255	0.09	169.41	5.27
12267AZ1_5	38.510	0.525	0.05070	0.00221	0.09	165.26	4.93
12267AZ1_6	37.710	0.514	0.05077	0.00279	0.06	168.72	4.93
12267AZ1_7	38.639	0.630	0.05126	0.00285	0.06	164.71	5.05
12267AZ1_8	37.738	0.720	0.05087	0.00272	0.09	168.59	5.47
12267AZ1_9	37.722	0.541	0.05103	0.00278	0.05	168.67	5.06
12267AZ1_10	37.012	0.556	0.05153	0.00284	0.06	171.86	5.15
12267AZ1_11	38.186	0.534	0.04974	0.00309	0.06	166.64	4.89
12267AZ1_12	38.620	0.596	0.05128	0.00272	0.07	164.79	5.01
12267AZ1_13	36.515	0.446	0.04989	0.00179	0.09	174.17	5.01
12267AZ1_14	38.651	0.595	0.05202	0.00317	0.07	164.66	5.07
12267AZ1_15	37.549	0.998	0.05104	0.00265	0.23	169.43	6.27
12267AZ1_16	36.977	0.902	0.05059	0.00198	0.29	172.02	6.16
12267AZ1_17	37.539	0.730	0.05161	0.00323	0.12	169.48	5.47
12267AZ1_18	37.878	0.800	0.05171	0.00316	0.12	167.98	5.63
12267AZ1_19	37.716	0.939	0.05222	0.00344	0.15	168.69	6.06
12267AZ1_20	37.317	0.843	0.05302	0.00300	0.17	170.47	5.82
12267AZ1_21	38.160	0.888	0.05231	0.00327	0.15	166.75	5.82
12267AZ1_22	37.181	1.058	0.05152	0.00305	0.22	171.09	6.62
12267AZ1_23	37.539	0.668	0.04947	0.00188	0.19	169.48	5.38
12267AZ1_24	37.772	1.100	0.05170	0.00226	0.33	168.45	6.52
12267AZ1_25	36.740	1.006	0.05369	0.00429	0.11	173.11	6.47
12267AZ1_26	36.764	0.869	0.05323	0.00364	0.10	173.00	5.82
12267AZ1_27	37.275	0.798	0.05234	0.00363	0.11	170.66	5.49
12267AZ1_28	37.658	0.724	0.05256	0.00294	0.13	168.95	5.25
12267AZ1_29	37.638	0.810	0.05075	0.00323	0.10	169.04	5.53
12267AZ1_30	37.528	1.031	0.05197	0.00408	0.12	169.53	6.15
12267AZ1_31	38.589	0.888	0.05038	0.00179	0.40	164.93	5.60
12267AZ1_32	37.123	0.649	0.05082	0.00270	0.13	171.35	5.22
12267AZ1_33	37.753	0.724	0.05106	0.00355	0.10	168.53	5.29
12267AZ1_34	38.270	0.651	0.05171	0.00294	0.09	166.28	4.96
12267AZ1_35	37.262	0.761	0.05347	0.00336	0.13	170.72	5.44
12267AZ1_36	37.308	0.592	0.05078	0.00219	0.19	170.51	4.99
12267AZ1_37	37.670	0.593	0.04967	0.00248	0.08	168.90	4.96
12267AZ1_38	38.715	0.644	0.05004	0.00208	0.13	164.40	4.88
12267AZ1_39	37.441	0.649	0.05061	0.00269	0.10	169.92	5.22
12267AZ1_40	37.922	1.006	0.04999	0.00200	0.46	167.79	6.07
12267AZ1_41	37.834	0.527	0.05119	0.00230	0.09	168.17	4.79
12267AZ1_42	37.418	0.510	0.04984	0.00184	0.19	170.02	4.82
12267AZ1_43	37.313	0.564	0.05034	0.00197	0.14	170.49	4.97
12267AZ1_44	37.198	0.568	0.05298	0.00264	0.08	171.01	4.94
12267AZ1_45	37.773	0.614	0.05181	0.00362	0.04	168.44	4.95
12267AZ1_46	37.020	0.528	0.05017	0.00214	0.13	171.82	4.94
12267AZ1_47	36.808	0.574	0.05061	0.00283	0.07	172.80	5.02
12267AZ1_48	36.413	0.773	0.05033	0.00383	0.07	174.65	5.67
12267AZ1_49	37.122	0.569	0.05053	0.00215	0.13	171.36	5.01
12267AZ1_50	37.540	0.642	0.05129	0.00297	0.09	169.47	5.06

[1] Data not corrected for common lead

Zircon U-Pb LA-ICP-MS data for sample 11BVA35-276

Analysis	Isotopic ratios[1]					Age (Ma)[2]	
	$^{238}U/^{206}Pb$	±2σ abs	$^{207}Pb/^{206}Pb$	±2σ abs	Rho	$^{206}Pb/^{238}U$	±2σ abs
12268AZ1_1	36.504	1.117	0.05090	0.00184	0.55	174.22	6.79
12268AZ1_3	35.168	2.170	0.05080	0.00285	0.68	180.75	12.02
12268AZ1_4	37.645	1.297	0.04951	0.00172	0.63	169.01	7.14
12268AZ1_5	35.215	2.929	0.05817	0.00596	0.53	143.68	-30.26 +16.60
12268AZ1_6	37.813	0.971	0.04983	0.00166	0.53	168.27	5.99
12268AZ1_7	37.806	0.826	0.05112	0.00178	0.44	168.30	5.62
12268AZ1_8	41.236	1.869	0.08074	0.00655	0.39	159.11	-29.00 +20.70
12268AZ1_9	39.612	9.731	0.05522	0.01350	0.51	160.72	39.23
12268AZ1_10	42.051	1.162	0.05223	0.00438	0.08	151.51	5.47
12268AZ1_11	38.585	1.381	0.04993	0.00239	0.51	164.94	7.00
12268AZ1_12	40.500	10.981	0.05599	0.02072	0.37	157.24	42.47
12268AZ1_13	37.799	0.786	0.05418	0.00586	0.03	168.33	5.36
12268AZ1_14	43.193	0.486	0.05068	0.00217	0.07	147.55	4.01
12268AZ1_15	43.681	1.982	0.05199	0.00328	0.45	145.92	7.41
12268AZ1_16	36.256	1.229	0.05160	0.00207	0.57	175.40	7.36
12268AZ1_17	40.858	1.984	0.05947	0.00402	0.44	164.36	-23.81 +14.68
12268AZ1_18	41.741	8.057	0.05440	0.01496	0.38	152.62	29.62
12268AZ1_19	37.432	1.197	0.05110	0.00415	0.13	169.96	6.72
12268AZ1_20	40.371	2.611	0.04986	0.00513	0.39	157.73	10.71
12268AZ1_21	37.196	0.812	0.04998	0.00177	0.40	171.02	5.69
12268AZ1_22	36.842	2.837	0.05158	0.00357	0.58	172.64	13.81
12268AZ1_23	54.151	7.018	0.07012	0.01158	0.40	136.04	-49.51 +46.58
12268AZ1_24	33.628	3.385	0.05746	0.00542	0.59	188.91	19.30
12268AZ1_25	38.343	5.256	0.11411	0.01363	0.76	154.99	-55.60 +42.42
12268AZ1_26	37.162	2.152	0.05016	0.00391	0.37	171.18	10.66
12268AZ1_27	36.754	2.909	0.04970	0.00286	0.72	173.05	14.20
12268AZ1_28	36.849	2.839	0.05004	0.00305	0.64	172.61	13.83
12268AZ1_29	48.455	3.856	0.05401	0.00330	0.67	131.69	10.89
12268AZ1_30	35.997	3.140	0.05095	0.00368	0.61	176.64	15.83
12268AZ1_31	36.752	3.046	0.05006	0.00323	0.67	173.06	14.82
12268AZ1_32	35.335	2.078	0.05225	0.00338	0.47	179.90	11.35
12268AZ1_33	36.496	3.395	0.05031	0.00441	0.53	174.26	16.54
12268AZ1_34	37.218	2.309	0.05367	0.00475	0.35	170.92	11.26
12268AZ1_35	38.415	2.686	0.05172	0.00270	0.69	165.66	12.18
12268AZ1_36	36.037	7.223	0.05263	0.00987	0.55	176.44	35.19
12268AZ1_37	38.295	0.554	0.05170	0.00260	0.06	166.18	4.74
12268AZ1_38	37.958	0.743	0.05169	0.00358	0.14	167.63	5.15
12268AZ1_39	41.346	4.905	0.05165	0.00861	0.40	154.06	18.42
12268AZ1_40	37.873	0.763	0.05255	0.00390	0.07	168.00	5.29
12268AZ1_41	37.487	0.726	0.05236	0.00319	0.07	169.71	5.25
12268AZ1_42	50.924	4.389	0.06679	0.00738	0.46	159.90	-29.34 +19.70
12268AZ1_43	38.122	0.558	0.04994	0.00168	0.23	166.92	4.78
12268AZ1_44	38.700	1.807	0.04926	0.00242	0.61	164.46	8.74
12268AZ1_45	38.139	1.387	0.05178	0.00312	0.27	166.85	7.26
12268AZ1_46	30.189	9.138	0.11795	0.15409	0.01	210.07	62.88
12268AZ1_47	36.832	0.522	0.05014	0.00153	0.22	172.69	4.91
12268AZ1_48	37.866	0.624	0.05273	0.00336	0.05	168.04	4.97
12268AZ1_49	38.689	2.396	0.05070	0.00371	0.44	164.51	10.82
12268AZ1_50	37.802	0.821	0.05096	0.00242	0.17	168.31	5.48

[1] Data not corrected for common lead

[2] Data not corrected for common lead, except underlined values

Zircon U-Pb LA-ICP-MS data for sample 11BVA38-304

Analysis	Isotopic ratios[1]					Age (Ma)[1]	
	$^{238}U/^{206}Pb$	±2σ abs	$^{207}Pb/^{206}Pb$	±2σ abs	Rho	$^{206}Pb/^{238}U$	±2σ abs
12269AZ1_1	30.164	0.626	0.05631	0.00520	0.04	210.24	6.58
12269AZ1_2	30.403	0.664	0.05746	0.00497	0.05	208.62	6.72
12269AZ1_3	29.644	0.548	0.05464	0.00462	0.05	213.87	6.49
12269AZ1_4	29.257	0.524	0.05453	0.00403	0.05	216.66	6.49
12269AZ1_5	29.060	0.550	0.05363	0.00445	0.03	218.10	6.68
12269AZ1_6	29.431	0.667	0.05485	0.00538	0.03	215.39	7.12
12269AZ1_7	29.062	0.591	0.05743	0.00561	0.02	218.09	6.86
12269AZ1_8	30.024	0.675	0.05481	0.00505	0.03	211.21	6.95
12269AZ1_9	28.638	0.434	0.05286	0.00313	0.05	221.26	6.35
12269AZ1_10	29.541	0.557	0.05486	0.00521	0.03	214.61	6.55
12269AZ1_11	30.336	0.559	0.05516	0.00423	0.03	209.07	6.35
12269AZ1_12	28.185	0.805	0.05782	0.00711	0.02	224.75	8.41
12269AZ1_13	30.188	1.007	0.05503	0.00508	0.12	210.08	8.61
12269AZ1_14	29.524	0.783	0.05447	0.00395	0.13	214.73	7.64
12269AZ1_15	29.943	0.689	0.05234	0.00321	0.14	211.77	7.07
12269AZ1_16	29.894	0.887	0.05616	0.00570	0.11	212.11	8.06
12269AZ1_17	29.178	0.901	0.05262	0.00550	0.06	217.23	8.45
12269AZ1_18	29.562	0.736	0.05343	0.00252	0.23	214.46	7.41
12269AZ1_19	29.431	0.682	0.05223	0.00345	0.13	215.39	7.20
12269AZ1_20	28.556	0.746	0.05282	0.00365	0.14	221.88	7.87
12269AZ1_21	29.994	0.736	0.05468	0.00403	0.13	211.42	7.26
12269AZ1_22	29.486	0.823	0.05359	0.00427	0.12	215.00	7.86
12269AZ1_23	29.144	0.882	0.05288	0.00473	0.11	217.49	8.38
12269AZ1_24	29.250	0.774	0.05487	0.00502	0.08	216.71	7.68
12269AZ1_25	28.467	0.860	0.05497	0.00449	0.15	222.56	8.56
12269AZ1_26	28.706	0.808	0.05434	0.00350	0.18	220.75	9.85
12269AZ1_27	29.516	0.945	0.05704	0.00477	0.15	214.79	10.24
12269AZ1_28	28.284	0.939	0.05761	0.00550	0.13	223.98	10.70
12269AZ1_29	29.130	0.674	0.05266	0.00342	0.12	217.59	9.10
12269AZ1_30	29.435	0.860	0.05515	0.00552	0.08	215.37	9.73
12269AZ1_31	28.335	1.119	0.05544	0.00591	0.15	223.58	11.73
12269AZ1_32	29.817	0.824	0.05484	0.00359	0.21	212.66	9.49
12269AZ1_33	29.198	0.814	0.05624	0.00435	0.16	217.08	9.68
12269AZ1_34	29.461	0.894	0.05203	0.00295	0.23	215.18	10.04
12269AZ1_35	29.529	0.984	0.06026	0.00702	0.10	214.69	10.22
12269AZ1_36	27.844	0.946	0.05378	0.00453	0.14	227.46	11.06
12269AZ1_37	29.819	1.021	0.05119	0.00277	0.34	212.64	10.59
12269AZ1_38	29.310	0.951	0.05261	0.00416	0.16	216.27	10.36
12269AZ1_39	29.509	0.530	0.05410	0.00352	0.07	214.83	8.48
12269AZ1_40	29.394	0.445	0.05166	0.00269	0.10	215.66	8.36
12269AZ1_41	29.448	0.553	0.05566	0.00450	0.05	215.27	8.61
12269AZ1_42	28.807	0.606	0.05530	0.00387	0.09	219.98	9.05
12269AZ1_43	28.861	0.540	0.05216	0.00386	0.05	219.58	8.73
12269AZ1_44	28.633	0.394	0.05025	0.00241	0.09	221.30	8.47
12269AZ1_45	28.711	0.564	0.05471	0.00387	0.09	220.71	9.04
12269AZ1_46	28.728	0.816	0.05483	0.00393	0.16	220.58	9.89
12269AZ1_48	29.505	0.987	0.05350	0.00661	0.08	214.86	10.10
12269AZ1_49	29.613	0.723	0.05153	0.00333	0.14	214.09	9.21
12269AZ1_50	28.760	0.741	0.05359	0.00441	0.08	220.34	9.57

[1] Data not corrected for common lead

Zircon U-Pb LA-ICP-MS data for sample 11BVA42-333

Analysis	Isotopic ratios[1]					Age (Ma)[1]	
	$^{238}U/^{206}Pb$	±2σ abs	$^{207}Pb/^{206}Pb$	±2σ abs	Rho	$^{206}Pb/^{238}U$	±2σ abs
122610AZ1_1	27.935	1.296	0.05746	0.00636	0.16	226.73	11.66
122610AZ1_2	28.027	1.139	0.05637	0.00506	0.20	226.00	10.52
122610AZ1_3	27.830	0.883	0.05924	0.00650	0.08	227.57	8.91
122610AZ1_4	28.428	0.851	0.05358	0.00483	0.08	222.86	8.40
122610AZ1_5	28.240	1.276	0.05955	0.00705	0.15	224.33	11.32
122610AZ1_6	27.515	1.501	0.05541	0.00548	0.28	230.13	13.49
122610AZ1_7	28.584	1.097	0.05612	0.00503	0.18	221.67	9.90
122610AZ1_8	28.359	1.175	0.05152	0.00504	0.17	223.40	10.55
122610AZ1_9	28.130	1.209	0.05410	0.00551	0.15	225.19	10.97
122610AZ1_10	28.708	0.939	0.05646	0.00507	0.14	220.73	8.84
122610AZ1_11	28.388	1.513	0.05729	0.00573	0.24	223.17	12.83
122610AZ1_12	29.615	0.615	0.05645	0.00444	0.07	214.08	6.72
122610AZ1_13	29.402	0.617	0.05584	0.00494	0.05	215.60	6.79
122610AZ1_14	29.049	0.746	0.05573	0.00618	0.05	218.18	7.56
122610AZ1_15	28.981	1.060	0.05400	0.00506	0.15	218.68	9.46
122610AZ1_16	28.223	1.034	0.06001	0.00671	0.11	224.46	9.67
122610AZ1_17	28.888	0.805	0.05547	0.00532	0.08	219.38	8.03
122610AZ1_18	29.317	0.926	0.05823	0.00587	0.07	216.22	8.44
122610AZ1_19	29.147	1.220	0.05470	0.00508	0.18	217.46	10.36
122610AZ1_20	29.312	1.337	0.05378	0.00517	0.19	216.26	11.07
122610AZ1_21	28.608	1.259	0.05783	0.00692	0.14	221.49	10.94
122610AZ1_22	29.433	0.885	0.05730	0.00602	0.06	215.38	8.13
122610AZ1_23	28.748	0.650	0.05329	0.00559	0.05	220.43	7.22
122610AZ1_24	29.155	1.402	0.05589	0.00610	0.19	217.40	11.52
122610AZ1_25	29.383	1.457	0.05723	0.00506	0.26	215.74	11.72
122610AZ1_26	28.648	0.879	0.05534	0.00457	0.12	221.18	8.34
122610AZ1_27	28.398	1.290	0.05347	0.00559	0.20	223.09	11.13
122610AZ1_28	29.248	1.461	0.05676	0.00589	0.22	216.72	11.65
122610AZ1_29	28.909	1.434	0.06002	0.00605	0.22	219.22	11.77
122610AZ1_30	28.564	1.008	0.05399	0.00425	0.21	221.83	9.16
122610AZ1_31	28.961	1.568	0.05222	0.00597	0.21	218.83	12.63
122610AZ1_32	29.762	1.418	0.05455	0.00445	0.28	213.04	11.08
122610AZ1_33	28.455	1.218	0.05515	0.00722	0.11	222.66	10.60
122610AZ1_34	29.353	1.026	0.05341	0.00505	0.13	215.96	8.85
122610AZ1_35	29.735	0.993	0.05473	0.00502	0.15	213.23	8.48
122610AZ1_36	29.453	1.079	0.05435	0.00476	0.17	215.24	9.14
122610AZ1_37	29.317	1.026	0.05412	0.00737	0.06	216.22	8.90
122610AZ1_38	30.534	0.704	0.05352	0.00417	0.07	207.74	6.66
122610AZ1_39	28.814	0.662	0.05565	0.00572	0.05	219.93	7.05
122610AZ1_40	30.472	0.447	0.05089	0.00216	0.15	208.16	5.54
122610AZ1_41	29.629	0.694	0.05261	0.00491	0.06	213.98	6.86
122610AZ1_42	29.805	0.800	0.05574	0.00558	0.07	212.74	7.36
122610AZ1_43	29.517	0.939	0.05302	0.00719	0.06	214.78	8.19
122610AZ1_44	29.109	0.784	0.05861	0.00581	0.06	217.74	7.56
122610AZ1_45	29.472	0.740	0.05167	0.00416	0.09	215.10	7.30
122610AZ1_46	28.927	0.767	0.05270	0.00432	0.08	219.09	7.57
122610AZ1_47	29.732	0.692	0.05509	0.00534	0.06	213.25	6.83
122610AZ1_48	29.489	0.913	0.05651	0.00656	0.06	214.98	8.08
122610AZ1_49	29.108	0.643	0.05557	0.00499	0.05	217.75	6.82
122610AZ1_50	29.193	0.961	0.05826	0.00587	0.08	217.12	8.51

[1] Data not corrected for common lead

Appendix 6: Hornblende/biotite Ar-Ar geochronology data

Hornblende Ar-Ar data for sample 11BVA27-199

Heating	Laser	Isotope Ratios										Age	
step	power(%)	40Ar/39Ar	1σ	37Ar/39Ar	1σ	36Ar/39Ar	1σ	Ca/K	% 40Ar atm	% 39Ar	40Ar*/39ArK	(Ma)	2σ
1	2.40 W	41.20	0.74	2.91	0.08	0.084	0.003	5.34	60.06	0.24	16.488	161.90	17.16
2	2.80 W	11.28	0.13	1.64	0.04	0.008	0.001	3.01	20.89	1.22	8.933	89.51	3.84
3	3.20 W	17.84	0.11	0.96	0.02	0.003	0.000	1.77	4.39	4.66	17.071	167.37	2.03
4	3.60 W	21.44	0.14	1.24	0.02	0.003	0.000	2.27	3.39	6.62	20.730	201.31	2.64
5*	3.80 W	21.85	0.11	1.89	0.03	0.001	0.000	3.46	1.29	9.38	21.594	209.24	2.08
6*	4.00 W	22.04	0.12	2.63	0.04	0.001	0.000	4.82	0.85	13.99	21.896	212.00	2.20
7*	4.10 W	21.76	0.12	2.47	0.04	0.001	0.000	4.53	0.45	7.01	21.704	210.24	2.20
8*	4.30 W	21.97	0.11	2.54	0.04	0.001	0.000	4.66	0.74	11.37	21.848	211.56	2.11
9*	4.50 W	21.94	0.11	2.53	0.04	0.001	0.000	4.64	0.60	11.61	21.845	211.53	2.13
10	4.70 W	21.47	0.11	2.75	0.05	0.001	0.000	5.05	0.50	5.86	21.402	207.48	2.25
11	4.90 W	21.55	0.11	3.06	0.05	0.001	0.000	5.62	0.66	4.80	21.451	207.93	2.67
12	5.10 W	21.23	0.12	3.42	0.06	0.001	0.000	6.27	0.77	6.00	21.114	204.84	2.28
13	5.30 W	20.18	0.13	3.58	0.07	0.002	0.000	6.58	1.49	1.97	19.926	193.91	2.60
14	6.00 W	20.10	0.11	4.48	0.08	0.002	0.000	8.23	1.53	3.56	19.855	193.25	2.23
15	7.00 W	19.97	0.11	5.42	0.09	0.003	0.000	9.97	1.71	4.43	19.705	191.87	2.16
16	8.00 W	20.91	0.11	4.72	0.08	0.002	0.000	8.67	1.46	3.81	20.674	200.80	2.29
17	9.00 W	20.61	0.13	7.66	0.13	0.003	0.000	14.11	2.06	3.46	20.298	197.34	2.49

Plateau age: 210.9 ± 1.6 Ma (2σ, including J-error of .6%), MSWD=1.16, p=0.32, includes 53.3% of the 39Ar, steps 5 through 9

Inverse isochron age: 209.4 ± 2.1 Ma, initial 40Ar/36Ar=235 ± 51, MSWD=5.0, p=0, 10 point isochron

***** Heating steps used for plateau age calculation

Biotite Ar-Ar data for sample 11BVA35-276

Heating	Laser	Isotope Ratios										Age	
step	power(%)	40Ar/39Ar	1σ	37Ar/39Ar	1σ	36Ar/39Ar	1σ	Ca/K	% 40Ar atm	% 39Ar	40Ar*/39ArK	(Ma)	2σ
1	2.40 W	8.50	0.08	0.26	0.01	0.013	0.001	0.47	45.12	0.39	4.666	47.34	3.85
2	2.80 W	10.38	0.06	0.12	0.00	0.008	0.000	0.21	23.54	1.86	7.936	79.80	1.89
3	3.20 W	16.12	0.08	0.04	0.00	0.004	0.000	0.07	6.57	4.72	15.063	148.57	1.57
4	3.30 W	17.41	0.09	0.03	0.00	0.002	0.000	0.05	2.69	3.34	16.941	166.26	1.78
5*	3.40 W	17.64	0.09	0.03	0.00	0.001	0.000	0.06	2.52	2.35	17.194	168.64	1.78
6*	3.50 W	17.39	0.09	0.02	0.00	0.001	0.000	0.04	1.91	3.77	17.060	167.38	1.65
7*	3.60 W	17.55	0.09	0.03	0.00	0.001	0.000	0.06	1.95	3.96	17.204	168.74	1.65
8*	3.70 W	17.65	0.09	0.10	0.00	0.001	0.000	0.19	2.03	5.44	17.288	169.52	1.68
9*	3.80 W	17.57	0.09	0.02	0.00	0.001	0.000	0.04	1.30	3.78	17.347	170.07	1.89
10*	3.90 W	17.49	0.10	0.03	0.00	0.001	0.000	0.05	1.19	3.90	17.282	169.47	1.95
11*	4.00 W	17.61	0.09	0.09	0.00	0.001	0.000	0.17	1.20	4.47	17.400	170.57	1.80
12*	4.10 W	17.53	0.09	0.05	0.00	0.001	0.000	0.09	1.06	3.32	17.340	170.00	1.93
13*	4.20 W	17.46	0.09	0.04	0.00	0.001	0.000	0.07	1.14	4.29	17.265	169.30	1.89
14*	4.30 W	17.48	0.09	0.04	0.00	0.001	0.000	0.07	1.31	4.24	17.252	169.18	1.81
15*	4.40 W	17.45	0.12	0.11	0.00	0.001	0.000	0.20	1.19	2.74	17.244	169.11	2.43
16*	4.60 W	17.38	0.09	0.11	0.00	0.001	0.000	0.20	1.12	5.07	17.185	168.56	1.75
17*	4.80 W	17.29	0.09	0.09	0.00	0.001	0.000	0.17	1.26	7.42	17.072	167.49	1.75
18	5.00 W	17.11	0.10	0.14	0.00	0.001	0.000	0.26	0.96	6.22	16.945	166.30	1.87
19	5.20 W	17.13	0.09	0.16	0.00	0.001	0.000	0.30	1.00	5.16	16.958	166.43	1.76
20	5.40 W	17.11	0.09	0.21	0.00	0.001	0.000	0.38	1.10	3.36	16.921	166.08	1.98
21	5.70 W	17.20	0.09	0.21	0.01	0.000	0.000	0.39	0.80	2.92	17.065	167.43	1.95
22	6.00 W	17.19	0.09	0.22	0.00	0.001	0.000	0.40	0.98	3.49	17.019	167.00	1.85
23	6.50 W	17.13	0.09	0.25	0.00	0.001	0.000	0.46	0.87	7.43	16.981	166.64	1.67
24	7.00 W	17.12	0.09	0.33	0.01	0.001	0.000	0.60	1.03	3.89	16.949	166.34	1.81
25	7.50 W	17.22	0.09	0.41	0.01	0.001	0.000	0.74	1.42	2.48	16.979	166.62	2.07

Plateau age: 169.0 ± 1.1 Ma (2σ, including J-error of .6%), MSWD=1.12, p=0.34, includes 54.7% of the 39Ar, steps 5 through 17

Inverse isochron age: 166.4 ± 1.8 Ma, initial 40Ar/36Ar=476 ± 230, MSWD=2.3, p=0.001, 22 point isochron

***** Heating steps used for plateau age calculation

Hornblende Ar-Ar data for sample 11BVA42-329

Heating	Laser	Isotope Ratios										Age	
step	power(%)	40Ar/39Ar	1σ	37Ar/39Ar	1σ	36Ar/39Ar	1σ	Ca/K	% 40Ar atm	% 39Ar	40Ar*/39ArK	(Ma)	2σ
1	2.20 W	15.03	18.4	0.58	0.71	0.047	0.061	-1.06	91.96	0.07	1.207	-12.46	128.70
2	2.70 W	165.34	214	5.69	7.37	0.235	0.304	10.47	41.61	0.07	96.928	793.94	1672.2
3	3.70 W	21.51	0.58	2.50	0.08	0.013	0.001	4.59	16.96	3.39	17.891	175.22	9.67
4	4.40 W	17.16	0.30	2.28	0.06	0.003	0.000	4.19	4.19	5.33	16.466	161.87	5.67
5	5.00 W	17.25	0.18	2.86	0.05	0.003	0.000	5.25	3.21	9.73	16.734	164.39	3.46
6*	5.70 W	17.72	0.13	4.42	0.08	0.002	0.000	8.12	1.82	18.30	17.457	171.16	2.59
7*	6.40 W	17.75	0.16	4.60	0.08	0.003	0.000	8.46	2.62	14.22	17.341	170.07	2.94
8*	7.10 W	17.82	0.22	4.71	0.10	0.003	0.000	8.66	2.84	7.83	17.368	170.33	4.26
9*	7.80 W	18.50	0.29	4.42	0.10	0.004	0.000	8.12	5.04	6.11	17.618	172.67	5.39
10*	8.40 W	18.17	0.12	5.38	0.09	0.003	0.000	9.88	2.69	28.99	17.746	173.87	2.23
11*	9.00 W	18.19	0.29	4.55	0.11	0.004	0.000	8.36	4.18	6.10	17.490	171.48	5.65

Plateau age: 171.9 ± 1.7 Ma (2σ, including J-error of .6%), MSWD=1.13, p=0.34, includes 81.6% of the 39Ar, steps 6 through 11

Inverse isochron age: 168.9 ± 4.7 Ma, initial 40Ar/36Ar=386 ± 210, MSWD=4.7, p=0, 11 point isochron

***** Heating steps used for plateau age calculation

Hornblende Ar-Ar data for sample 11BVA42-332

Heating	Laser	Isotope Ratios										Age	
step	power(%)	40Ar/39Ar	1σ	37Ar/39Ar	1σ	36Ar/39Ar	1σ	Ca/K	% 40Ar atm	% 39Ar	40Ar*/39ArK	(Ma)	2σ
1	2.20 W	4.71	0.15	0.24	0.01	0.011	0.004	0.44	71.38	0.24	1.349	13.80	21.97
2	2.60 W	6.27	0.05	0.18	0.00	0.006	0.000	0.33	29.35	1.99	4.433	44.96	2.87
3	3.00 W	12.06	0.08	0.08	0.00	0.004	0.000	0.15	9.63	4.17	10.900	108.60	2.03
4	3.60 W	16.68	0.10	0.08	0.00	0.002	0.000	0.14	3.20	15.98	16.144	158.62	1.81
5*	3.80 W	18.02	0.10	0.08	0.00	0.001	0.000	0.15	2.07	14.97	17.652	172.75	1.82
6*	4.00 W	18.11	0.10	0.19	0.00	0.001	0.000	0.34	2.18	9.75	17.715	173.34	1.90
7*	4.30 W	18.00	0.10	0.23	0.00	0.001	0.000	0.41	1.52	11.47	17.728	173.46	1.89
8*	4.80 W	17.95	0.11	0.30	0.01	0.001	0.000	0.55	1.45	18.01	17.692	173.13	1.96
9	5.30 W	17.42	0.09	0.34	0.01	0.001	0.000	0.63	0.94	10.86	17.265	169.14	1.73
10	5.80 W	17.02	0.09	0.46	0.01	0.001	0.000	0.85	1.10	6.33	16.841	165.17	1.90
11	6.30 W	16.81	0.25	0.58	0.01	0.001	0.000	1.07	1.28	3.20	16.603	162.93	4.85
12	7.00 W	16.96	0.09	0.71	0.01	0.001	0.000	1.31	1.24	3.04	16.760	164.41	2.43

Plateau age: 173.2 ± 1.4 Ma (2σ, including J-error of .6%), MSWD=0.114, p=0.95, includes 54.2% of the 39Ar, steps 5 through 8

Inverse isochron age: 170.1 ± 3.2 Ma, initial 40Ar/36Ar=294.99 ± 0.45, MSWD=14, p=0, 9 point isochron (forced through air argon initial composition)

***** Heating steps used for plateau age calculation

Hornblende Ar-Ar data for sample 11BVA42-333

Heating	Laser	Isotope Ratios										Age	
step	power(%)	40Ar/39Ar	1σ	37Ar/39Ar	1σ	36Ar/39Ar	1σ	Ca/K	% 40Ar atm	% 39Ar	40Ar*/39ArK	(Ma)	2σ
1*	2.20 W	102.01	22.78	5.11	1.19	0.202	0.121	9.39	58.09	0.03	42.910	394.25	571.29
2*	2.60 W	32.08	1.30	7.73	0.38	0.060	0.017	14.24	53.57	0.22	14.976	147.56	97.01
3*	3.00 W	22.73	0.48	3.00	0.11	0.008	0.007	5.50	8.80	0.48	20.770	201.57	36.59
4*	3.70 W	25.76	0.26	7.38	0.15	0.012	0.001	13.58	10.91	3.24	23.073	222.60	7.83
5*	4.30 W	23.07	0.14	5.72	0.10	0.002	0.000	10.53	0.84	60.81	22.973	221.68	2.55
6*	4.60 W	22.69	0.14	5.27	0.09	0.002	0.000	9.68	0.38	29.47	22.689	219.11	2.60
7	5.00 W	22.18	0.25	5.83	0.15	0.003	0.001	10.72	1.56	2.84	21.920	212.10	7.18
8	5.80 W	21.58	0.20	5.30	0.13	0.002	0.002	9.74	0.57	1.90	21.542	208.64	9.21
9	6.80 W	21.64	0.25	5.18	0.17	0.003	0.006	9.52	1.60	1.02	21.370	207.07	31.43

Plateau age: 220.5 ± 2.2 Ma (2σ, including J-error of .6%), MSWD=1.20, p=0.31, includes 94.2% of the 39Ar, steps 1 through 6

Inverse isochron age: 218.8 ± 3.2 Ma, initial 40Ar/36Ar=365 ± 190, MSWD=2.2, p=0.05, 9 point isochron

***** Heating steps used for plateau age calculation

QUEST-Northwest Total Field Magnetics (Aeroquest Airborne, 2012) with Geological Line Features

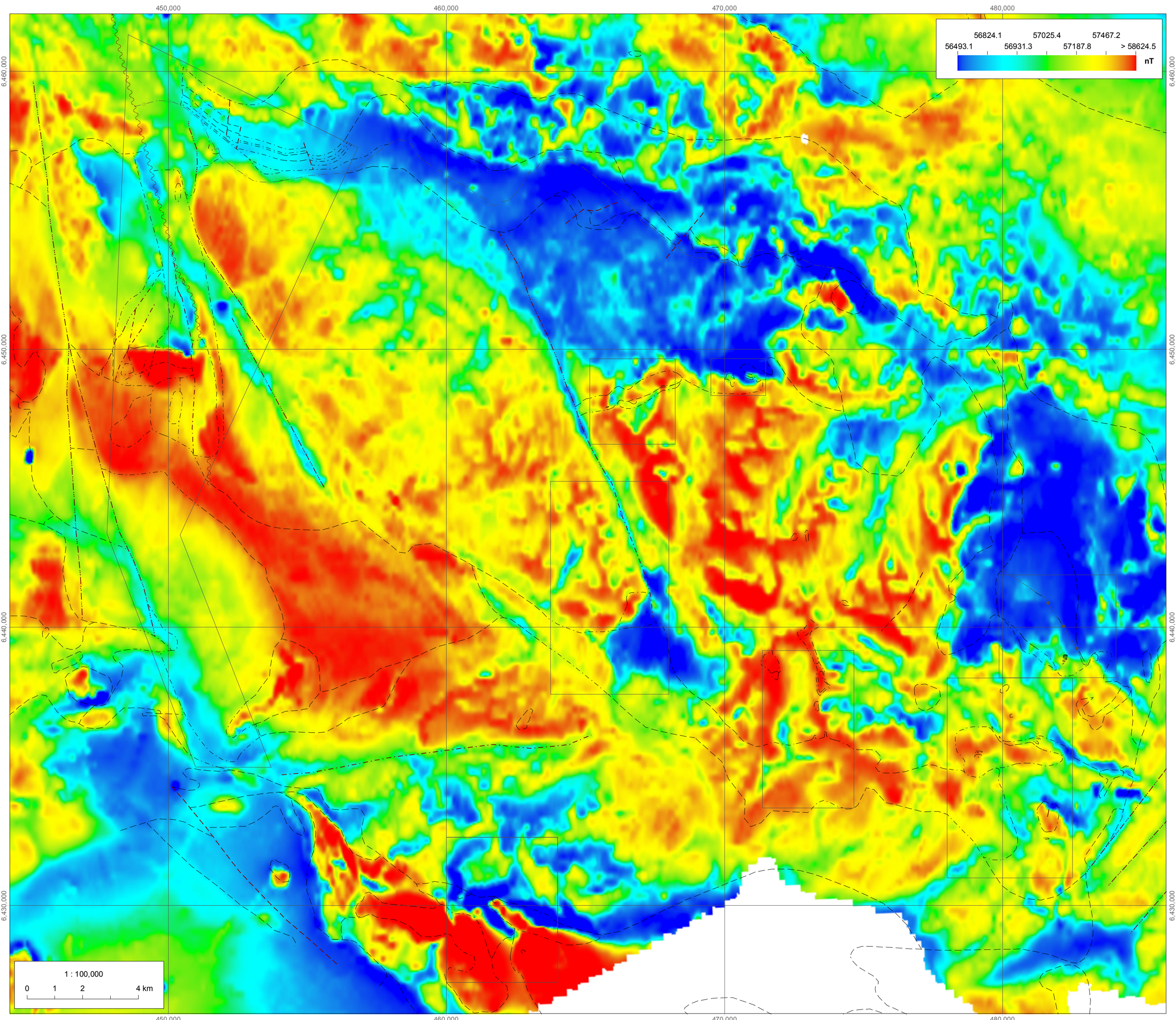

QUEST-Northwest First Vertical Derivative of Total Magnetic Field (Aeroquest Airborne, 2012) with Geological Line Features

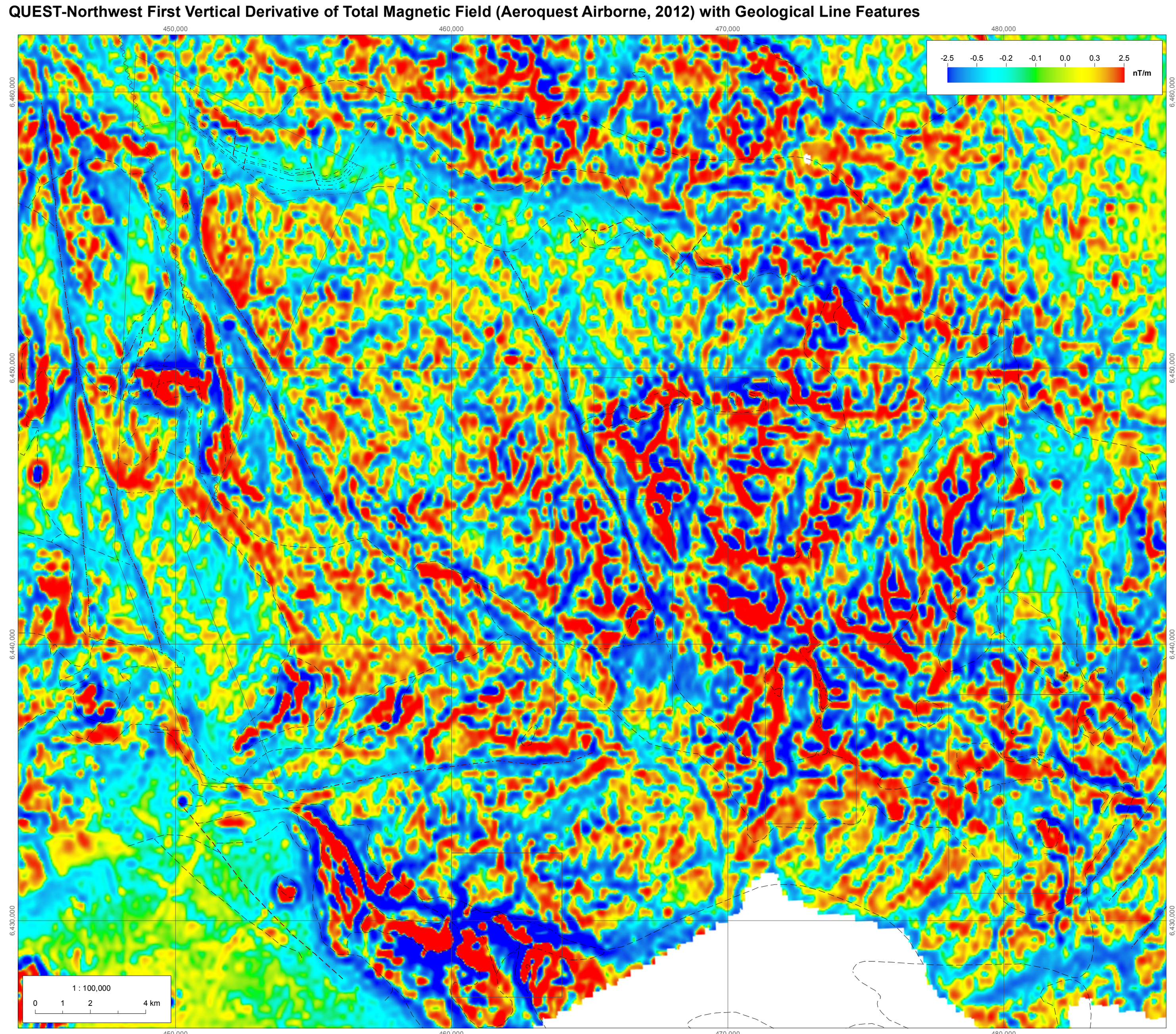

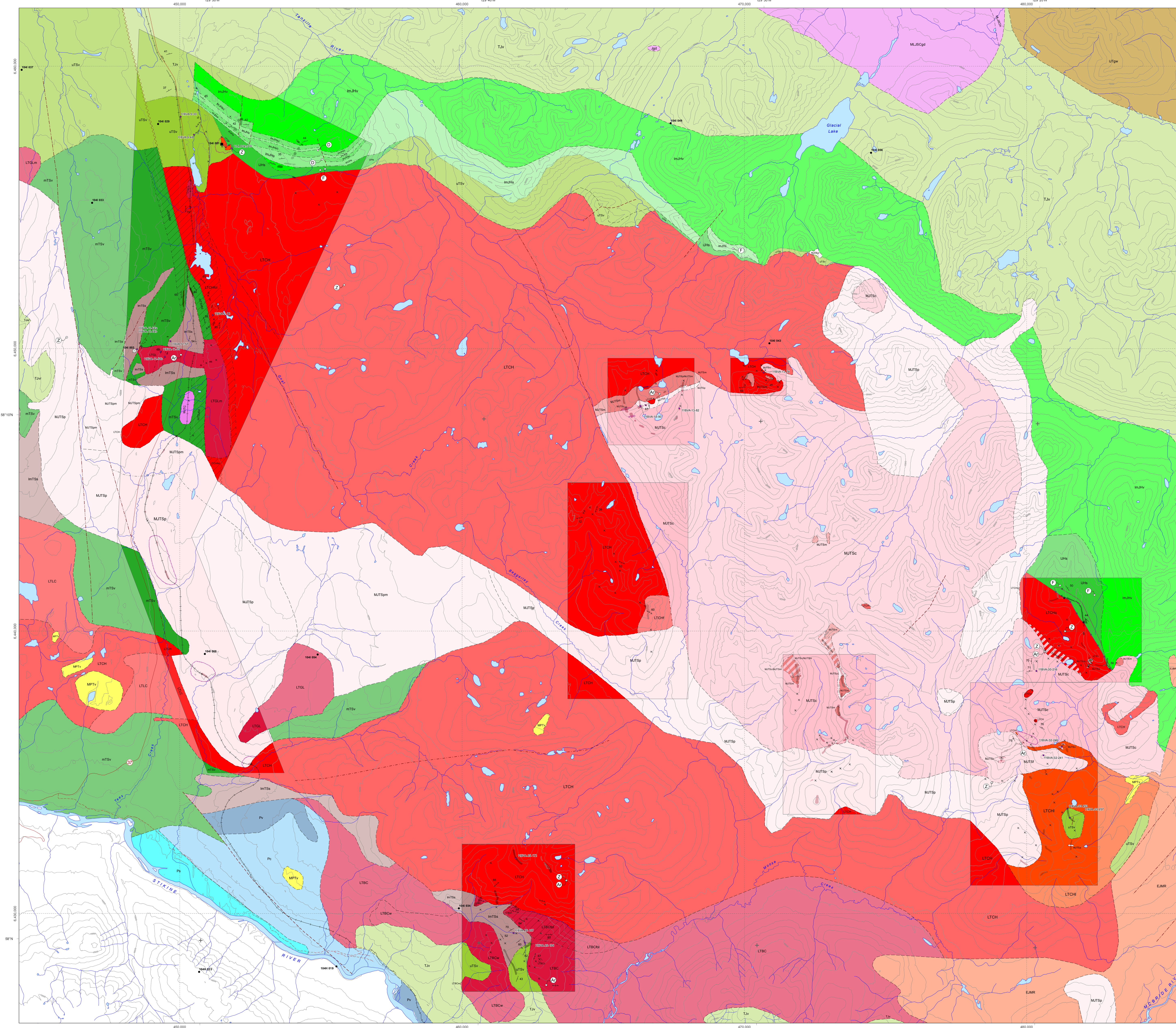

Previous Mapping in the Region

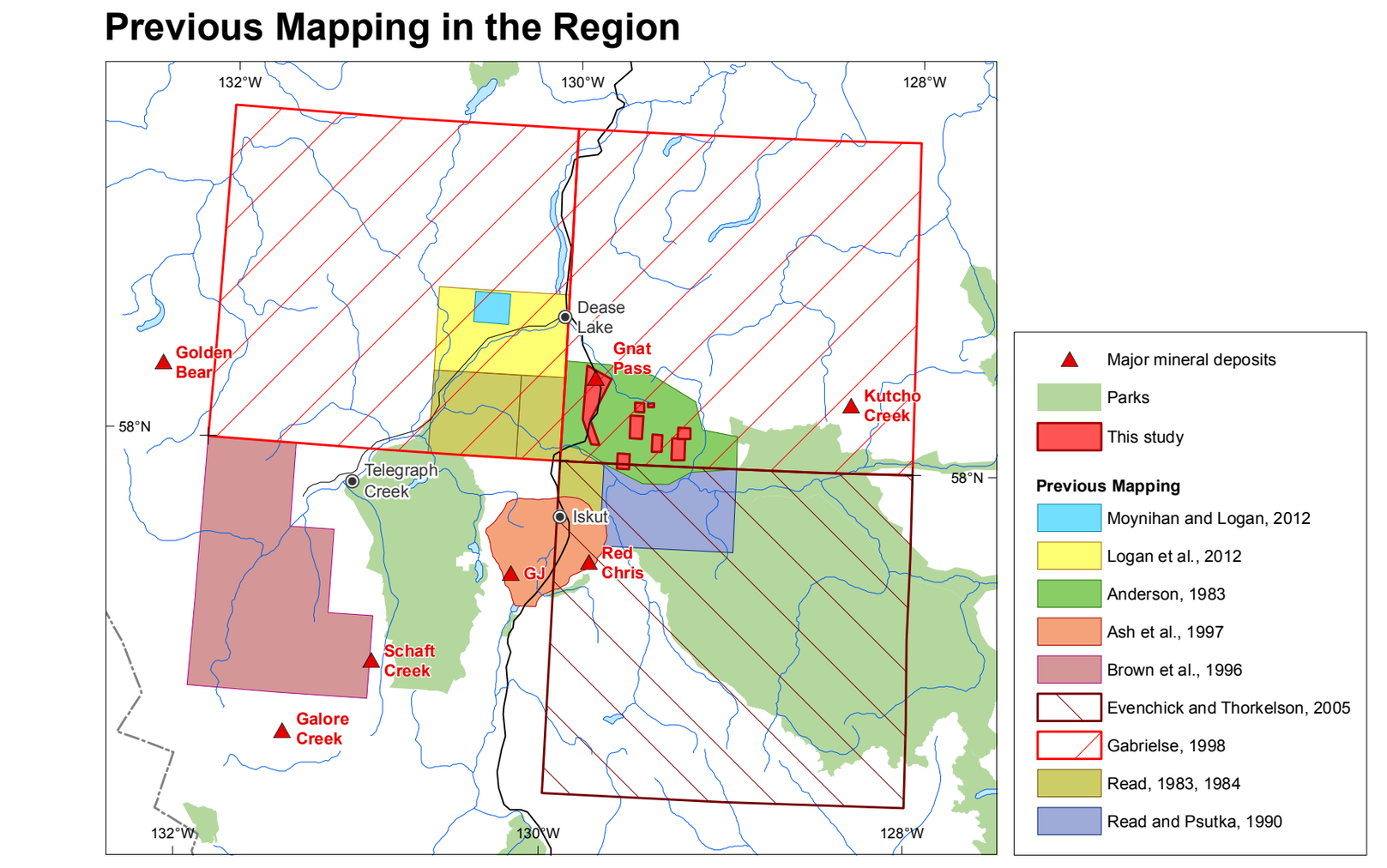

Note: Outcrops visited and detailed mapping done in this study are distinguished from regional geology data by using increasingly lighter shades of a particular colour. The darkest shades are used to depict outcrops, intermediate shades are used for geological units in detailed mapping areas, and the lightest shades are used for regional geological units.

The different shades are shown in the legend in following order: outcrops, detailed mapping geological units, regional mapping geological units. See example here:

Outcrop — Detailed mapping geological units — Regional mapping geological units

MIOCENE TO PLEISTOCENE
Tuya Formation
- MPTv — Alkali olivine basalt, tuff.

JURASSIC
- Jgd — Granodiorite, granite; age unknown.

MIDDLE TO LATE JURASSIC
Snowdrift Creek Pluton
- MLJSCgd — Biotite-hornblende quartz monzodiorite; moderately foliated; marginal magnetic, likely mafic, phase (SCm).

MIDDLE JURASSIC
HOTAILUH BATHOLITH
Tees Creek Intrusive
- MJTC — Hornblende feldspar porphyritic hypabyssal intrusive; bleached and pervasive alteration.

Three Sisters Pluton
- MJTSp — Potassic phase; biotite granite, quartz-syenite and quartz-monzonite, includes pink biotite porphyry dikes; marginal magnetic phase (TSpm); hornblende-biotite granite of Evenchick and Thorkelson (2005). 169.01 ± 0.8 Ma (U-Pb zircon), 169.6 ± 1 Ma (U-Pb zircon).
- MJTSc — Central phase; biotite and hornblende-biotite (rare biotite-hornblende) quartz-monzonite and quartz-monzodiorite. Equigranular, to K-feldspar porphyritic and locally with diorite xenoliths. 169.0 ± 1.3 Ma (U-Pb zircon), 169.0 ± 1.1 Ma (Ar-Ar biotite).
- MJTSm — Mafic phase; hornblende quartz diorite, lesser biotite-clinopyroxene-hornblende quartz-diorite. Stubby equant and acicular hornblende crystals. 171.9 ± 1.7 Ma (Ar-Ar hornblende).
- MJTSf — Fine-grained mafic-intermediate phase; hornblende-biotite-quartz diorite. Equigranular to often plagioclase porphyritic. 173.2 ± 1.4 Ma (Ar-Ar hornblende).

EARLY JURASSIC
HOTAILUH BATHOLITH
McBride River Pluton
- EJMR — Hornblende-biotite granodiorite and quartz-monzodiorite; equigranular, 1-5 mm crystals; contains abundant rounded, clear to grey quartz grains (Anderson, 1983). 184 ± 8 Ma (U-Pb zircon).

LOWER TO MIDDLE JURRASSIC
Hazelton Formation
- lmJHv — Augite and plagioclase-hornblende porphyry breccia and flows; granule, pebble and cobble-sized volcanic conglomerate, augite crystal-rich volcaniclastic sandstone and felsic tuff.
- lmJHs — Alternating grey and black parallel laminated siltstone, calcareous siltstone. Regional mapping geological units also include fine- to medium-grained feldspathic +/- lithic arenite, tuff and minor interbedded conglomerate.
- lmJHsc — Fine- to medium-grained feldspathic +/- lithic arenite, tuff and minor interbedded conglomerate.
- lJHs — Basal conglomerate, quartz-bearing feldspathic-arenite; graphitic siltstone and micrite of Anderson (1983), calcareous sandstone and siltstone of Smith and Garagan (1990).

LOWER JURRASSIC
Takwahoni Formation
- lJTgw — Greywacke, shale and conglomerate; mainly Pliensbachian (Gabrielse, 1998).

UPPER TRIASSIC TO LOWER JURASSIC
- TJv — Undivided Hazelton and Stuhini Group volcanic rocks; maroon and grey aphyric and plagioclase porphyritic breccia, tuff and flows (TJvr).

LATE TRIASSIC
HOTAILUH BATHOLITH
Gnat Pass Intrusive
- LTGP — Plagioclase porphyritic hypabyssal intrusive; sparse quartz and/or hornblende phenocrysts, pervasive bleaching, with local brecciation and carbonate alteration. 216.5 ± 1.4 Ma (U-Pb zircon).

Beggerlay Creek Pluton
- LTBC — Clinopyroxene-hornblende to hornblende-clinopyroxene gabbro (BC); serpentinized websterite (BCw) and rare plagioclase-bearing clinopyroxenite (BCc). Commonly equigranular, 3-5 mm interlocking crystal, locally foliated along the margins. 210.9 ± 1.6 Ma (Ar-Ar hornblende).

Cake Hill Pluton
- LTCHq — Hornblende (tabular) monzogranite and granodiorite. Equigranular, 3-4 mm, with ubiquitous 4-7 mm quartz blebs. 216.2 ± 1.2 Ma (U-Pb zircon).
- LTCHf — Foliated biotite(?)-hornblende diorite and quartz diorite; equigranular, 1-3 mm crystals.
- LTCHl — Leucocratic and epidote-altered hornblende-quartz monzodiorite, granodiorite, quartz-diorite and tonalite(?). Equigranular, 2-3 mm crystals, tabular hornblende common.
- LTCH — Hornblende (tabular), to lesser biotite-hornblende quartz monzodiorite and quartz monzonite. Commonly equigranular, 3-4 mm crystals; trace titanite ubiquitous; trace magnetite in places; massive to moderately foliated. 218.2 ± 1.3 Ma (U-Pb zircon), 220.5 ± 2.2 Ma (Ar-Ar hornblende), 221 ± 3 Ma (U-Pb zircon).

Latham Creek Pluton
- LTLC — Biotite hornblende quartz monzodiorite, hornblende augite monzodiorite and rare diorite; common marginal foliation.

Gnat Lakes Ultramafite
- LTGLm — Clinopyroxene-hornblende gabbro; equigranular 1-5 mm hornblende crystals; clinopyroxene metagabbro, monzodiorite and monzograbbro of Gabrielse (1998).
- LTGL — Plagioclase-bearing hornblendite to clinopyroxene-hornblende gabbro. 223.3 ± 2.0 Ma (Ar-Ar hornblende).

UPPER TRIASSIC
Stuhini Group
- uTSv — Massive, brecciated and rare pillowed augite porphyritic basalt, plagioclase porphyritic andesitic basalts and aphyric basalt; tuffs, breccias and volcaniclastic horizons and lesser mudstone, shale, sandstone with minor limestone.

MIDDLE TRIASSIC
Stuhini Group
- mTSv — Augite porphyry metabasalt, meta-andesite, breccia, tuff and flows, argillite.

LOWER AND MIDDLE TRIASSIC
- lmTSs — Argillite, siliceous argillite, limestone and minor chert.

CARBONIFEROUS AND PERMIAN
Stikine Assemblage
- Pc — Massive white limestone, interlayered with chert and minor calcareous shale.
- Ps — Phyllitic greenstone, phyllite, sericite schist and limestone (Evenchick and Thorkelson, 2005).

CARBONIFEROUS AND OLDER
Stikine Assemblage
- Pv — Dark and light green phyllitic greenstone, grey phyllite, minor chert and rare limestone (Evenchick and Thorkelson, 2005).

References

Aeroquest Airborne (2012): Report on a helicopter-borne magnetic survey (Aeroquest job # 11-046) for Geoscience BC; Geoscience BC Report 2012-2, 11 pages.
Anderson, R.G. (1983): Geology of the Hotailuh batholith and surrounding volcanic and sedimentary rocks, north-central British Columbia; unpublished Ph.D. thesis, Carleton University, 669 pages.
Anderson, R.G. and Bevier, M.L. (1992): New Late Triassic and Early Jurassic U-Pb zircon ages from the Hotailuh batholith, Cry Lake map area, north-central British Columbia; in Radiogenic Age and Isotope Studies (Report 6); Geological Survey of Canada, Paper 92-2, pages 145-152.
Anderson, R.G., Loveridge, W.D., and Sullivan, R.W. (1982): U-Pb isotopic ages of zircon from the Jurassic plutonic suite, Hotailuh batholith, north-central British Columbia; in Current Research, Part C, Geological Survey of Canada, Paper 22-1C, pages 133-137.
Ash, C.H., Macdonald, R.W.J., Stinson, P.K., Fraser, T.M., Nelson, K.J., Arden, K.M. and Lefebure, D.V. (1997): Geology and mineral occurrences of the Tatogga Lake area; B.C. Ministry of Energy, Mines and Petroleum Resources, Open File 1997-3.
Brown, D.A., Gunning, M.H. and Greig, C.J. (1996): The Stikine Project: Geology of western Telegraph Creek map area, northwestern British Columbia; B.C. Ministry of Energy, Mines and Petroleum Resources, Bulletin 95, 175 pages.
Evenchick, C. A. and Thorkelson, D.J. (2005): Geology of the Spatsizi River map area, north-central British Columbia; Geological Survey of Canada, Bulletin 577, 276 pages.
Gabrielse, H. (1998): Geology of Cry Lake and Dease Lake Map areas, north-central British Columbia; Geological Survey of Canada, Bulletin 504, 147 pages.
Henderson, C.M. and Perry, D.G. (1981): A Lower Jurassic heteroporid bryozoan and associated biota, Turnagain Lake, British Columbia; Canadian Journal of Earth Sciences, Volume 18, pages 457-468.
Iverson, O., Mahoney, J.B. and Logan, J.M. (2012): Dease Lake Geoscience Project, Part IV: Tsaybahe group: lithological and geochemical characterization of Middle Triassic volcanism in the Stikine Arch, North-central British Columbia. B.C. Ministry of Energy and Mines, Geological Fieldwork 2011, Paper 2012-1, pages 17-22.
Logan, J.M., Moynihan, D.P., Diakow, L.J. and Van Straaten, B.I. (2012): Dease Lake - Little Tuya River Geology, NTS 104J/ 08 and 07E; Geoscience BC Map 2012-08-1 and British Columbia Geological Survey Open File 2012-04, 1 sheet.
Moynihan, D.P. and Logan, J.M. (2012): Dease Lake Geoscience Project, Part III: Age, emplacement and mineralization of the Cretaceous Snow peak pluton; B.C. Ministry of Energy and Mines, Geological Fieldwork 2011, Report 2012-1, pages 69-74.
Read, P.B. (1983): Geology, Classy Creek (10J/2E) and Stikine Canyon (104J/1W), British Columbia; Geological Survey of Canada, Open File 940.
Read, P.B. (1984): Geology Klastline River (104G/16E), Ealue Lake (104H/13W), Cake Hill (104I/4W) and Stikine Canyon (104J/1E), British Columbia; Geological Survey of Canada, Open File 1080.
Read, P.B. and Psutka, J.F. (1990): Geology of Ealue Lake east-half (104H/13E) and Cullivan Creek (104H/14) map areas, British Columbia; Geological Survey of Canada, Open File 2241.
Smith, G. and Garagan, T. (1990): Summary report on the 1989 exploration program on the Gnat Pass property; B.C. Ministry of Energy, Mines and Petroleum Resources, Assessment Report 20408, 156 pages.
van Straaten, B.I., Logan, J.M. and Diakow, L.J. (2012): Dease Lake Geoscience Project, Part II: Preliminary report on the Mesozoic magmatic history and metallogeny of the Hotailuh batholith and surrounding volcanic and sedimentary rocks; B.C. Ministry of Energy and Mines, Geological Fieldwork 2011, Paper 2012-1, pages 99-120.
Zagorevski, A., Joyce, N., Mihalynuk, M. and Logan, J. (2011): Regional U/Pb zircon and Ar/Ar geochronology of Carboniferous to Early Jurassic Stikinia; AME BC Mineral Exploration Roundup, January 2011, poster presentation.

Data Sources

MinFile data

BC Geological Survey (2012): MINFILE BC mineral deposits database; B.C. Ministry of Energy, Mines and Natural Gas, URL <http://minfile.ca> [November 2012]

Aeromagnetic data

Aeroquest Airborne (2012): Report on a Helicopter-Borne Magnetic Survey (Aeroquest Job #11-046) for Geoscience BC; Geoscience BC, Report 2012-2, 11 p. URL <http://www.geosciencebc.com/s/Report2012-02.asp> [January 2012]

Topographic data

BC TRIM (2006): British Columbia Terrain Resource Information Mapping (TRIM) Digitial Map Products; B.C. Ministry of Forests, Lands and Natural Resource Operations, Crown Registry and Geographic Base Branch. URL <http://archive.ilmb.gov.bc.ca/crgb/pba/trim/> [May 2011]

Natural Resources Canada (2007): National Topographic Data Base, tiles 104H13, 104H14, 104I03, 104I04, 104I05, 104I06; Natural Resources Canada, Earth Sciences Sector, Centre for Topographic Information, URL <http://geogratis.cgdi.gc.ca/geogratis/en/product/search.do?id=F3D83500-2564-D61E-4F37-FEF860E6DDC0> [September 2012]

Massey, N.W.D, MacIntyre, D.G., Desjardins, P.J. and Cooney, R.T. (2005): Digital Geology Map of British Columbia: Whole Province; B.C. Ministry of Energy, Mines and Natural Gas, Geofile 2005-1, URL <http://www.empr.gov.bc.ca/Mining/Geoscience/PublicationsCatalogue/GeoFiles/Pages/2005-1.aspx> [November 2007]

Natural Resources Canada (2007): Atlas of Canada base maps; Natural Resources Canada, Earth Sciences Sector, URL <http://geogratis.gc.ca/geogratis/en/option/select.do?id=0BCF289A-0131-247B-FDBD-4CC70989CBCB> [November 2007]

Acknowledgments

Cartography by James M. Logan from British Columbia Geological Survey and Fion Ma from Geoscience BC

Summary of zircon U-Pb and hornblende/biotite Ar-Ar geochronology samples taken from the Hotailuh batholith.

Sample no.	Type	UTM E	UTM N	Unit	Rock description	Age (Ma)*	Population	Statistics	Reference
11BVA31-232	U/Pb, Zrn	478,755	6,434,626	MJ TSp	Hbl-bearing Bt monzogranite	169.1±0.8	50/50 grains	MSWD=0.93, p=0.62	This study
11BVA35-276	Ar/Ar, Bt	480,640	6,439,273	MJ TSc	Hbl-bearing Bt Qtz-monzonite to monzogranite	169.0±1.1	13/25 steps, 54.7% of ^{39}Ar	MSWD=1.12, p=0.34	This study
11BVA35-276	U/Pb, Zrn	480,640	6,439,273	MJ TSc	Hbl-bearing Bt Qtz-monzonite to monzogranite	169.0±1.3	29/49 grains	MSWD=0.64, p=0.93	This study
11BVA42-329	Ar/Ar, Hbl	466,997	6,448,398	MJ TSm	Acicular Hbl-rich Qtz-diorite	171.9±1.7	6/11 steps, 81.6% of ^{39}Ar	MSWD=1.13, p=0.34	This study
11BVA42-332	Ar/Ar, Hbl	479,794	6,436,014	MJ TSf	Fine grained Hbl-Bt Qtz-diorite	173.2±1.4	4/12 steps, 54.2% of ^{39}Ar	MSWD=0.114, p=0.95	This study
11BVA27-199	Ar/Ar, Hbl	462,983	6,427,463	LT BC	Cpx-bearing Hbl-rich gabbro	210.9±1.6	5/17 steps, 53.3% of ^{39}Ar	MSWD=1.16, p=0.32	This study
11JLO32-319 (DDH G-89-8 55.47-60.05 m)	U/Pb, Zrn	451,832	6,457,090	LT GP	Plag-porphyritic hypabyssal intrusion	216.5±1.4	44/49 grains	MSWD=0.78, p=0.85	This study
11BVA38-304	U/Pb, Zrn	481,362	6,439,991	LT CHq	Hbl-bearing granodiorite to monzogranite	216.2±1.2	45/49 grains	MSWD=0.73, p=0.90	This study
11BVA42-333	Ar/Ar, Hbl	463,692	6,431,161	LT CH	Hbl Qtz-monzonite	220.5±2.2	6/9 steps, 94.2% of ^{39}Ar	MSWD=1.20, p=0.31	This study
11BVA42-333	U/Pb, Zrn	463,692	6,431,161	LT CH	Hbl Qtz-monzonite	218.2±1.3	47/50 grains	MSWD=0.76, p=0.88	This study
ZE09-057C (Z10117)	Ar/Ar, Hbl	450,041	6,449,776	LT GL	Layered to discordant hornblendite - pyroxenite	223.3±2.0			Zagorevski et al. (2011)
11OiV4-48	U/Pb, detrital Zrn	455,036	6,456,696	lmJHs	Siltstone and fine-grained sandstone	Carboniferous, Middle Triassic, Late Triassic, Early and Middle Jurassic peaks			Iverson et al. (2012)
11OiV4-52	U/Pb, detrital Zrn	454,891	6,457,018	lmJHsc	Volcanic lithic feldspathic arenite	Middle Triassic, Late Triassic, Early Jurassic and Middle Jurassic peaks			Iverson et al. (2012)
AN-77-356	U/Pb, Zrn	445,998	6,450,395	MJ TSp	Quartz syenite, biotite hornblende granite	169.6±1			Anderson et al. (1982)
AN-78-467	U/Pb, Zrn	492,021	6,434,632	EJ MR	Granodiorite	184±8			Anderson and Bevier (1992)
AN-78-569-3	U/Pb, Zrn	455,820	6,452,253	LT CH	Quartz monzonite	221±3			Anderson and Bevier (1992)

* Crystalization age for U-Pb zircon analyses. Cooling age (plateau age) for Ar-Ar analyses. 2 SD error

Selected assay results of mineralized rock samples collected during 2011 field work.

Mineral occur.	Station no.	UTM E	UTM N	Unit	Au*	Ag	Cu	Mo	W	Sn	Bi	As	Sb	Ba	Pb	Zn	Rb	Sr	Cd	Ni	Co
	Units				ppb	ppm	ppm	ppm	ppm	ppm	ppm	ppm	ppm	ppm	ppm	ppm	ppm	ppm	ppm	ppm	ppm
	Detection limit				2	0.1	0.1	0.1	0.1	0.1	0.1	1	0.1	1	0.1	1	0.1	1	0.1	0.1	0.2
Gnat P.	11BVA5-30	450,034	6,458,207	LTGP	12	0.1	161	<0.1	1.0	0.3	0.9	30	4.2	463	4	5	79	211	<0.1	3	109
Gnat P.	11BVA9-48	450,502	6,457,572	LTGP	4	<0.1	34	0.4	0.5	0.6	0.1	7	2.4	598	2	23	66	182	<0.1	2	6
Gnat P.	11JLO32-319	451,832	6,457,090	LTGP	41	0.6	7221	16.7	0.6	0.6	0.1	5	1.0	510	7	32	134	315	0.2	4	8
Dalv.	11BVA11-62a	448,489	6,449,977	lmTSs	14	<0.1	87	<0.1	29.5	0.9	4.8	535	54.9	53	2	3	64	38	<0.1	230	31
Dalv.	11BVA11-62b	448,489	6,449,977	lmTSs	570	2	463	0.5	9.8	1.2	61.0	>10000	205	36	32	21	38	121	<0.1	53	93
Gnat Cr.	11BVA2-12	451,163	6,451,183	LTCH	1703	81.7	>10000	5.5	<0.1	0.1	483	<1	1.4	50	79	125	62	599	0.5	5	18
Gnat L. um.	11BVA11-57	449,665	6,450,261	lmTSs	<2	<0.1	72	1.9	0.3	3.9	0.3	<1	0.3	341	11	33	64	21	<0.1	21	11
Gnat L. um.	11BVA11-58b	449,472	6,449,706	LTGLf	<2	0.1	87	8.2	0.8	0.9	0.1	5	1.8	1005	8	78	19	689	<0.1	39	22
Gnat L. um.	11BVA11-59	449,321	6,449,882	LTGL	5	0.2	402	3.7	0.2	1.3	0.1	2	1.9	245	4	93	5	424	0.2	30	96
Gnat L. um.	*Acme Dup (11BVA-11-59)*	449,321	6,449,882	LTGL	*4*																
Mat	11BVA26-184	462,220	6,428,961	lmTSs	2	0.2	139	7.0	0.4	0.7	<0.1	4	<0.1	27	5	129	2	80	0.4	146	20
Mat	11BVA26-187	461,821	6,429,303	lmTSs	<2	0.1	133	0.9	0.2	0.6	<0.1	22	0.4	36	73	57	2	272	0.2	63	39
Mat N	11BVA25-172	461,904	6,431,947	LTCH	39	9.1	>10000	0.7	0.2	0.2	5.4	<1	0.4	3102	13	86	32	1120	0.1	25	22
Pat	11BVA13-74	470,681	6,449,148	LTCH?	32	1.1	2962	2.2	0.4	1.8	1.0	12	0.7	392	4	24	25	568	<0.1	10	20
Pat W	11BVA14-82	467,697	6,447,881	MJTSc	21	0.7	7079	0.1	2.4	1.1	0.6	19	1.3	1083	2	49	117	159	0.2	2	15
Pat W	11BVA15-90	466,323	6,447,968	MJTSp	<2	<0.1	131	2.0	0.1	0.5	<0.1	4	<0.1	1179	4	7	84	461	<0.1	2	8
3 Sis. N	11BVA30-216	480,344	6,438,583	MJTSc	9	0.2	3645	6.4	>200	3.4	<0.1	3	0.4	130	3	92	19	195	0.2	5	51
3 Sis.	11BVA32-241	480,590	6,435,596	MJTSf	80	<0.1	3520	0.8	6.1	0.7	0.2	<1	0.2	41	2	59	2	270	<0.1	3	15
3 Sis.	11BVA32-246	481,249	6,435,903	LTCH	<2	<0.1	144	3.8	3.2	2.7	<0.1	<1	<0.1	188	3	9	4	550	<0.1	2	15
3 Sis. S	11BVA33-253	481,447	6,433,699	uTSv	<2	<0.1	55	6.8	1.1	0.8	0.1	5	0.2	40	1	3	2	1028	<0.1	10	124
3 Sis. S	11BVA33-257	481,525	6,433,380	uTSv	14	0.4	3367	314	33.3	3.1	2.4	11	2.7	51	2	58	9	521	<0.1	11	123
3 Sis. S	*Acme Dup (11BVA-33-257)*	481,525	6,433,380	uTSv		*0.3*	*3452*	*332*	*39*	*3.2*	*2.3*	*9*	*2.6*	*51*	*2*	*59*	*9*	*537*	*<0.1*	*11*	*122*
3 Sis. S	*11BVA33-257Dup*	481,525	6,433,380	uTSv	*14*	*0.3*	*2925*	*240*	*32*	*4.6*	*2.4*	*8*	*3.1*	*50*	*2*	*54*	*7*	*560*	*<0.1*	*12*	*105*

Abbreviations used for mineral occurrences: Gnat P. = Gnat Pass, Gnat Cr. = Upper Gnat Creek, Dalv. = Dalvenie, Gnat L. um. = Gnat Lakes ultramafite, 3 Sis. = Three Sisters, W = west, N = north, S = south.

* Analyzed by lead-collection fire assay fusion followed by ICP-ES. All other elements analyzed by four-acid digestion followed by ICP-MS.

MinFile (labelled by MinFile number): Developed Prospect, Prospect, Showing
Altered / mineralized rock samples (labelled by SampleID)
Sample: fossil, isotopic dating method (U-Pb zircon, Ar-Ar hornblende/biotite, U-Pb detrital zircon) — F, Z, Ar, D
Outcrop location (Stations)
Bedding: inclined
Fabric: spaced fracture cleavage, schistosity or magmatic foliation: inclined, vertical
Vein: inclined
Geological contact: defined, approximate, inferred
Unconformity: defined, approximate, inferred
Fault: defined, approximate, inferred, geophysical lineament
Ductile shear zone: inferred
Alteration zone / gossan
Roads: Highway 37, rough tracks
Abandoned railroad
Elevation contours (100 m intervals): Major, Minor
Foliated lithology
Study area

BC Geological Survey Open File 2012-06
Geoscience BC Map 2012-10-1

Geology of the Hotailuh Batholith northwestern British Columbia

NTS Sheets 104I/03, 04
Parts of NTS Sheets 104I/05, 06, 104H/13, 14

Bram I. van Straaten, James M. Logan, and Larry J. Diakow

1 : 50,000

0 1 2 4 km

Universal Transverse Mercator Projection, Zone 9
Horizontal Datum: North American Datum 1983

December 2012

Suggested Reference:
van Straaten, B.I., Logan, J.M. and Diakow, L.J. (2012): Geology of the Hotailuh Batholith, northwestern British Columbia; British Columbia Ministry of Energy, Mines, and Natural Gas, British Columbia Geological Survey Open File 2012-06 and Geoscience BC Map 2012-10-1, 1:50,000 scale.